

Crystals, Glasses and Gels

Synthesis and Phase Behavior of Soft Colloids

Jeroen Appel

Thesis committee

Promotor

Prof. Dr. F.A.M. Leermakers
Personal chair at Physical Chemistry and Soft Matter
Wageningen University

Co-promotor

Dr. J. Sprakel
Associate professor, Physical Chemistry and Soft Matter
Wageningen University

Other members

Prof. Dr. A. H. Velders, Wageningen University
Dr. C. V. Nikiforidis, Wageningen University
Dr. H. B. Eral, Delft University of Technology
Dr. I. K. Voets, Eindhoven University of Technology

This research was conducted under the auspices of the Graduate School VLAG (Advanced studies in Food Technology, Agrobiotechnology, Nutrition and Health Sciences).

Crystals, Glasses and Gels

Synthesis and Phase Behavior of Soft Colloids

Jeroen Appel

Thesis

submitted in fulfillment of the requirements for the degree of doctor

at Wageningen University

by the authority of the Rector Magnificus

Prof. Dr. A.P.J. Mol,

in the presence of the Thesis Committee appointed by the Academic Board

to be defended in public

on Wednesday 15 February 2017

at 4 p.m. in the Aula.

Jeroen Appel
Crystals, Glasses and Gels
Synthesis and Phase Behavior of Soft Colloids
148 pages

PhD thesis, Wageningen University, Wageningen, NL (2017)
With references, with summary in English

ISBN: 978-94-6343-010-4
DOI: <http://dx.doi.org/10.18174/396263>

Colloid science is an old discipline, older than polymer science, atom theory, quantum mechanics, biochemistry, electrolyte solution theory and environmental science, and, for that matter, older than its offsprings nanoscience and soft matter science.

Johannes Lyklema, *Colloidal Models. A bit of history*, Journal of Colloid and Interface Science **446** (2014), 308-316.

Contents

1	Introduction	1
<i>I</i>	<i>Synthesis of Novel Colloids</i>	
2	Facile Synthesis of Monodisperse Micron-Sized Latex Particles with Highly Carboxylated Surfaces	19
3	Conjugated Polymer Shells on Colloidal Templates by Seeded Suzuki-Miyaura Dispersion Polymerization	35
4	Temperature Controlled Sequential Gelation in Composite Microgel Suspensions	53
<i>II</i>	<i>Crystals, Glasses and Gels</i>	
5	Substitutional Impurity-Induced Vitrification in Microgel Crystals	73
6	Mechanics at the Glass-to-Gel Transition of Thermoresponsive Microgel Suspensions	91
7	General Discussion	115
	Summary	129
	List of Publications	132
	Acknowledgements	134
	About the Author	137
	Overview of Completed training Activities	138

Chapter 1

Introduction

Soft Matter and Colloids

Classically, four phases or states of matter are identified: plasmas, gasses, liquids and solids (Figure 1.1). Each phase has specific characteristics in structure, dynamics and mechanics. For example, one can distinguish the plasma and gas phase from the liquid and solid phase, based on the number of atoms or molecules per unit volume. Liquids and solids belong to the class of condensed matter, held together by cohesive bonds resulting from attractive intermolecular (or interatomic) interactions. In typical condensed materials, the atoms or molecules interact strongly and it is the cohesive collection of constituting particles that is responsible for the often complex structure and mechanics of these phases. A liquid is a phase of matter in which the bonds holding the particles together are weak enough to break and reform due to thermal fluctuations. As a result, a liquid flows and cannot hold a particular shape. By contrast, a solid achieves a finite elastic modulus by strong and (typically) irreversible cohesive bonds between its atomic or molecular constituents as a result of which it resists deformation and can be shaped and molded.

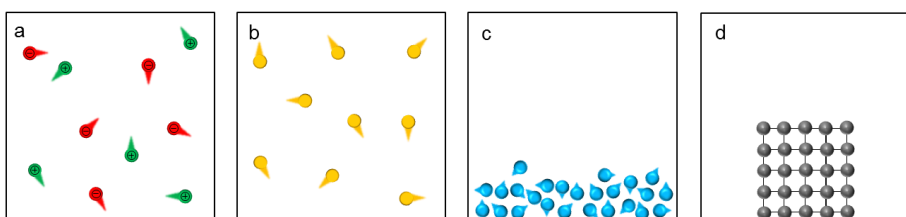


Figure 1.1: The four classical phases of matter. a) An ionized gas with no defined shape or volume forms a plasma. b) Molecules without intermolecular interactions and no defined shape or volume form a gas. c) Molecules or atoms with weak cohesive interactions between them form a liquid. d) Molecules or atoms with specific and permanent interactions between them have a defined volume and shape and form a solid.

Liquids and solids have been extensively studied as they are the corner stone of many materials used by man, such as plastics, metals and ceramics. Interestingly, there are also materials that have characteristics of both liquid and solid phases, combining properties of both phases in one material depending on for example the rate of deformation.^[1] Such soft solid, or viscoelastic materials, form the realm of study in soft matter science. Soft materials, or complex fluids, encompass a wide variety of matter, such as creams, emulsions, foams, paints and many more. Soft materials are also prevalent in nature, where water, proteins, lipids, DNA and many more molecules form cellular structures, cells, and tissues, together being the building blocks of life. In general, soft materials are composed of microscopic building blocks, such as colloids, polymers or surfactants, suspended or dissolved in a fluid. Despite its diversity, soft materials share several key features: they are typically inhomogeneous at mesoscopic length scales which governs their properties,^[2] they are easily deformed or structurally altered by weak thermal and mechanical fluctuations that are in the order of a few $k_B T$,^[3] and they often exhibit complexity.^[4,5]

In this thesis, we focus on colloidal dispersions, a prototypical class of soft materials, which by definition consist of a continuous phase and a suspended phase. The colloidal dispersions discussed in this thesis are suspensions of solid (or soft solid) particles of microscopic size, typically between tens of nanometers and several micrometers, suspended in a fluid. An important feature of colloidal systems is that the particles are in the size range where they can be observed in real space and time by optical microscopy, yet are small enough to exhibit Brownian motion. As such, colloidal suspensions have become a well-established experimental model to explore and test the thermal physics of materials.^[6-9] Interestingly, the physicochemical interplay between the particle surfaces and the fluid in which they are suspended, determines most of the suspension characteristics enabling the exploration of a rich variety of phases of matter, both in- and out-of-equilibrium.

The study of colloidal suspensions relies to a large extent on control of the physical stability of the suspension against aggregation. Such stability, can be achieved by electrostatic or steric repulsion, which prevents aggregation of the particles due to van der Waals forces. Moreover, by chemically controlling the surface functionality of the particles, the balance between repulsive and attractive forces, and their range and magnitude, can

be tailored precisely. Additionally, by matching the density of the continuous and suspended phase, gravitational effects such as sedimentation can be minimized, an essential feature to enable the mimicking of atomic states of matter where gravitational effects are typically negligible.^[6] Using optical microscopy, individual particles can be imaged and their positions in space and time analyzed with high accuracy using automated tracking routines,^[10] which allows for detailed studies of suspension characteristics at the single particle level. Often, particles are labeled with a fluorescent dye, making them visible with fluorescence microscopy, and if the refractive index of the fluid is comparable to that of the particles, non-invasive studies deep within the sample can be performed using confocal fluorescence microscopy. Figure 1.2 illustrates these important criteria for studying colloidal suspensions as experimental models for condensed matter.

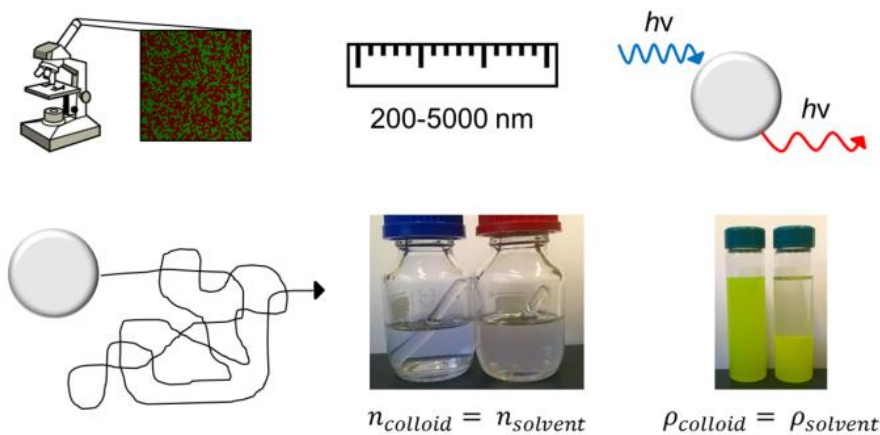


Figure 1.2: Basic requirements for microscopy studies of colloidal suspensions. Illustrated from top left to bottom right. Particles size should be above the optical resolution of the microscopes in order to discriminate individual particles. Fluorescently labeled particles allow for discriminating different particles in mixed systems and 3D imaging in confocal microscopy. Brownian motion of the particles allows for studying system dynamics. A comparable refractive index of the particles and the suspending medium limits light scattering and allows for imaging deeper in the sample. A comparable density of the particles and the suspending medium will limit the effects of gravity, in the bottom right picture, the left flask contains a density matched suspension, the right flask contains a suspension of colloids with a density higher than the suspending medium which have sedimented due to gravity.

The “Colloids as Big Atoms” paradigm was first postulated by Albert Einstein in his seminal paper on Brownian motion.^[11] With the advent of synthetic methods to produce well defined particles, the development of high-resolution microscopy methods and automated particle tracking algorithms, this paradigm has evolved into a mature field of study within the condensed matter community. Of particular note is the important paper by Pusey and van Megen who showed how the theoretical model of hard spheres could be realized in experiments using surface-functionalized colloids.^[12] Colloids are a powerful system for studying individual and collective phenomena of objects at the nanometer and micrometer scale. There are many unresolved phenomena in condensed matter physics which could be explored using well-defined colloidal systems and carefully designed experiments, such as crystal nucleation kinetics,^[13-17] the complex and heterogeneous dynamics in glasses,^[18-21] and the effect of impurities in crystals.^[22,23] While the phase transition between liquid and solid states, such as the liquid-gel or liquid-glass transition have been studied in great detail using colloidal systems,^[12,24-26] solid-solid transformations remain much less explored. In this thesis we focus on developing new colloids and studying phase transformations between colloidal crystals, glasses and gels.

In order to study these phase transformations, the experimental systems must obey three crucial criteria: i) particles should be monodisperse, with well-defined properties and be prepared through reproducible synthesis protocols, ii) the particles should ideally be responsive to environmental triggers such that their properties and interactions can be controlled experimentally, iii) the suspensions should be suitable for various experimental techniques, such as microscopy, rheology and light scattering, which for example requires matching of refractive index and density of particles and suspending solvent. Therefore, this thesis starts with the exploration of novel synthesis methods for colloids that meet these criteria, which are then used to study solid-solid phase transformations.

Colloid Synthesis

Colloidal particles are objects with dimensions from tens of nanometers to several micrometers. To synthesize these microscopic objects, we use processes in which small molecular precursors condense, typically through a nucleation-and-growth process, to form the final colloidal object. Solid colloidal particles can be categorized in three main groups based on their chemical composition, namely organic, inorganic and hybrid particles.

Organic polymer or ‘latex’ colloids are generally synthesized by radical polymerization reactions of three different types depending on the solubility of the precursors and the nature of the stabilizers, namely: emulsion, dispersion and precipitation polymerizations. In an emulsion polymerization, a liquid monomer is emulsified in a reaction medium, which is immiscible with both the monomer and the final polymer that forms the particles. Dissolved in the reaction medium is a free radical generator which initiates the polymerization of the emulsified monomer. At the start, radical oligomers aggregate in small clusters of collapsed insoluble polymer until a stable nucleus is formed, which grows into a particle by continued polymerization of monomer within these droplets. Emulsion polymerizations typically give rise to small particles between 10-500 nm.^[27] In a dispersion polymerization, both the monomer and initiator are soluble in the reaction medium. However, the reaction medium is a poor solvent for the polymers, which aggregate into nuclei and form particles. Since the monomer is soluble in the initial reaction mixture, nucleation is postponed and large particle sizes result; dispersion polymerizations are typically used to create particles of one to several micrometers. Different approaches to dispersion polymerizations, e.g. using palladium-catalyzed polycondensation reactions, have also been developed in recent years.^[28] Both emulsion and dispersion polymerizations consume monomers after the nucleation phase as monomers diffuse from the reaction medium into the growing particles. A precipitation polymerization reaction starts with the same reaction mixture as a dispersion polymerization however, in this case the reaction mixture is such a poor solvent for the polymer that after nucleation, monomers can hardly diffuse into the particles and growth of the particles is due to precipitation of the polymer on the surface of the particle. Due to this different growth mechanism, it is usually more difficult to have low polydispersity in

precipitation polymerizations, even though exceptions exist as demonstrated in the synthesis of microgels in Chapter 4.

In addition to initiators and monomers, the reaction mixtures in these free-radical polymerizations can also contain a plethora of additives such as surfactants, polymers and fluorescent dyes, which enables tailoring of particle size,^[29-31] shape,^[32-35] surface functionality^[36-40] and labelling.^[41,42] Together with the broad range of physicochemical properties of monomers applicable in these types of reactions this has led to reports describing many different colloids with interesting properties. For example, through careful selection of particle and the suspending fluid, a suspension is created in which light is not scattered by particles and in which solvent and particle exhibit the same density such that gravitational effects are minimized.^[43,44] These are advantages features for the use of colloids to study the properties of condensed phases, for example using confocal fluorescence microscopy.

Inorganic colloidal particles are also synthesized in a reaction fluid from a small reactive precursor. However, rather than forming from a collapsed polymer, inorganic particle nuclei consist of amorphous or crystalline phases of inorganic materials stabilized by small organic molecules on the particle surface. Particle growth proceeds from the surface which in the case of crystalline nuclei can result in faceted growth. This can lead to particles with unusual non-spherical shapes, such as cubes,^[34] pyramids^[33] and stars.^[32] Unfortunately, these non-isotropic shapes are difficult to maintain during growth and as a consequence such particles are usually restricted to sizes well below 100 nm. However, with advanced synthetic methods spheres, rods and cubes, as shown in Figure 1.3, and several other geometries are within experimental range also for micrometer sized particles.

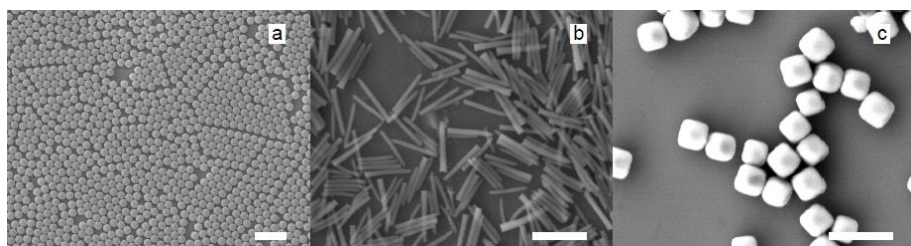


Figure 1.3: Differently shaped micron sized colloids, a) polystyrene spheres, b) silica rods and c) hematite cubes. Scale bars 5 μm .

Hybrid particles are particles either with a layered structure such as core-shell particles, where the core and the shell are made up of different materials or composite particles in which a blend of distinct materials forms the particle. While such a complex architecture may be advantageous for some experiments or applications, as we will show in this thesis, it places important constraints on the synthetic procedures, typically involving multi-step synthesis. A technique that is widely employed, is to use seed particles and synthesize a homogeneous shell or localized protrusion on them.^[45-47] Loading micron sized particles with nanoparticles or molecules, by swelling and de-swelling is another often used technique to create composite particles with unique properties.^[42] This has resulted in the synthesis of particles with remarkable features, such as self-propulsion,^[48] targeted drug delivery^[49] and controllable self-organization.^[39,50]

Phase Behavior of Colloidal Suspensions

The phase behavior of colloidal suspensions depends strongly not only on the concentration of colloids in the suspending fluid, but also on the interaction potential between particles.^[26] These parameters can be controlled through the experimental design of both the particles and the suspending medium. With these two parameters only, six phases can be found in monodisperse colloidal systems; the gas, liquid, gel, attractive-glass, repulsive-glass and crystalline phase. While the colloidal gas and liquid phases are interesting, we focus our attention to the colloidal solid phases (crystals, glasses and gels), which are shown in Figure 1.4.

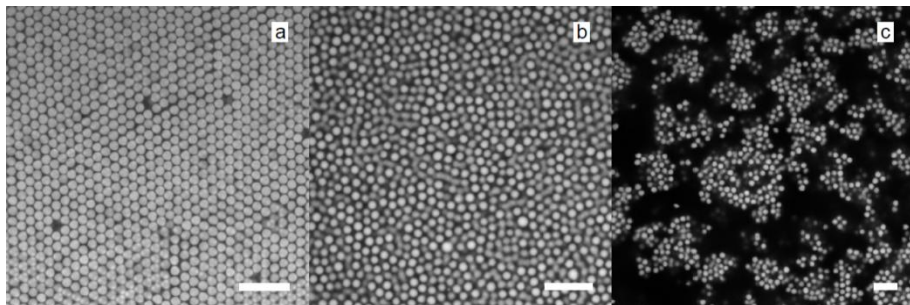


Figure 1.4: Confocal microscopy images of pTFEMA-pTBMA colloids in three different solid-like phases. A colloidal crystal (a), colloidal glass (b) and colloidal gel phase (c). Scale bars 10 μm .

In a colloidal crystal, particles are ordered into a regular lattice which exhibits long-ranged positional, orientational and translational order, in direct analogy to atomic or molecular crystals. The liquid-to-crystal transition is often induced by changing the particle volume fraction, which plays the role of an inverse temperature. In some cases, crystals can form at relatively low colloid concentrations, if there are long range repulsive interactions between the particles, for example due to electrostatic forces in media with very low salt concentrations.^[51] It is more common to study systems which exhibit only short range interactions, which means that higher colloid concentrations are needed to form thermodynamically stable crystal phases. For the most common colloidal crystal symmetries, the face-centered cubic and hexagonally close-packed lattices, the maximum packing density is that of close packing of spheres with a volume fraction of $\phi = 0.74$,^[12] however, stable crystals can form in hard sphere suspensions at significantly lower volume fractions.^[52] Often short range interactions are produced by aspecific forces between particle surfaces, such as electrostatic or steric interactions, however more complex interactions can be designed, for example using surface-tethered biomolecules, which allows the generation of more complex crystal phases.^[53]

A colloidal glass is a concentrated ensemble of particles ($\phi \approx 0.58$) which are jammed into a disordered, aperiodic, non-equilibrium state.^[54,55] Ultimately, the glass phase should crystallize; however, kinetic trapping of the particles in cages formed by their neighbors, slows down crystal nucleation to such a degree that the glass phase can be metastable for extended periods. We can distinguish two types of glasses; if the particles have repulsive interactions, a repulsive glass can form due to geometric hindrance alone, while the presence of attractive interactions between the particles can cause a bonding-dominated solid phase which is denoted as an attractive-glass.^[56] These two different disordered solids are of particular interest as they appear structurally identical, yet dynamically very different.^[57]

Finally there is the colloidal gel phase, which is formed when colloidal particles aggregated due to attractive interactions at volume fractions below the colloidal glass transition ($\phi \approx 0.58$). Gels can be mechanically stable down to very low concentrations, even as low as $\phi = 0.01$, depending on the attraction strength.^[58] Similar to a colloidal

glass, colloidal gels are in a non-equilibrium state attempting to approach a crystalline phase but becoming kinetically trapped. This also means that over time, these disordered phases will age and evolve structurally.

In the past, a wealth of studies has been dedicated to the transformation from liquid to solid states in colloidal suspensions. By contrast, much less is known about the transformations from one solid phase into the other, while such solid-solid transitions are also important in the context of material science as a whole.

Outline of this thesis

Colloidal suspensions are an experimental model system for studying structural and mechanical properties of soft materials. These properties are manifested differently in colloidal solid-like phases such as crystals, glasses and gels. To further understand these properties and relations between them, it is necessary to develop well-defined colloids and employ techniques such as microscopy and rheology to study the structure and mechanics of their suspensions. This thesis presents five experimental chapters dealing with the synthesis and characterization of colloids and their suspensions, with particular interest in solid-solid phase transformations in dense suspensions.

In the first section “Synthesis of Novel Colloids”, we present different methods to synthesize and characterize well-defined colloids with new properties. **Chapter 2** presents a facile one-step method to prepare monodisperse and well defined fluorescent latex particles in aqueous solution. The method allows for control over the particle size in a size range that is suitable for optical microscopy studies, furthermore the incorporation of fluorescent dye makes these colloids perfectly detectable with fluorescence microscopy. Carboxylic acid groups on the surface of these colloids provide high stability against aggregation and allow for surface modifications. **Chapter 3** presents a technique to synthesize conjugated polymer shells on colloidal templates. Using a seeded polymerization technique, a variety of conjugated shells can be synthesized on organic as well as inorganic colloids. Moreover, the, as synthesized, core-shell particles retain the monodispersity and shape of the core particle. **Chapter 4** presents a two-step method to synthesize core-shell microgels with a latex core and a temperature responsive microgel shell. The latex core can incorporate a fluorescent dye, making these particles suitable for fluorescence microscopy

and the thermoresponsivity of the microgel shell can be tuned with the monomer composition. A two-component mixture of core-shell microgels demonstrates how a combination of microscopy and rheology is used to study phase transition in colloidal suspensions and sets the stage for the second section.

Section two “Crystals, Glasses and Gels”, presents two chapters on phase transitions in suspensions of soft colloids. **Chapter 5** is a microscopy study on the crystal-to-glass transition, induced by impurity particles. Large impurities in a crystal of smaller microgel particles with a size ratio of 0.67 induce a crystal-to-glass transition as the concentration of impurities increases. Interestingly, there is a substitution phenomenon at low impurity concentrations, where an impurity particle substitutes four tetrahedrally coordinated lattice particles in an face centered cubic packed crystal. **Chapter 6** presents a rheological study on the glass-to-gel transition in a suspension of thermoresponsive microgels. The glass-to-gel transition is a transition between two amorphous colloidal solid states and interestingly, the rheological data shows a clear distinction in the viscoelastic properties of these two states, with a discontinuity at the transition point. Finally, in **Chapter 7**, the most important results of the five experimental chapters are discussed in a broader scientific perspective.

References

- [1] V. Trappe and D. A. Weitz, *Scaling of the Viscoelasticity of Weakly Attractive Particles*, Phys. Rev. Lett., **85** (2000), 449-452.
- [2] J. C. Crocker, M. T. Valentine, E. R. Weeks, T. Gisler, P. D. Kaplan, A. G. Yodh and D. A. Weitz, *Two-Point Microrheology of Inhomogeneous Soft Materials*, Phys. Rev. Lett., **85** (2000), 888-891.
- [3] F. Gittes, B. Schnurr, P. D. Olmsted, F. C. MacKintosh and C. F. Schmidt, *Microscopic Viscoelasticity: Shear Moduli of Soft Materials Determined from Thermal Fluctuations*, Phys. Rev. Lett., **79** (1997), 3286-3289.
- [4] S. Jain and F. S. Bates, *On the Origins of Morphological Complexity in Block Copolymer Surfactants*, Science, **300** (2003), 460-464.
- [5] R. Mezzenga, P. Schurtenberger, A. Burbidge and M. Michel, *Understanding foods as soft materials*, Nature Materials, **4** (2005), 729-740.
- [6] W. C. K. Poon, *Colloids as Big Atoms*, Science, **304** (2004), 830-831.
- [7] E. R. Weeks, J. C. Crocker, A. C. Levitt, A. Schofield and D. A. Weitz, *Three-Dimensional Direct Imaging of Structural Relaxation Near the Colloidal Glass Transition*, Science, **287** (2000), 627-631.
- [8] A. Yethiraj and A van Blaaderen, *A colloidal model system with an interaction tunable from hard sphere to soft and dipolar*, Nature, **421** (2003), 513-517.
- [9] P. J. Lu, and D. A. Weitz, *Colloidal Particles: Crystals, Glasses and Gels*, Annu. Rev. Condens. Matter Phys., **4** (2013), 217-233.
- [10] Y. X. Gao and M. L. Kilfoil, *Accurate detection and complete tracking of large populations of features in three dimensions*, Opt. Express, **17** (2009), 4685-4704.
- [11] A. Einstein, *Über die von der molekularkinetischen Theorie der Wärme geforderte Bewegung von in ruhenden Flüssigkeiten suspendierten Teilchen*, Annalen der Physik, **17** (1905), 549-560.
- [12] P. N. Pusey and W. van Megen, *Phase behavior of concentrated suspensions of nearly hard colloidal spheres*, Nature, **320** (1986), 340-342.
- [13] S. Auer and D. Frenkel, *Prediction of absolute crystal-nucleation rate in hard-sphere colloids*, Nature, **409** (2001), 1020-1023.
- [14] A. Cacciuto, S. Auer and D. Frenkel, *Onset of heterogeneous crystal nucleation in colloidal suspensions*, Nature, **428** (2004), 404-406.

- [15] Y. Peng, F. Wang, Z. Wang, A. M. Alsayed, Z. Zhang, A. G. Yodh and Y. Han, *Two-step nucleation mechanism in solid–solid phase transitions*, Nature Materials, **14** (2015), 101-108.
- [16] Y. Wang, Y. Wang, X. Zheng, E. Ducrot, J. S. Yodh, M. Weck and D. J. Pine, *Crystallization of DNA-coated colloids*, Nature Communications, **6** (2015).
- [17] B. Li, D. Zhou and Y. Han, *Assembly and phase transitions of colloidal crystals*, Nature Reviews Materials, **1** (2016), 15011.
- [18] E. R. Weeks, J. C. Crocker, A. C. Levitt, A. Schofield and D. A. Weitz, *Three-Dimensional Direct Imaging of Structural Relaxation Near the Colloidal Glass Transition*, Science, **287** (2000), 627-631.
- [19] W. K. Kegel and A. van Blaaderen, *Direct Observation of Dynamical Heterogeneities in Colloidal Hard-Sphere Suspensions*, Science, **287** (2000), 290-293.
- [20] B. Abou, D. Bonn and J. Meunier, *Aging dynamics in a colloidal glass*, Phys. Rev. E, **64** (2001), 021510-021515.
- [21] S. Golde, T. Palberg and H. J. Schöpe, *Correlation between dynamical and structural heterogeneities in colloidal hard-sphere suspensions*, Nature Physics, (2016).
- [22] V. W. A. de Villeneuve, R. P. A. Dullens, D. G. A. L. Aarts, E. Groeneweld, J. H. Scherff, W. K. Kegel and H. N. W. Lekkerkerker, *Colloidal Hard-Sphere Crystal Growth Frustrated by Large Spherical Impurities*, Science, **309** (2005), 1231-1233.
- [23] R. Higler, J. Appel and J. Sprakel, *Substitutional impurity-induced vitrification in microgel crystals*, Soft Matter, **9** (2013), 5372-5379.
- [24] V. J. Anderson and H. N. W. Lekkerkerker, *Insights into phase transition kinetics from colloid science*, Nature, **416** (2002), 811-815.
- [25] V. Trappe, V. Prasad, L. Cipelletti, P. N. Segre and D. A. Weitz, *Jamming phase diagram for attractive particles*, Nature, **411** (2001), 772-775.
- [26] P. J. Lu, and D. A. Weitz, *Colloidal Particles: Crystals, Glasses and Gels*, Annu. Rev. Condens. Matter Phys., **4** (2013), 217-233.
- [27] M. Egen and R. Zentel, *Surfactant-Free Emulsion Polymerization of Various Methacrylates: Towards Monodisperse Colloids for Polymer Opals*, Macromol. Chem. Phys., **205** (2004), 1479-1488.
- [28] A. J. C. Kuehne, M. C. Gether and J. Sprakel, *Monodisperse conjugated polymer particles by Suzuki–Miyaura dispersion polymerization*, Nature Communications, **3** (2012).
- [29] L. Antl, J. W. Goodwin, R. D. Hill, R. H. Ottewill, S. M. Owens, S. Papworth and J. A. Waters, *The preparation of poly(methyl*

- methacrylate) latices in non-aqueous media*, Colloids and Surfaces, **17** (1986), 67-78.
- [30] E. Matijević, *Preparation and Properties of Uniform Size Colloids*, Chem. Mater., **5** (1993), 412-426.
- [31] B. Liu, M. Zhang, G. Wu and H. Zhang, *Synthesis of large-scale, monodisperse latex particles via one-step emulsion polymerization through in situ charge neutralization*, Colloids and Surfaces A: Physicochemical and Engineering Aspects, **500** (2016), 127-136.
- [32] S. M. Lee, Y. Jun, S. N. Cho and J. Cheon, *Single-Crystalline Star-Shaped Nanocrystals and Their Evolution: Programming the Geometry of Nano-Building Blocks*, J. Am. Chem. Soc., **124** (2002), 11244–11245.
- [33] B. Koo, R. N. Patel and B. A. Korgel, *Synthesis of CuInSe₂ Nanocrystals with Trigonal Pyramidal Shape*, J. Am. Chem. Soc., **131** (2009), 3134–3135.
- [34] L. Rossi, S. Sacanna, W. T. M. Irvine, P. M. Chaikin, D. J. Pine and A. P. Philipse, *Cubic crystals from cubic colloids*, Soft Matter, **7** (2011), 4139-4142.
- [35] S. Sacanna, M. Korpics, K. Rodriguez, L. Colón-Meléndez, S. -H. Kim, D. J. Pine and G. -R. Yi, *Shaping colloids for self-assembly*, Nature Communications, **4** (2013).
- [36] S. F. Lascelles and S. P. Armes, *Synthesis and characterization of micrometre-sized, polypyrrole-coated polystyrene latexes*, J. Mater. Chem., **7** (1997), 1339-1347.
- [37] J. I. Amelvy, G. -F. Unali, Y. Li, S. Granger-Bevan, and S. P. Armes, *Synthesis of Sterically Stabilized Polystyrene Latex Particles Using Cationic Block Copolymers and Macromonomers and Their Application as Stimulus-Responsive Particulate Emulsifiers for Oil-in-Water Emulsions*, Langmuir, **20** (2004), 4345-4354.
- [38] M. A. Correa-Duarte, V. Salgueiriño-Maceira, B. Rodríguez-González, L. M. Liz-Marzán, A. Kosiorek, W. Kandulski and M. Giersig, *Asymmetric Functional Colloids Through Selective Hemisphere Modification*, Advanced Materials, **17** (2005), 2014-2018.
- [39] M. -P. Valignat, O. Theodoly, J. C. Crocker, W. B. Russel and P. M. Chaikin, Reversible self-assembly and directed assembly of DNA-linked micrometer-sized colloids, Proceedings of the National Academy of Sciences of the United States of America, **102** (2005), 4225-4229.
- [40] E. Spruijt, H. E. Bakker, T. E. Kodger, J. Sprakel, M. A. C. Stuart and J. van der Gucht, *Reversible assembly of oppositely charged hairy colloids in water*, Soft Matter, **7** (2011), 8281-8290.

- [41] B. J. Battersby, G. A. Lawrie, A. P. R. Johnston and M. Trau, *Optical barcoding of colloidal suspensions: applications in genomics, proteomics and drug discovery*, Chemical Communications, **14** (2002), 1435-1441.
- [42] C. Xu and E. Bakker, *Multicolor Quantum Dot Encoding for Polymeric Particle-Based Optical Ion Sensors*, Analytical Chemistry, **79** (2007), 3716-3723.
- [43] E. R. Weeks, J. C. Crocker, A. C. Levitt, A. Schofield and D. A. Weitz, *Three-Dimensional Direct Imaging of Structural Relaxation Near the Colloidal Glass Transition*, Science, **287** (2000), 627-631.
- [44] A. Yethiraj and A van Blaaderen, *A colloidal model system with an interaction tunable from hard sphere to soft and dipolar*, Nature, **421** (2003), 513-517.
- [45] Y. Lu, Y. Mei, M. Drechsler and M. Ballauff, Thermosensitive Core–Shell Particles as Carriers for Ag Nanoparticles: Modulating the Catalytic Activity by a Phase Transition in Networks, Angewandte Chemie International Edition, **45** (2006), 813-816.
- [46] J. R. Wolters, G. Avvisati, F. Hagemans, T. Vissers, D. J. Kraft, M. Dijkstra and W. K. Kegel, *Self-assembly of “Mickey Mouse” shaped colloids into tube-like structures: experiments and simulations*, Soft Matter, **11** (2015), 1067-1077.
- [47] Y. Wang, Y. Wang, D. R. Breed, V. N. Manoharan, L. Feng, A. D. Hollingsworth, M. Weck and D. J. Pine, *Colloids with valence and specific directional bonding*, Nature, **491** (2012), 51-55.
- [48] G. Volpe, I. Buttinoni, D. Vogt, H. J. Kümmurer and C. Bechinger, *Microswimmers in patterned environments*, Soft Matter, **7** (2011), 8810-8815.
- [49] J. K. Oh, R. Drumright, D. J. Siegwart and K. Matyjaszewski, *The development of microgels/nanogels for drug delivery applications*, Progress in Polymer Science, **33** (2008), 448-477.
- [50] F. Li, D. P. Josephson and A. Stein, *Colloidal assembly: the road from particles to colloidal molecules and crystals*, Angewandte Chemie International Edition, **50** (2011), 360-388.
- [51] E. R. Russel, F. Spaepen and D. A. Weitz, *Anisotropic elasticity of experimental colloidal Wigner crystals*, Phys. Rev. E, **91** (2015), 032310.
- [52] K. Kremer, M. O. Robbins and G. S. Grest, *Phase Diagram of Yukawa Systems: Model for Charge-Stabilized Colloids*, Phys. Rev. Lett., **57** (1986), 2694-2697.

- [53] M. T. Casey, R. T. Scarlett, W. B. Rogers, I. Jenkins, T. Sinno and J. C. Crocker, *Driving diffusionless transformations in colloidal crystals using DNA handshaking*, Nature Communications, **3** (2012).
- [54] T. G. Mason and D. A. Weitz, Linear Viscoelasticity of Colloidal Hard Sphere Suspensions near the Glass Transition, Phys. Rev. Lett., **75** (1995), 2770-2773.
- [55] E. R. weeks and D. A. Weitz, Properties of Cage Rearrangements Observed near the Colloidal Glass Transition, Phys. Rev. Lett., **89** (2002), 095704.
- [56] F. Sciortino, Disordered materials: *One liquid, two glasses*, Nature Materials, **1** (2002), 145-146.
- [57] T. van de Laar, R. Higler, K. Schröen and J. Sprakel, *Discontinuous nature of the repulsive-to-attractive colloidal glass transition*, Scientific Reports, **6** (2016).
- [58] V. Trappe and P. Sandkühler, *Colloidal gels—low-density disordered solid-like states*, Current Opinion in Colloid & Interface Science, **8** (2004), 494-500.

I

Synthesis of Novel Colloids

Chapter 2

Facile Synthesis of Monodisperse Micron-Sized Latex Particles with Highly Carboxylated Surfaces

A facile method for the aqueous synthesis of monodisperse and micrometer-sized colloids with highly carboxylated surfaces is presented. The method is applied to three different monomers, styrene, methyl methacrylate, and 2,2,2-trifluoroethyl methacrylate, and illustrates tuning of the size and monodispersity in the reactions. High surface density of carboxylic acids of up to 10 COOH/nm² from potentiometric titrations, is achieved through copolymerization with itaconic acid. The versatility of this system is highlighted by creating highly fluorescent and monodisperse particles that can be index matched in aqueous solution and through surface modification via the carboxylic acid groups using standard amidation chemistry.

This chapter was published as:

Jeroen Appel, Sabine Akerboom, Remco G. Fokkink and Joris Sprakel,
Facile One-Step Synthesis of Monodisperse Micron-Sized Latex Particles with Highly Carboxylated Surfaces, Macromolecular Rapid Communications, **34** (2013), 1284-1288.

2.1 Introduction

Colloids are extensively used as building blocks for creating novel functional materials through their assembly into two- and three dimensional structures.^[1] For example, undirected colloidal assembly is used for creating artificial opals.^[2-4] Such an artificial opal can then be turned into an inverse photonic crystal via post-assembly chemical modifications.^[5] Colloids can also be directed in their assembly processes, with external fields, such as light^[6] or electric^[7] or magnetic fields.^[8] Alternatively, functional groups or molecules at the surface of the colloids, that introduce specific interactions, can also be used to direct their assembly^[9,10] and allow even for orthogonal assembly.^[11] Colloids are also useful probes in optical microscopy, as their well-defined shape and size allows them to be detected and tracked with high accuracy. They are used as embedded probes in microrheology to determine mechanical properties of soft materials and cells.^[12,13] In microfluidics, colloidal suspensions are used to study flow properties through narrow channels and around obstacles.^[14]

A wide variety of organic, inorganic, and hybrid colloids can be synthesized, yet polymer colloids, or latex particles, are preferred because of their facile preparation methods, which give low polydispersities.^[15,16] Monodispersity is a key factor for colloidal crystallization and for the interpretation of the results from particle-tracking algorithms such as those used in particle-tracking microrheology. The broad array of functional monomers that can be copolymerized with the bulk monomer has led to a broad array of organic colloids with specific characteristics. Colloidal stability, another important requirement, originates from electrostatic repulsion and/or steric hindrance^[17] and thus depends on the surface characteristics of the colloids. Also for functionalization of the colloids, the surface groups are crucial as they are used as scaffolds for modifications.^[18-20] Among the most utilized colloids are polymeric colloids with carboxylic acids at their surface; they are highly stable against aggregation and can be easily modified with amide or ester chemistry. While such colloids are easily prepared through surfactant free emulsion polymerization (SFEP) with carboxylic comonomers, colloid diameters in a single step reaction typically do not exceed 500 nm.^[21-23] The use of colloidal particles in colloid physics experiments requires particle sizes well above the optical diffraction limit of

(confocal)microscopes, such that individual particles can be automatically recognized even when they are densely packed. They can be synthesized via seeded emulsion polymerization^[24] or two stage dispersion polymerization.^[25] However, these methods are less straightforward, time consuming, and generally detrimental to monodispersity. Reese and Asher^[26] demonstrate a method to generate monodisperse particles with mixed surfaces consisting of carboxylic acids, hydroxyl groups and sulfate moieties; in this case, approximately 30-50% of the surface charges originate from carboxylic groups.

In this chapter, we describe a simple method for the synthesis of highly monodisperse micron-sized latex colloids in water, in a single step reaction yielding high carboxylic acid charge densities at the particle surface without any other surface groups present. We emphasize the low polydispersity, adjustable size, up to well over one micrometer in diameter, and high carboxylic acid surface coverage obtained with this method, as well as its applicability to different hydrophobic monomers. We also show that the carboxylic acid groups can be used for further surface functionalization. Finally, we also prepare particles from fluorinated monomers, which allow for refractive index matching in aqueous media, making them a useful system for optical characterization.

2.2 Experimental Section

2.2.1 Materials

Styrene, methyl methacrylate (MMA), itaconic acid (IA), 2,2,2-trifluoroethyl methacrylate (TFEMA), *N*-hydroxysulfosuccinimide sodium salt (sulfo-NHS), 4,4'-azobis(4-cyanovaleric acid) (ACVA), dimethyl sulfoxide (DMSO), *N*-(3-dimethylaminopropyl)-*N'*-ethylcarbodiimide hydrochloride (EDC), phosphate buffered saline (PBS), and sodium hydroxide were obtained from Sigma-Aldrich (Munich, Germany). The fluorescent dyes pyrromethene 546 and pyrromethene 605 were obtained from Exciton (Dayton OH, USA). mPEG-NH₂ (molecular weight [MW] 5000 g/mol) was obtained from Nanocs (New York NY, USA). Heptakis(6-amino-6-deoxy)- β -cyclodextrine heptahydrochloride (CD) was obtained from CycloLab (Budapest, Hungary). All chemicals were used as received.

2.2.2 Preparation of Colloids

Colloids were prepared in a single step SFEP. The different reaction mixtures used for the colloids discussed in this chapter are given in Tables 2.1-2.3. The general synthesis procedure was the following: All materials except the initiator were charged in a one neck round-bottom flask, including a 2.5 cm magnetic stirring bar. ACVA was dissolved in 0.2 M sodium hydroxide (28 mg/mL). The flask was sealed with a rubber septum and the reaction mixture was flushed with nitrogen for 15 min. The flask was then placed in an oil bath at 85 °C and stirred at 500 rpm, after 15 min the initiator was injected into the reaction mixture. The reaction was allowed to proceed for 12 hours at 85 °C, stirring at 500 rpm. The reaction mixtures were then filtered and the polystyrene colloids were washed three times with DI water using centrifugation. The pMMA and pTFEMA colloids were used for characterization straight from the reaction mixture.

2.2.3 Characterization

Particle sizes and polydispersities were determined using static light scattering (SLS), performed on an ALV instrument equipped with an ALV7002 external correlator, and a 300 mW Cobolt Samba-300 DPSS laser operating at a wavelength of 532 nm. A dust free toluene reference was used. Measurements were performed in 25 mm quartz cuvettes (Hellma). Detector: Thorn RFIB263KF Photo Multiplier Detector: ALV 50/100/200/400/600 μm pinhole detection system. Goniometer: ALV-SP/86. The scattering intensity was recorded at scattering angles between $40^\circ \leq \theta \geq 125^\circ$ at 1° intervals, and the resulting scattering curves were fitted to a form factor for polydisperse hard spheres, to extract both the mean particle radius and its polydispersity.

Samples for scanning electron microscopy (SEM) were deposited on a silicon wafer, then sputtered with a thin layer of gold using a JEOL JFC-1300 autofine sputtercoater. Images were recorded on a JEOL JAMP-9500F Field Emission Auger Microprobe.

Potentiometric titrations with sodium hydroxide were performed on colloidal dispersions and monitored with a Mettler Toledo InLab Micro electrode. The colloidal dispersions had a starting salt concentration of $[\text{NaCl}] = 50 \times 10^{-3} \text{ M}$. From the titration curves, the number of carboxylic

acids were determined, which were then converted into the surface area (nm^2) per carboxylic acid.

ζ potentials were recorded on a Malvern Zetasizer 2000, on colloidal dispersions with $[\text{NaCl}] = 50 \times 10^{-3}$ M at pH 4.1 and 9.9.

Bright field and confocal fluorescence microscopy images were recorded with a Zeiss LSM 5 EXCITER Axiovert 200M confocal microscope, equipped with a $100\times$ oil-immersion objective.

Table 2.1: Reaction mixtures of the p(styrene) colloids.

	Water (g)	Styrene (g)	IA (g)	ACVA (g)	Dye (g)
pSIA5	125	5	0.1	0.05	-
pSIA15	125	15	0.3	0.15	-
pSIA25	125	25	0.5	0.25	-
pSIA35	125	35	0.7	0.35	-
pSIA55	125	55	1.1	0.55	-
pSIA35-546	125	35	0.7	0.35	0.01
pSIA35-605	125	35	0.7	0.35	0.01

Table 2.2: Reaction mixtures of the p(MMA) colloids.

	Water (g)	MMA (g)	IA (g)	ACVA (g)	Dye (g)
pMMAIA5	125	5	0.1	0.05	-
pMMAIA15	125	15	0.3	0.15	-
pMMAIA25	125	25	0.5	0.25	-
pMMAIA35	125	35	0.7	0.35	-
pMMAIA55	125	55	1.1	0.55	-
pMMAIA55-546	125	55	1.1	0.55	0.01
pMMAIA55-605	125	55	1.1	0.55	0.01

Table 2.3: Reaction mixtures of the p(TFEMA) colloids.

	Water (g)	TFEMA (g)	IA (g)	ACVA (g)	Dye (g)
pTFEMAIA5-546	125	5	0.1	0.05	0.01
pTFEMAIA5-605	125	5	0.1	0.05	0.01

2.2.4 Surface Modification

Post synthesis surface modifications were performed on the carboxylic acids at the surface of the particles, using a EDC/sulfo-NHS mediated amidation. We coupled both mono-amine functionalized polyethylene glycol of MW 5000 g/mol and a cyclodextrin functionalized with seven amine groups. The reactions were performed in PBS with pH 7.4 and an ionic strength of 150×10^{-3} M. To 1 mL of a 1 wt% suspension of the colloids was added 2 mg EDC, 2 mg sulfo-NHS, and either 5 mg mPEG-NH₂ (PEG+) or 2 mg CD (CD+). The amidation reaction was allowed to proceed for 4 hours at room temperature. As a control experiment, to check for unspecific binding through physical adsorption, colloids and mPEG-NH₂ (PEG-) or CD (CD-) were mixed without addition of the conjugating agents EDC and sulfo-NHS and were incubated at room temperature for 4 h. The colloids were then washed three times with 1 mL PBS and their ζ potentials were recorded in PBS.

2.3 Results and Discussion

SFEP is a general method to synthesize latex colloids. It is a simple one step procedure and typically gives colloids with low polydispersities. Surface charge, to ensure colloidal stability, is typically achieved with a persulfate initiator and can be increased with acidic comonomers such as acrylic acid (AA) and methacrylic acid (MA).^[21-23] However, a drawback of the method is that the size of the particles produced, while maintaining monodispersity, typically does not exceed 500 nm in diameter. With the carboxyl functional azo initiator ACVA, in the absence of any comonomers, we could already obtain colloids with diameters of up to 800 nm. However, these colloids only exhibit low surface charge densities, as only the initiator provides charge. To increase the surface charge density we copolymerize the insoluble monomer with itaconic acid (IA) at 2 wt% to monomer. Compared with MA, IA doubles the charge density, as it has two carboxylic acids per monomer. The number of carboxylic groups per particle is determined from titration curves for the polystyrene colloids (pSIA). These are then converted into a parking area, which gives typical area per carboxylic group. The parking area is a convenient way of comparing surface charge between particles of different

diameters, where a low parking area number corresponds to a high charge distribution. We found surprisingly small parking areas between 0.07 and 0.23 nm² (Table 2.4), which indicates a carboxylic load of up to 10 carboxylic groups per nm²; this high carboxylic load ensures good colloidal stability, even under extreme saline or alkaline conditions, and allows for efficient surface modifications. Such high carboxylic acid loads at the particle surface are indicative of a hairy surface layer of polymers enriched in carboxylic acid groups. We further verify the high surface charge density by determining the ζ potential. We measure ζ potentials of colloidal dispersions at an ionic strength of 50×10^{-3} M at pH 4.1 and pH 9.9 (Table 2.4). At a given pH, the ζ potential between different batches of particles is relatively constant, verifying the reproducibility of our method. At higher pH, more protons dissociate from the carboxylic acid groups, increasing the amount of negative charge on the colloidal surface. Therefore, there is a significant decrease in ζ potential of ≈ -40 mV from pH 4.1 to pH 9.9.

Table 2.4: Parking area and ζ potential of the synthesized latex colloids.

	Parking Area nm ² /COOH Group	ζ potential (mV) pH 4.1	ζ potential (mV) pH 9.9
pSIA5	7	-39.6	-78.2
pSIA15	23	-34.3	-74.7
pSIA25	14	-39.3	-77.7
pSIA35	19	-40.5	-78.2
pSIA55	15	-32.6	-73.9
pSIA35-546	-	-39.4	-75.8
pSIA35-605	-	-33.4	-77.5
pMMAIA5	-	-	-
pMMAIA15	-	-31.8	-77.6
pMMAIA25	-	-32.8	-80.0
pMMAIA35	-	-31.6	-78.5
pMMAIA55	-	-32.1	-70.3
pMMAIA55-546	-	-31.9	-68.6
pMMAIA55-605	-	-29.5	-70.6
pTFEMAIA5-546	-	-33.2	-85.2
pTFEMAIA5-605	-	-32.8	-84.5

We synthesize colloids of polystyrene and pMMA in five different monomer to water ratios, with ACVA at 1 wt% and IA at 2 wt%. The size and polydispersity of these colloids is then determined with SLS by fitting the scattering curves to a form factor for polydisperse hard spheres and the results are given in Table 2.5. For the polystyrene, colloids we measured diameters between 600 and 1400 nm. The pMMA colloids have diameters between 250 and 1000 nm. In both cases, the monodispersity is excellent with relative standard deviations in most cases between 5% and 6%. This shows that with the given method, contrasting earlier synthetic protocols, carboxylated colloids with sizes well over 500 nm and with high monodispersity can be obtained in a simple single step reaction. The polystyrene and pMMA particles show a clear and reproducible increase of colloid size with increasing monomer to water ratio as can be seen in Figure 2.1. This is convenient because it enables the choice of particle size before synthesis.

Table 2.5: Diameter and polydispersity of the synthesized latex colloids.

	Diameter (nm)	Polydispersity (R_w/R_n)	Rel. St. Dev. (%)
pSIA5	625	1.02	7.2
pSIA15	959	1.01	5.6
pSIA25	1046	1.01	5.5
pSIA35	1171	1.01	4.7
pSIA55	1404	1.01	4.6
pSIA35-546	1336	1.01	4.6
pSIA35-605	1361	1.00	3.6
pMMAIA5	258	1.01	5.7
pMMAIA15	773	1.01	6.3
pMMAIA25	746	1.01	5.0
pMMAIA35	909	1.01	6.0
pMMAIA55	1022	1.01	6.6
pMMAIA55-546	984	1.01	5.4
pMMAIA55-605	1169	1.01	5.0
PTFEMAIA5-546	771	1.01	4.3
PTFEMAIA5-605	776	1.00	3.4

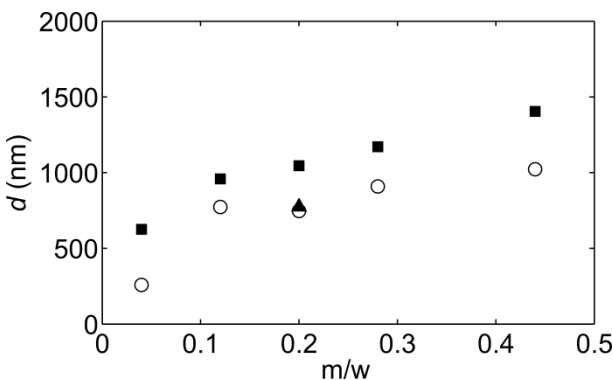


Figure 2.1: Particle diameters as a function of monomer-to-water ratio (m/w). Polystyrene (black squares), pMMA (open circles), pTFEMA (black triangle).

Low polydispersity is a precondition for many colloidal assembly studies, as it allows for the colloids to assemble into 2D hexagonally packed films or 3D crystal structures. A dispersion of polystyrene colloids with a relative standard deviation of 7.2% (pSIA5) is dried on a microscope slide. These colloids have the highest polydispersity determined for our series of experiments. The dried film is imaged with a 100 \times oil-immersion objective with bright field microscopy, the image is shown in Figure 2.2a. A hexagonally packed film of the colloids is visible; this highlights, that even the least monodisperse sample we produced, is still monodisperse enough to allow the formation of extended crystalline structures. Higher magnification images are captured with SEM of particles deposited on silicon wafers and sputtered with a thin gold layer. These SEM images are taken at 3300magnification for polystyrene (pSIA35) and pMMA (pMMAIA25) colloids and are shown in Figures 2.2b,c, respectively. Also in these images, hexagonally packed areas are present; moreover, at this magnification, the surface of the colloids appears smooth.

Under appropriate conditions, colloidal particles can assemble into 2D and 3D microstructures. To quantify the structure of these materials, 3D confocal scanning microscopy is often used; however, this requires that the particles are fluorescently labeled, to allow for fluorescence detection, and that the refractive index of the colloids is matched to that of the suspending fluid, to eliminate diffusive scattering that inhibits acquisition of high quality images.

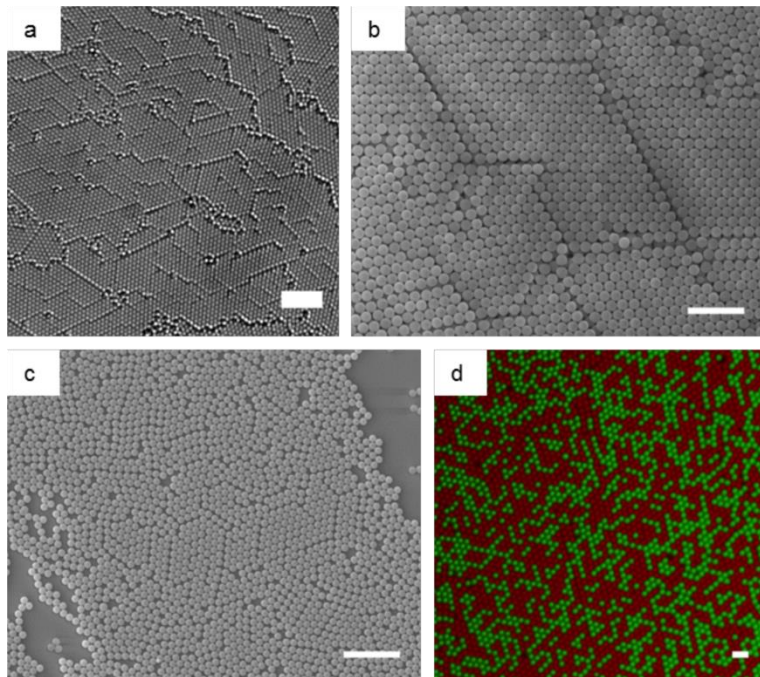


Figure 2.2: Microscopy images of different colloids synthesized, a) 100 \times bright field microscopy image of a dried film of pSIA5 colloids, b) 3300 \times SEM image of pSIA35 colloids, c) 3300 \times SEM image of pMMAIA25 colloids, d) 100 \times confocal microscopy image of a dried film of mixed pSIA35-546/605. Scale bars 5 μm .

We synthesized polystyrene, pMMA and pTFEMA colloids with the fluorescent dyes pyrromethene 546 and pyrromethene 605. These dyes easily dissolve in the monomers used and do not affect the synthesis. The polystyrene colloids pSIA35546 and pSIA35605 are synthesized according to the same reaction recipe, but with different fluorescent dyes. The diameters determined by SLS are 1336 nm for pSIA35-546 and 1361 nm for pSIA35-605, which is less than 2% variance in diameter. A dried film of mixed pSIA35-546 and pSIA35-605 is made on a microscopy slide and imaged with confocal microscopy. Cocrystallization of the two types of colloids is clearly visible in Figure 2.2d and demonstrates the reproducibility of our synthetic approach.



Figure 2.3: pTFEMA colloids refractive index matched in a solvent of 50 vol% DMSO/water. a) pTFEMAIA5-546 (yellow) and pTFEMAIA5-605 (pink) colloids dispersed in water and in 50 vol% DMSO/water, b) 100 \times confocal microscopy image of colloidal crystal of pTFEMAIA5-546 in 50 vol% DMSO/water, taken from a z-stack of images at a depth of 20 μm . Scale bar 5 μm .

pTFEMA colloids have a refractive index of ≈ 1.42 , which is the lowest refractive index of the colloids synthesized for this study. Dispersed in 50 vol% DMSO/water, the pTFEMA colloids are refractive index matched leading to transparent solutions in which scattering is minimized. This is illustrated in Figure 2.3a. To further highlight that our method allows the synthesis of index-matched particles in aqueous solutions, we form a colloidal crystal through sedimentation of a suspension of pTFEMAIA5-546 colloids suspended in a 50 vol% DMSO/water mixture. A three-dimensional image stack with a depth of 47 μm is made, using a confocal microscope. Figure 2.3b shows an image of the crystal structure from the z-stack at a depth of 20 μm . This illustrates that index-matching allows deep penetration of the confocal imaging system without significant loss of image quality.

Table 2.6: ζ potentials of surface modified latex colloids.

ζ potential (mV)	
PEG+	2.4
PEG-	-39.5
CD+	5.9
CD-	-39.1

The colloidal crystal shown in Figure 2.3b, is an example of the undirected assembly of monodisperse particles. However, colloids can also be directed in their assembly process, through the aid of functional groups at the surface of the colloids. For example, carboxylic acids can be coupled to amines, via

an amidation reaction, mediated by EDC/sulfo-NHS. We use this amidation reaction, to show that the colloids prepared here are suitable for surface modification. Mono-amine functionalized polyethylene glycol of MW 5000 (PEG+) and a heptaamine-functionalized cyclodextrin (CD+) are coupled to the surface of polystyrene colloids (pSIA35). Successful coupling will neutralize the surface charge on the colloids, which we determine by measurement of the ζ potential. As a negative control, these reactions are also performed without EDC/sulfo-NHS (PEG- and CD-). The results of these coupling reactions are given in Table 2.6, which shows that the EDC/sulfo-NHS coupling increases the ζ potential of the colloids to values around 0 mV. The ζ potential of the negative controls is maintained at ≈ -40 mV. This demonstrates a successful and nearly full conversion of the carboxylic groups at the surface of the colloid.

2.4 Conclusion

In this chapter, we present a facile method for the synthesis in water of monodisperse micron-sized colloids with highly carboxylated surfaces. The method is based on a SFEP and applied to different monomers. We successfully synthesize colloids of polystyrene, pMMA, and pTFEMA with diameters over 1 μm in a single step synthesis. The method allows for control over the colloid size via monomer-to-water ratio while retaining excellent monodispersity, well within the limits for applications such as artificial opals. The colloidal surface is highly carboxylated, due to the use of itaconic acid as comonomer, making the colloids highly stable and suitable for surface modifications. Moreover, a fluorescent dye can be easily incorporated, and through the use of fluorinated monomers, resulting in low refractive index polymers, they can be refractive index matched in an aqueous solvent.

References

- [1] F. Li, D. P. Josephson and A. Stein, *Colloidal Assembly: The Road from Particles to Colloidal Molecules and Crystals*, Angewandte Chemie International Edition, **50** (2011), 360-388.
- [2] M. Egen and R. Zentel, *Surfactant-Free Emulsion Polymerization of Various Methacrylates: Towards Monodisperse Colloids for Polymer Opals*, Macromolecular Chemistry and Physics, **205** (2004), 1479-1488.
- [3] G. von Freymann, V. Kitaev, B. V. Lotsch and G. A. Ozin, *Bottom-up assembly of photonic crystals*, Chem. Soc. Rev., **42** (2013), 2528-2554.
- [4] A. Stein, B. E. Wilson and S. G. Rudisill, *Design and functionality of colloidal-crystal-templated materials-chemical applications of inverse opals*, Chem. Soc. Rev., **42**(2013):2763-2803.
- [5] B. Lange, F. Fleischhaker and R. Zentel, *Chemical Approach to Functional Artificial Opals*, Macromolecular Rapid Communications, **28** (2007), 1291-1311.
- [6] D. G. Grier, *A revolution in optical manipulation*, Nature, **424** (2003), 810-816.
- [7] S. R. Yeh, M. Seul and B. I. Shraiman, *Assembly of ordered colloidal aggregates by electricfield-induced fluid flow*, Nature, **386** (1997), 57-59.
- [8] T. Ding, K. Song, K. Clays and C. H. Tung, *Fabrication of 3D Photonic Crystals of Ellipsoids: Convective Self-Assembly in Magnetic Field*, Advanced Materials, **21** (2009), 1936-1940.
- [9] P. L. Biancaniello, A. J. Kim and J. C. Crocker, *Colloidal Interactions and Self-Assembly Using DNA Hybridization*, Phys. Rev. Lett., **94** (2005), 58302.
- [10] T. B. Norsten, B. L. Frankamp and V. M. Rotello, *Metal Directed Assembly of Terpyridine-Functionalized Gold Nanoparticles*, Nano Letters, **2** (2002), 1345-1348.
- [11] L. M. Demers, S. J. Park, T. A. Taton, Z. Li and C. A. Mirkin, *Orthogonal Assembly of Nanoparticle Building Blocks on Dip-Pen Nanolithographically Generated Templates of DNA*, Angewandte Chemie International Edition, **40** (2001), 3071-3073.

- [12] J. C. Crocker and B. D. Hoffman, *Multiple Particle Tracking and Two Point Microrheology in Cells*, Methods in Cell Biology, **83** (2007), 141-178.
- [13] J. C. Crocker, M. T. Valentine, E. R. Weeks, T. Gisler, P. D. Kaplan, A. G. Yodh and D. A. Weitz, *Two-Point Microrheology of Inhomogeneous Soft Materials*, Phys. Rev. Lett., **85** (2000), 888-891.
- [14] D. Genovese and J. Sprakel, *Crystallization and intermittent dynamics in constricted microfluidic flows of dense suspensions*, Soft Matter, **7** (2011), 3889-3896.
- [15] J. W. Goodwin, R. H. Ottewill and R. Pelton, *Studies on the preparation and characterization of monodisperse polystyrene lattices V: The preparation of cationic lattices*, Colloid and Polymer Science, **257** (1979), 61-69.
- [16] J. W. Goodwin, R. H. Ottewill, R. Pelton, G. Vianello and D. E. Yates, *Control of particle size in the formation of polymer lattices*, British Polymer Journal, **10** (1978), 173-180.
- [17] J.Th.G. Overbeek. *Recent developments in the understanding of colloid stability*, Journal of Colloid and Interface Science, **58** (1977), 408-422.
- [18] D. Bartczak and A. G. Kanaras, *Preparation of Peptide-Functionalized Gold Nanoparticles Using One Pot EDC/Sulfo-NHS Coupling*, Langmuir, **27** (2011), 10119-10123.
- [19] F. Thielbeer, K. Donaldson and M. Bradley, *Zeta Potential Mediated Reaction Monitoring on Nano and Microparticles*, Bioconjugate Chemistry, **22** (2011), 144-150.
- [20] D. Bastos-Gonzalez, J. L. Ortega-Vinuesa, D. E. F. J. Lasnieves and R. Hidalgo-Alvarez, *Carboxylated Latexes for Covalent Coupling Antibodies, I*. Journal of Colloid and Interface Science, **176** (1995), 232-239.
- [21] G. W. Ceska, *The effect of carboxylic monomers on surfactant-free emulsion copolymerization*, Journal of Applied Polymer Science, **18** (1974), 427-437.
- [22] G. W. Ceska, *Carboxyl-stabilized emulsion polymers*, Journal of Applied Polymer Science, **18** (1974), 2493-2499.
- [23] P. H. Wang and C.Y. Pan, *Emulsion copolymerization of styrene with acrylic or methacrylic acids distribution of the carboxylic group*, Colloid and Polymer Science, **279** (2001), 98-103.

- [24] M. Slawinski, J. Meuldijk, A. M. Van Herk and A. L. German, *Seeded emulsion polymerization of styrene: Incorporation of acrylic acid in latex products*, Journal of Applied Polymer Science, **78** (2000), 875-885.
- [25] S. Song, W. Zhang, Z. Hu and Z. Zhang, *Monodisperse micrometer-size carboxyl-functionalized polystyrene particles obtained by two-stage radiation-induced dispersion polymerization*, Colloids and Surfaces A: Physicochemical and Engineering Aspects, **348** (2009), 1-8.
- [26] C. E. Reese and S. A. Asher, *Emulsifier-Free Emulsion Polymerization Produces Highly Charged, Monodisperse Particles for Near Infrared Photonic Crystals*, Journal of Colloid and Interface Science, **248** (2002), 41-46.

Chapter 3

Conjugated Polymer Shells on Colloidal Templates by Seeded Suzuki-Miyaura Dispersion Polymerization

The self-assembly of colloidal conjugated polymers presents a versatile and powerful route towards new functional optoelectronic materials and devices. However, this strategy relies on the existence of chemical protocols to prepare highly monodisperse colloids of conjugated polymers in high yields. Here, a recently developed Suzuki-Miyaura dispersion polymerization method is adopted to synthesize core-shell particles, in which a conjugated polymer shell is grown onto non-conjugated organic and inorganic colloidal templates. By chemically anchoring aryl halide groups at the particle surface, a conjugated polymer shell can be attached to a wide variety of organic and inorganic microparticles. In this way, both spherical and non-spherical hybrid conjugated polymer particles are prepared, and it is shown that the method can be applied to a variety of conjugated polymers. This new method offers independent control of the size, shape and photophysical properties of these novel conjugated polymer particles.

This chapter was published as:

Jan Bart ten Hove, Jeroen Appel, Johanna M. van den Broek, Alexander J. C. Kuehne and Joris Sprakel, *Conjugated Polymer Shells on Colloidal Templates by Seeded Suzuki-Miyaura Dispersion Polymerization*, *Small*, **10** (2014), 957-963.

3.1 Introduction

Conjugated polymers present a viable alternative to inorganic materials for photonic applications. The materials are generally non-toxic and processable from solution; this opens up a wide field of applications, ranging from biological markers and probes^[1-5] to photonic structures.^[6,7] Much of the research in this field is dedicated to the tuning of the optical properties of conjugated polymers through manipulation of the electronic structure on the molecular scale^[8, 9] and fine-tuning of component architectures on the device scale.^[9,10] Surprisingly, control of the material properties on the mesoscale, where we find the colloidal domain, remains relatively unexplored. A few recent examples employ top-down and templating techniques to obtain colloidal conjugated polymeric materials. Reprecipitation of a conjugated polymer solution into a non-solvent as well as polymerization within miniemulsion droplets both lead to finely dispersed conjugated polymer particles; yet, both techniques yield polydisperse particles, limiting their usefulness for a variety of photonic applications.^[11-17] Furthermore, complex architectures such as core-shell and Janus particles cannot be produced due to insufficient control during synthesis so that the resulting particles lack definition.^[18] However, when bottom-up self-assembly strategies are employed, new structure and functionality can be achieved in conjugated polymer materials and well-defined macromolecular and colloidal building blocks can be obtained. The self-assembly toolbox developed in soft matter science can be put to work, to either facilitate the creation of new functionalities by molecular self-assembly that are not achievable through traditional approaches or to allow the fabrication of polymer photonics by colloidal self-assembly.

Monodisperse particles of conjugated polymers can be templated in monodisperse emulsion droplets produced by microfluidics, yet often only in relatively low yields compared to bulk synthesis methods.^[19,20] Recently, a new strategy to directly synthesize monodisperse conjugated polymer nanoparticles by adopting Suzuki-Miyaura cross-coupling to a dispersion polymerization protocol was presented.^[21] This versatile method allows the direct synthesis of monodisperse spherical particles in a size range of approximately 100-1000 nm, of a variety of light-emitting polymers. Post-processing also allows the fabrication of ellipsoidal particles through melt-

stretching of the spherical colloids from the Suzuki-Miyaura dispersion polymerization.

In this chapter we develop a method for a seeded Suzuki-Miyaura dispersion polymerization to fabricate core-shell particles in which a core particle can be decorated with a conjugated polymer shell, after appropriate surface functionalization. This allows the direct synthesis of a conjugated polymer shell on both spherical and anisometric organic and inorganic particles. The absorption and emission characteristics can be tuned through the choice of conjugated monomers. Our results open the way for the direct synthesis of a new class of highly monodisperse conjugated colloidal building blocks in high yield.

3.2 Experimental Section

3.2.1 Preparation of Colloids

Silica Microparticles: Commercially available silica particles of $1.2 \mu\text{m}$ ($\text{\AA}ngstr\"om$ -Sphere) and $3.9 \mu\text{m}$ (Bangs Laboratories) in diameter were dispersed in ethanol by overnight sonication and mechanical stirring. To prepare these silica particles for use as seeds in a Suzuki dispersion polymerization the following procedure was applied: to the dispersion trimethoxy-(octyl)silane (TMOS, 0.75 mL) and (3-aminopropyl)-triethoxysilane (APTES, 0.25 mL) were added after which the reaction was incubated for 2 hours. The aminated particles were then cleaned through repeated centrifugation and resuspension in dichloromethane (DCM). Finally, we functionalised the particles through reacting bromobenzoic acid, which can partake in the Suzuki polymerization, with the amine groups at the surface; N,N' -dicyclohexylcarbodiimide (DCC, 70 mg), 4-Dimethylaminopyridine (DMAP, 15 mg) and 4-bromobenzoic acid (50 mg) were added to the amine-functionalized particles in DCM. After incubating for 2 hours, the particles were repeatedly washed in DCM, followed by resuspension in propanol. XPS measured a surface composition of 46.6% of octyl chains, 43.8% of amine groups and 9.6% of bromobenzene groups, which suggests a yield of 19% in the DCC-mediated coupling of bromobenzoic acid.

Hematite Microcubes: Hematite (Fe_2O_3) cubes were synthesized following a standard protocol^[22,23]. An aqueous 6.0 M NaOH stock solution (360 mL) was added drop-wise to a stirred solution of 2.0 M FeCl_3 (400 mL) over a period of 30 minutes. Upon completion of addition, water (40 mL) was added and stirring was continued for 10 minutes. The mixture was then aged in a convection oven for at least 7 days at 100 °C in absence of any stirring. This resulted in particles with a diameter of approximately 1.2 μm . The particles were cleaned by repeated washing in water and ethanol. Functionalization of the surface with bromobenzoic acid groups was performed in the same way as for the silica microparticles. XPS measured 17.1% octyl chains, 64.0% amine groups and 18.9% bromobenzene groups at the particle surface; this indicates a yield of 23% for the DCC-mediated coupling of bromobenzoic acid.

Poly(styrene-co-bromostyrene) Microparticles: Polystyrene microparticles, with bromostyrene groups at the surface, were prepared through a classical dispersion copolymerization: to a 250 mL roundbottom flask was added poly(vinylpyrrolidone) (PVP, 4.5 g), styrene (12.5 g), 4-bromostyrene (500 L) and 1-propanol (125 g). After degassing by bubbling N_2 , the reaction mixture was heated to 70 °C. The polymerization was initiated by injecting a solution of azobisisobutyronitrile (AIBN, 125 mg) dissolved in styrene (1 mL); the reaction was left to complete for 24 h. The resulting particles, with a diameter of 1.6 μm , were cleaned through repeated centrifugation and resuspension in 1-propanol.

Seeded SuzukiMiyaura Dispersion Polymerization: For the growth of a conjugated polymer shell around the seed particles described above, we adopt the procedure outlined in reference 21. A typical reaction proceeds as follows: a 50 mL three-necked roundbottom flask was charged with a solution (6.6 mL) containing 100 g/L poly(vinylpyrrolidone) and 20 g/L Triton X-45 surfactant in 1-propanol, functionalized core particles (100 mg) pre-suspended in 1-propanol (3 mL). A stock solution containing equimolar amounts of monomers functionalised with either two terminal bromines or two boronic acid pinacol ester moieties, at a total concentration of 1.2×10^{-2} M of monomer, is added to the reaction (1 mL). The reaction vessel was placed in an oil bath at 65 °C and a tip sonicator was inserted through a rubber septum; low-power sonication was maintained throughout the reaction. The reaction mixture was degassed for 15 min by bubbling N_2 after which the catalyst tetrakis(triphenylphosphine) palladium(0) (2 mg) was

added. After addition of the palladium catalyst, the reaction mixture was continuously purged with N₂. The reaction was initiated by injecting a 5 g/L solution of potassium tert-butoxide in 1-propanol (1.5 mL). The reaction was stopped after 3 hours by removing the reaction vessel from the oil bath and exposure to oxygen. The particles were washed at least three times by centrifugation in ethanol.

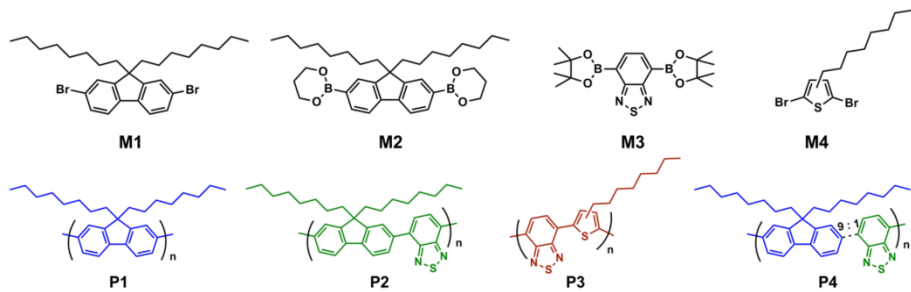


Figure 3.1: Chemical structures of the monomers 9,9-dioctyl-2,7-dibromo fluorene (**M1**), 9,9-dioctylfluorene-2,7-diboronic acid bis(1,3-propanediol) ester (**M2**), 2,1,3-benzothiadiazole-4,7-bis(boronic acid pinacol ester) (**M3**), 2,5-dibromo-3-octyl thiophene (**M4**) and the polymers (**P1-4**).

In this chapter, we grow shells of 4 different conjugated polymers, which are illustrated in Figure 3.1: **P1**) poly(dioctylfluorene), formed by reacting equimolar amounts of 9,9-dioctyl-2,7-dibromofluorene (**M1**) and 9,9-dioctylfluorene-2,7-diboronic acid bis(1,3-propanediol) ester (**M2**), **P2**) poly(dioctylfluorene-alt-benzothiadiazole), through reacting equimolar amounts of **M1** and 2,1,3-benzothiadiazole-4,7-bis(boronic acid pinacol ester) (**M3**), **P3**) poly(benzothiadiazole-alt-octyl thiophene) through reaction of equimolar amounts of **M3** and 2,5-dibromo-3-octyl thiophene (**M4**) and **P4**) poly(dioctylfluorenecoenzothiadiazole) by reacting 3 parts **M1**, 2 parts **M2** and 1 part **M3**.

3.2.2 Characterization

X-ray photoelectron spectroscopy (XPS) was performed on a JEOL JPS-9200 system, with an energy resolution of <0.65 eV.

Absorption spectra were recorded on a Hitachi U-300 spectrometer on particles suspended in a mixture of water and DMSO to minimize the effects of diffuse scattering.

Confocal microscopy images were recorded on a Zeiss Axiovert 200M microscope with a Zeiss LSM5 exciter module through illumination at $\lambda = 450$ nm and detection at $\lambda > 470$ nm.

Scanning electron microscopy (SEM) images are recorded on a JAMP-9500F field emission Auger microprobe in secondary electron imaging mode; samples were prepared by deposition from suspension onto a cleaned silicon wafer. A crystal of the core-shell particles was formed by sedimentation of a suspension of core-shell particles in a glass capillary; after sedimentation and drying, the capillary was broken in half to image the formed crystal.

3.3 Results and Discussion

The Pd-catalyzed Suzuki-Miyaura polycondensation reaction is typically applied in a good solvent for monomers, catalyst and resulting polymer. However, to create colloidal particles during the polycondensation reaction, the solvent should be selective for the monomers, catalyst and short conjugated oligomers and a non-solvent for higher molecular weight polymer; 1-propanol satisfies these requirements. Equal amounts of conjugated dibromo and diboronic acid ester functionalized monomers are polymerized using a classical Suzuki-Miyaura catalyst ($\text{PPh}_3)_4\text{Pd}(0)$ and potassium *tert*-butoxide as base. Once the growing conjugated polymer chains reach a critical chain length, they precipitate from solution to form colloidal particles.

For the polymers we use here, i.e., poly(dioctylfluorene) (**P1**), poly(dioctylfluorene-alt-benzothiadiazole) (**P2**), poly(benzothiadiazole-alt-octyl thiophene) (**P3**) and poly(dioctylfluoreneco-benzothiadiazole) (**P4**) these critical molecular weights are around 10-15 kDa.^[21] To prevent aggregation of the precipitating nuclei and growing particles, poly(vinylpyrrolidone-co-vinylacetate) and Triton X-45 are applied as stabilizers as described previously.^[21]

To successfully accomplish a seeded dispersion polymerization, in which individual core particles are coated by a homogeneous and monodisperse shell, it is necessary that chains that become insoluble in the solvent preferentially precipitate onto the seed particles that are present in the reaction mixture.^[24] If the interactions between the surface of the seeds

and the polymer chain are carefully tuned, the heterogeneous condensation of a polymer shell onto a seed particle should be thermodynamically favorable over the homogeneous nucleation of a new colloid in the solution. Addition of non-functional silica seed particles to a Suzuki-Miyaura dispersion polymerization before the nucleation of conjugated polymer particles, results in a poorly controlled reaction. The polymerization product consists of highly aggregated core particles bridged by conjugated polymer, which forms during the polymerization. An example is shown in Figure 3.2a.

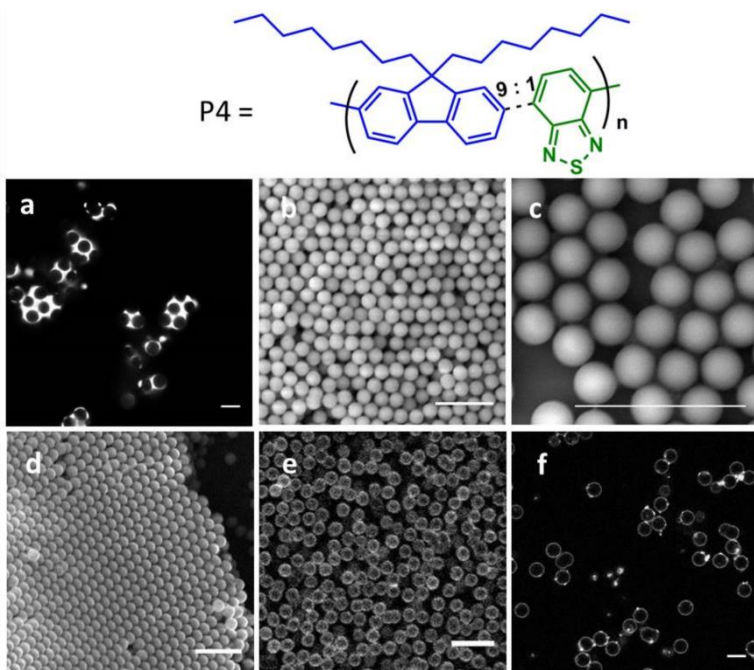


Figure 3.2: top: illustration of the polymer **P4**, a) confocal image of the product when non-functionalized 4 micron silica particles are used as seeds in a Suzuki-Miyaura dispersion polymerization of **P4**, b) SEM image of 1.2 micron silica seed particles, c) same particles after surface functionalization and coating with conjugated polymer **P4**, d) photonic crystal assembled from these core-shell particles and their confocal microscopy image in e), f) confocal microscopy image of 4 micron silica-conjugated polymer shell particles. Scale bars are 5 μm .

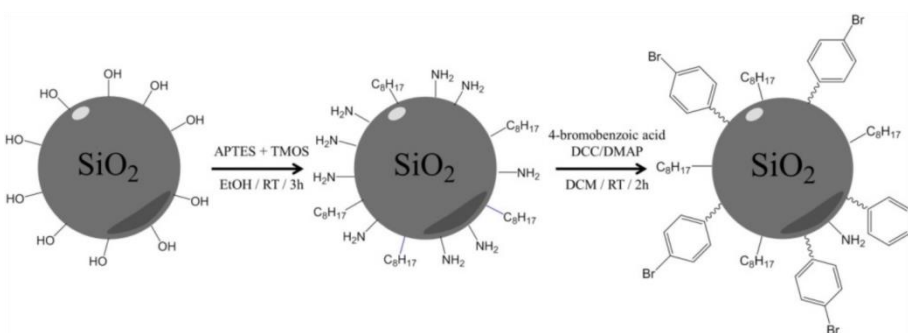


Figure 3.3: Schematic illustration of the two-step surface modification strategy to express aryl halide functionality at the surface of silica seed particles.

To ensure anchoring of the growing polymer and condensation of the polymer chains onto the particle surface, we functionalize the seed particles with aryl halide groups, which partake in the polycondensation reaction. This functionalization is accomplished in a two-step approach, as illustrated in Figure 3.3. First, the surface of the silica particles is functionalized using a mixture of an octyl- and aminefunctional silane; the alkyl residues ensure colloidal stability against aggregation during the functionalization and early stages of the dispersion polymerizations. In absence of these stabilizing octyl groups we find that the amine-functionalized particles aggregate rapidly and irreversibly. In a subsequent step, the primary amines at the particle surface are coupled to 4-bromobenzoic acid, using Steglich active-ester conditions to provide aryl halide functionality at the particle surface. The efficiency of this approach is verified through elemental surface analysis using XPS. We find that the particle surface is composed of 46.6% of octyl chains, 43.8% of unreacted amine groups and 9.6% of bromobenzene groups, after successful modification. This confirms a yield of approximately 20% in the coupling of bromobenzoic acid to the surface amines.

The seeded dispersion polymerization, in which bromobenzene functionalized silica seed particles of $1.2 \mu\text{m}$ in diameter are used, proceeds in a very controlled manner. Through the use of monodisperse seed particles, as shown in Figure 2b, we obtain monodisperse core-shell particles as shown in Figure 2c. The monodispersity of these core-(conjugated-shell) particles is verified by light scattering experiments before and after the seeded Suzuki-Mizyaura dispersion polymerization; no measurable change in monodispersity was found within the accuracy of the measurements. This is

furthermore highlighted by the facile assembly of the particles into large crystalline structures, as illustrated in Figure 2d. Moreover, the shell, composed of polymer **P4**, can be easily visualized using confocal microscopy, in which the fluorescent shell is distinctly visible around a dark, unlabeled core particle (Figure 2e). The same approach is also successfully applied to much larger particles; conjugated polymer shells were also grown around 4 μm functionalized silica particles, as shown in Figure 2f.

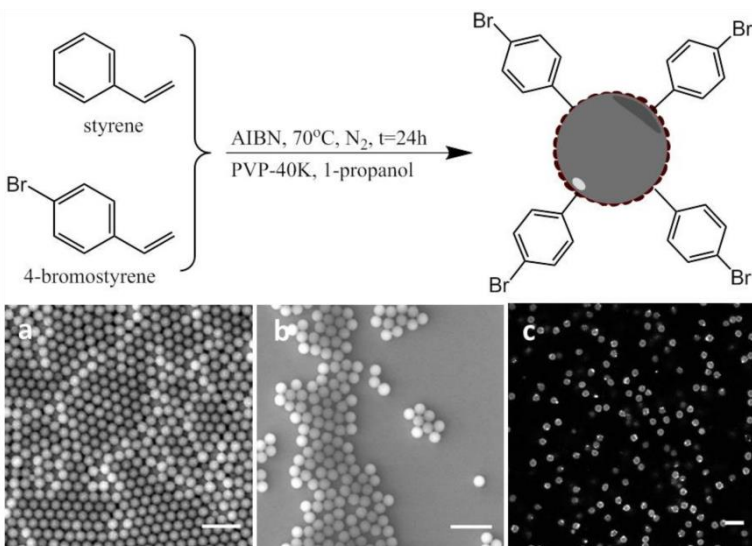


Figure 3.4: Top: schematic illustration of the formation of poly(styrene-co-bromostyrene) particles in a free-radical dispersion polymerisation. Bottom: SEM images of poly(styrene-co-bromostyrene) microparticles before (a) and after (b) **P4** shell growth, c) confocal image of the core-shell particles. Scale bars are 5 μm .

To highlight the versatility of this method, we also apply organic particles as seeds in the Suzuki-Miyaura dispersion polymerization. Here the presence of aryl halides at the particle surface is also desired to ensure good anchoring of the conjugated polymers to the seed particles. We prepare these latex particles through dispersion copolymerization of styrene and bromostyrene^[25], as illustrated in Figure 3.4; this results in highly monodisperse polymer colloids, with a diameter of 1.6 μm , with bromobenzene groups residing at the surface (Figure 3.4a). In addition, these particles can be decorated with a conjugated polymer shell, in this case polymer **P4**, while retaining their monodispersity, as confirmed by electron-

and confocal microscopy in Figure 3.4b,c. Previously, we have only been able to obtain monodisperse particles from binary monomer systems. This has been attributed to different reactivities and reaction rates of the monomers, which would lead to deviant chain-growth and hence polydispersity. However, here we are able to retain monodispersity while extending the polymer to a ternary system with only 10% of benzothiadiazole units distributed in a polyfluorene backbone. This showcases the precise controllability of this type of dispersion polymerization.

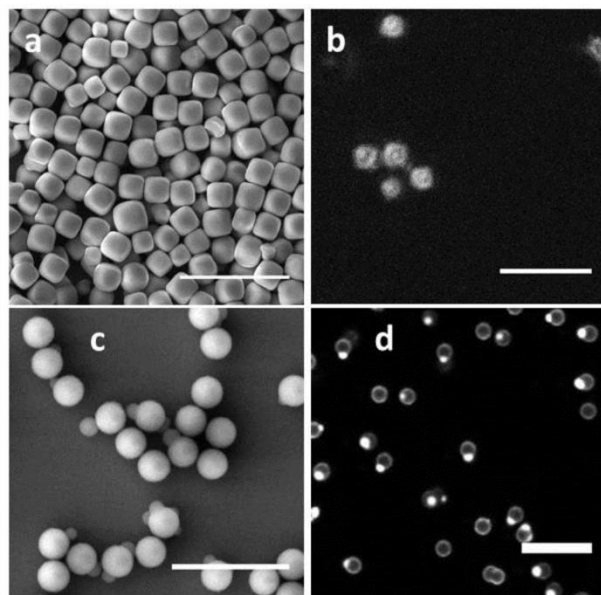


Figure 3.5: a) SEM image of hematite cubes used as seed particles and b) confocal image of hematite core-**P4** shell particles, SEM (c) and confocal (d) images of the anisometric particles that result from a seeded dispersion polymerization of **P4** with a total monomer concentration of 48 mM and 1.2 micron silica seed particles. Scale bars are 5 μm .

A variety of strategies is available to generate photonic structures from spherical particles by self-assembly^[26-28]; however, with spherical particles only close-packed structures with hexagonal symmetries can be formed. In return, this leads to limitations in the tuneability and variability of the photonic bandgap and optical material properties. A much wider variety of crystal structures can be formed from anisometric, e.g., cuboidal or

ellipsoidal particles, which has pronounced effects on their scattering and photonic properties.^[29, 30] Ellipsoidal particles of conjugated polymers can be made by melt-stretching of spherical conjugated polymer particles; by this however, ellipsoidal colloids can only be produced in low yields.^[21, 31] We therefore explore the application of anisometric seed particles to efficiently obtain nonspherical core-conjugated shell particles. Hematite is a form of iron oxide and represents an interesting template for this purpose as it can be made, in large quantities, in a wide variety of shapes such as rounded cylinders, peanuts and quasi-cubes.^[22] We prepare hematite quasi-cubes, through an established sol-gel method^[22,23], resulting in narrowly dispersed cubic colloidal particles, with distinctly rounded corners, and a diameter of approximately 1.2 μm as shown in Figure 3.5a. Also the iron oxide surface of these hematite particles can be functionalized following the protocol described for the silica particles; for these hematite cubes we found a surface composed of 17.1% octyl chains, 64.0% unreacted amines and 18.9% bromobenzene groups. Upon growing a conjugated polymer shell we obtain cubic conjugated polymer colloids with monodisperse shell thicknesses, as shown in Figure 3.5b.

Surprisingly, we found another strategy to produce particles with a nonspherical shape. While at low monomer concentrations, chain growth is sufficiently slow to ensure the majority of formed and precipitating chains to collapse onto the seed particles, at higher monomer concentrations, chains grow so rapidly that secondary nuclei appear to form in the reaction mixture. Interestingly, we see that these secondary nuclei merge and anchor onto the seed particles, which results in particles with distinct, and highly fluorescent, protrusions as shown by electron- and confocal microscopy in Figure 3.5c,d. Recently, these types of anisometric particles have received significant attention due to their ability to mimic molecular interactions.^[32-35] Purity of these types of particles could in principle be improved by separating particles with different numbers of protrusions through sucrose-gradient centrifugation or field-flow fractionation.

Depending on the application of interest, the optoelectronic properties of the polymer shells must be tuned to meet the specific need in question. To demonstrate that our method is flexible, and allows the growth of a variety of conjugated polymer shells, we tune the absorption and luminescence of our particles, through changes in the monomer composition. This allows us to grow blue-emitting shells of poly(diocetylfluorene) (**P1**),

green-emitting shells of poly(dioctylfluorene-alt-benzothiadiazole) (**P2**) and red-emitting shells of poly(benzothiadiazole-co-octyl thiophene) (**P3**), as shown in Figure 3.6. We note that the spectra are independent of the presence of a seed particle, and correspond to those of homogeneous films of the conjugated polymers, as also observed for homogeneous conjugated polymer particles.^[21] Within the same approach of a well-controlled seeded Suzuki-Miyaura dispersion polymerization, we demonstrate control and independent tuneability of the size, shape and photophysical properties of these novel conjugated polymer particles.

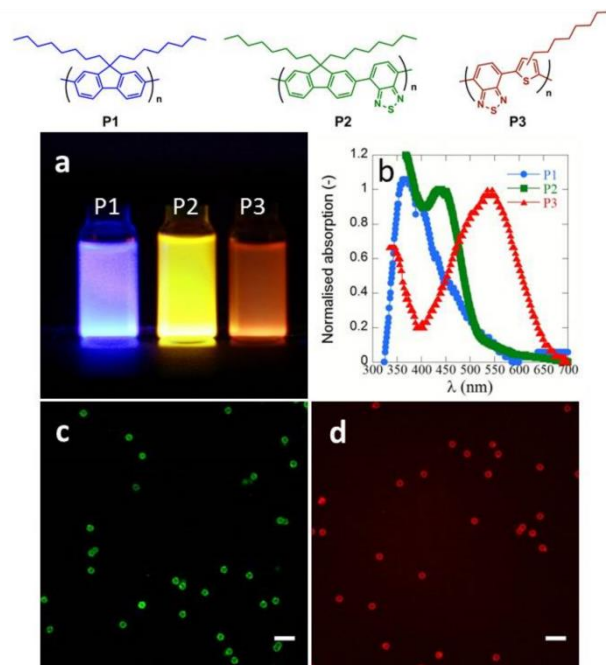


Figure 3.6: Tuning absorption and emission of the polymer shell: top: structures of polymers **P1-P3** a) Photograph showing the luminescence of $1.2\ \mu\text{m}$ silica core-conjugated polymer shell particles with **P1**, **P2** and **P3** conjugated polymers, b) Corresponding absorption spectra of the dispersed core-shell particles, and corresponding confocal microscopy images of $1.2\ \mu\text{m}$ silica core-**P2** (c) and -**P3** (d) shell particles.

3.4 Conclusion

In this chapter we present a strategy for the synthesis of conjugated polymer shells on colloidal templates. After appropriate surface modification of the colloidal seeds, either inorganic, such as silica or hematite, or organic, such as polystyrene microspheres, a variety of conjugated polymer shells are grown in a single step while retaining the monodispersity of the original particles. Even non-spherical particles can be produced, either through the use of non-spherical templates, such as hematite quasi-cubes, or through merging of secondary nuclei in the reaction mixture with the conjugated shell. In this way, a wide new range of colloidal conjugated building blocks can be created for the fabrication of polymeric optoelectronic materials.

References

- [1] S. Kim, C. K. Lim, J. Na, Y.D. Lee, K. Kim, K. Choi, J. F. Leary and I. C. Kwon, *Conjugated polymer nanoparticles for biomedical in vivo imaging*, Chem. Commun., **46** (2010), 1617-1619.
- [2] C. Wu, B. Bull, K. Christensen and J. McNeill, *Ratiometric Single-Nanoparticle Oxygen Sensors for Biological Imaging*, Angewandte Chemie International Edition, **48** (2009), 2741-2745.
- [3] C. Wu, B. Bull, C. Szymanski, K. Christensen and J. McNeill, *Multicolor Conjugated Polymer Dots for Biological Fluorescence Imaging*, ACS Nano, **2** (2008), 2415-2423.
- [4] J. Yu, C. Wu, S. P. Sahu, L. P. Fernando, C. Szymanski and J. McNeill. *Nanoscale 3D Tracking with Conjugated Polymer Nanoparticles*, Journal of the American Chemical Society, **131** (2009), 18410-18414.
- [5] X. Zhang, J. Yu, C. Wu, Y. Jin, Y. Rong, F. Ye and D. T. Chiu, *Importance of Having Low-Density Functional Groups for Generating High-Performance Semiconducting Polymer Dots*, ACS Nano, **6** (2012), 5429-5439.
- [6] I. D. W. Samuel and G. A. Turnbull, *Organic Semiconductor Lasers*, Chemical Reviews, **107** (2007), 1272-1295.
- [7] Y. Yang, G. A. Turnbull and I. D. W. Samuel, *Hybrid optoelectronics: A polymer laser pumped by a nitride light-emitting diode*, Applied Physics Letters, **92** (2008), 163306.
- [8] A. Bianco, S. Perissinotto, M. Garbugli, G. Lanzani and C. Bertarelli, *Control of optical properties through photochromism: a promising approach to photonics*, Laser & Photonics Reviews, **5** (2011), 711-736.
- [9] Y. Tokoro, H. Yeo, K. Tanaka and Y. Chujo, *Synthesis and tuning of optical properties of conjugated polymers involving benzo[h]quinoline-based neutral pentacoordinate organosilicon complexes in the main chain*, Polym. Chem., **4** (2013), 5237-5242.

- [10] A. J. C. Kuehne, M. Kaiser, A. R. Mackintosh, B. H. Wallikewitz, D. Hertel, R. A. Pethrick and K. Meerholz, *Sub-Micrometer Patterning of Amorphous- and-Phase in a Crosslinkable Poly(9,9-dioctylfluorene): Dual-Wavelength Lasing from a Mixed-Morphology Device*, Advanced Functional Materials, **21** (2011), 2564-2570.
- [11] T. Adachi, L. Tong, J. Kuwabara, T. Kanbara, A. Saeki, S. Seki and Y. Yamamoto, *Spherical Assemblies from π -Conjugated Alternating Copolymers: Toward Optoelectronic Colloidal Crystals*, Journal of the American Chemical Society, **135** (2013), 870-876.
- [12] S. Grigalevicius, M. Forster, S. Ellinger, K. Landfester and U. Scherf, *Excitation Energy Transfer from Semi-Conducting Polymer Nanoparticles to Surface-Bound Fluorescent Dyes*, Macromolecular Rapid Communications, **27** (2006), 200-202.
- [13] T. Kietzke, D. Neher, K. Landfester, R. Montenegro, R. Günntner and U. Scherf, *Novel approaches to polymer blends based on polymer nanoparticles*, Nature Materials, **2** (2003), 408-412.
- [14] N. Kurokawa, H. Yoshikawa, N. Hirota, K. Hyodo and H. Masuhara, *Size-Dependent Spectroscopic Properties and Thermochromic Behavior in Poly(substituted thiophene) Nanoparticles*, ChemPhysChem, **5** (2004), 1609-1615.
- [15] K. Landfester, R. Montenegro, U. Scherf, R. Günntner, U. Asawapirom, S. Patil, D. Neher and T. Kietzke, *Semiconducting Polymer Nanospheres in Aqueous Dispersion Prepared by a Miniemulsion Process*, Advanced Materials, **14** (2002), 651-655.
- [16] T. Piok, S. Gamerith, C. Gadermaier, H. Plank, F. P. Wenzl, S. Patil, R. Montenegro, T. Kietzke, D. Neher, U. Scherf, K. Landfester and E. J. W. List, *Organic Light-Emitting Devices Fabricated from Semiconducting Nanospheres*, Advanced Materials, **15** (2003), 800-804.
- [17] F. Wang, M.Y. Han, K. Y. Mya, Y. Wang and Y. H. Lai, *Aggregation-Driven Growth of Size-Tunable Organic Nanoparticles Using Electronically Altered Conjugated Polymers*, Journal of the American Chemical Society, **127** (2005), 10350-10355.
- [18] C. Negele, J. Haase, A. Leitenstorfer and S. Mecking, *Polyfluorene Nanoparticles and Quantum Dot Hybrids via Miniemulsion Polymerization*, ACS Macro Letters, **1** (2012), 1343-1346.

- [19] W. C. Jeong, J. M. Lim, J. H. Choi, J. H. Kim, Y. J. Lee, S. H. Kim, G. Lee, J. D. Kim, G. R. Yi and S. M. Yang, *Controlled generation of submicron emulsion droplets via highly stable tip-streaming mode in microfluidic devices*, Lab Chip, **12** (2012), 1446-1453.
- [20] A. J. C. Kuehne and D. A. Weitz, *Highly monodisperse conjugated polymer particles synthesized with drop-based microfluidics*, Chem. Commun., **47** (2011), 12379-12381.
- [21] A. J. C. Kuehne, M. C. Gather and J. Sprakel, *Monodisperse conjugated polymer particles by Suzuki-Miyaura dispersion polymerization*, Nature Communications, **3** (2012).
- [22] T. Sugimoto, M. M. Khan, A. Muramatsu and H. Itoh, *Formation mechanism of monodisperse peanut-type- Fe_2O_3 particles from condensed ferric hydroxide gel*, Colloids and Surfaces A: Physicochemical and Engineering Aspects, **79** (1993), 233-247.
- [23] L. Rossi, S. Sacanna, W. T. M. Irvine, P. M. Chaikin, D. J. Pine and A. P. Philipse, *Cubic crystals from cubic colloids*, Soft Matter, **7** (2011), 4139-4142.
- [24] E. Bourgeat-Lami and J. Lang, *Encapsulation of Inorganic Particles by Dispersion Polymerization in Polar Media: 1. Silica Nanoparticles Encapsulated by Polystyrene*, Journal of Colloid and Interface Science, **197** (1998), 293-308.
- [25] K. P. Lok and C. K. Ober, *Particle size control in dispersion polymerization of polystyrene*, Canadian Journal of Chemistry, **63** (1985), 209-216.
- [26] P. Jiang, T. Prasad, M. J. McFarland and V. L. Colvin, *Two-dimensional nonclose-packed colloidal crystals formed by spincoating*, Applied Physics Letters, **89** (2006), 011908.
- [27] J. Vos and W. L. Wijnhoven, *Preparation of Photonic Crystals Made of Air Spheres in Titania*, Science, **281** (1998), 802-804.
- [28] Y. H. Ye, F. LeBlanc, A. Haché and V. V. Truong, *Self-assembling three-dimensional colloidal photonic crystal structure with high crystalline quality*, Applied Physics Letters, **78** (2001).
- [29] J. M. Meijer, F. Hagemans, L. Rossi, D. V. Byelov, S. I. R. Castillo, A. Snigirev, I. Snigireva, A. P. Philipse and A. V. Petukhov, *Self-Assembly of Colloidal Cubes via Vertical Deposition*, Langmuir, **28** (2012), 7631-7638.

- [30] E. Yablonovitch, T. J. Gmitter and K. M. Leung, *Photonic band structure: The face-centered-cubic case employing nonspherical atoms*, Phys. Rev. Lett., **67** (1991), 2295-2298.
- [31] C. C. Ho, A. Keller, J. A. Odell and R. H. Ottewill, *Preparation of monodisperse ellipsoidal polystyrene particles*, Colloid and Polymer Science, **271** (1993), 469-479.
- [32] D. J. Kraft, W. S. Vlug, C. M. van Kats, A. van Blaaderen, A. Imhof and W. K. Kegel, *Self-Assembly of Colloids with Liquid Protrusions*, Journal of the American Chemical Society, **131** (2009), 1182-1186.
- [33] Y. Wang, Y. Wang, D. R. Breed, V. N. Manoharan, L. Feng, A. D. Hollingsworth, M. Weck and D. J. Pine, *Colloids with valence and specific directional bonding*, Nature, **491** (2012), 51-55.
- [34] S. Sacanna, L. Rossi and D. J. Pine, *Magnetic Click Colloidal Assembly*, Journal of the American Chemical Society, **134** (2012), 6112-6115.
- [35] S. Sacanna, M. Korpics, K. Rodriguez, L. Colón-Meléndez, S. H. Kim, D. J. Pine and G. R. Yi, *Shaping colloids for self-assembly*, Nature Communications, **4** (2013).

Chapter 4

Temperature Controlled Sequential Gelation in Composite Microgel Suspensions

Depending on the volume fraction and interparticle interactions, colloidal suspensions can exhibit a variety of physical states, ranging from fluids, crystals, and glasses to gels. For microgel particles made of thermoresponsive polymers, both parameters can be tuned using environmental parameters such as temperature and ionic strength, making them excellent systems to experimentally study state transitions in colloidal suspensions. Using a simple two-step synthesis it is shown that the properties of composite microgels, with a fluorescent latex core and a responsive microgel shell, can be finely tuned. With this system the transitions between glass, liquid, and gel states for suspensions composed of a single species are explored. Finally, a suspension of two species of microgels with different transition temperatures, is demonstrated to gel in a sequential manner. Upon increasing temperature a distinct core-sheath structure is formed with a primary gel composed of the species with lowest transition temperature, which acts as a scaffold for the aggregation of the second species.

This chapter was published as:

Jeroen Appel, Niek de Lange, Hanne M. van der Kooij, Ties van de Laar, Jan Bart ten Hove, Thomas E. Kodger and Joris Sprakel: *Temperature Controlled Sequential Gelation in Composite Microgel Suspensions*, Particle and Particle Systems Characterization, **32** (2015), 764-770.

4.1 Introduction

Colloidal gels are kinetically arrested structures formed from aggregated colloidal particles. They find common use in a variety of consumer products, such as foods and cosmetics,^[1,2] to impart solid-like mechanical properties even at low solid fractions to otherwise liquid suspensions. While much effort has focused on the microscopic gel structure, the attractive interactions between the colloidal building blocks, and their relation to the mechanical properties of colloidal gels, establishing direct links remains challenging.^[3-12] This is caused to a large extent by the sensitivity of colloidal gels to their mechanical history. Colloidal gels are inherently nonequilibrium structures, which emerge due to diverging time scales during spinodal decomposition of a phase separating suspension.^[6] Any mechanical agitation of such a system causes irreversible changes to both microstructure and mechanical properties. Extensive preshear protocols can be utilized to liquefy colloidal gels, in attempts to create reproducible initial conditions for further experimentation, yet these will typically introduce strong anisotropy into the material.^[13] Ideally, gelation and liquefaction should be reversible and triggerable by means of an environmental parameter, such as temperature. We previously demonstrated that this is possible by using thermoresponsive polymers which exhibit a lower-critical solution temperature (LCST), in which the attractive forces that drive gelation can be turned on and off on demand.^[14]

Here, we explore the use of thermoresponsive microgel particles as a controllable system to study colloidal gelation. Microgel particles are crosslinked polymer gel particles of colloidal dimensions swollen with the liquid in which they are dispersed, making them compressible and deformable. The degree of swelling of the microgel is governed by a balance between internal osmotic pressure and elasticity due to crosslinks between the polymer chains. The osmotic pressure depends strongly on the solvent quality, and thus influences the equilibrium size of the microgel. For microgels composed of poly(N-isopropylacrylamide), or co-polymers thereof, the solvent quality is temperature dependent due to unfavorable hydrogen bonding between amide groups and the aqueous solvent at temperatures above the LCST. This allows, under specific conditions, tuning

of the interactions between the microgels from repulsive to attractive; providing the ability to switch between glass, liquid, and gel states.^[15]

In this chapter, we first explore the conditions that allow switching between the different physical states of glass, liquid, and gel in suspensions of a single microgel species. Subsequently, we demonstrate how mixing multiple microgel species with different transition temperatures allows for even more complex switching between physical states by an environmental trigger. In mixed suspensions, we observe sequential gelation, for which an initial gel is formed at the first transition temperature by one species of microgel. This gel then acts as a scaffold for the aggregation of the second species when its transition temperature is crossed. This is further evidenced by a stepwise increase of the elastic modulus at the two transition temperatures.

4.2 Experimental Section

4.2.1 Materials

Styrene, methyl methacrylate, 2,2,2-trifluoroethyl methacrylate, divinylbenzene, *N*-isopropylacrylamide, *N*-(hydroxymethyl)acrylamide, acrylamide, methacrylic acid, *N,N'*-methylenebis(acrylamide), 3-sulfopropyl methacrylate potassium salt, potassium persulfate, and sodium dodecyl sulfate were purchased from Sigma-Aldrich. Pyrromethene 546 and pyrromethene 605 were purchased from Exciton. All chemicals were used as received. Deionized water with a resistivity of 18.3 MΩ·cm was obtained from a Merck Millipore water purification system.

4.2.2 Preparation of Colloids

Latex Core Particle Synthesis: Aqueous dispersed latex core particles were synthesized by free radical emulsion polymerization. In a 100 mL round bottom flask, 13.5 g latex monomer, 1.5 g NIPAM, 0.025 g SDS, 0.005 g fluorescent dye, and 50 g water were stirred, flushed, with nitrogen and heated to 75 °C. After 15 minutes the reaction is initiated by addition of 0.025 g potassium persulfate dissolved in 1 mL water. The reaction was

allowed to proceed for 24 hours at 75 °C, after which the particles are filtered and washed three times with water using centrifugation.

Composite Microgel Synthesis: Composite microgels, consisting of a latex core and a microgel shell were synthesized by seeded precipitation polymerization. In a 100 mL round bottom flask, 0.25 g latex core particles, 1.25 g microgel monomer, and 50 g water were stirred, flushed, with nitrogen and heated to 75 °C. After 15 minutes the reaction is initiated by addition of 0.050 g potassium persulfate dissolved in 1 mL water. The reaction was allowed to proceed for 4 hours at 75 °C, after which the particles are filtered and washed three times with water using centrifugation.

4.2.3 Characterization

Dynamic Light Scattering: Particle size was determined by light scattering techniques performed with a Malvern Nanosizer ZS. Operating at a scattering angle of 173°. Correlation data were analyzed with correlogram analysis software from Malvern. Particles were suspended in deionized water, a solution of 1×10^{-3} M sodium hydroxide or solutions of various concentrations of sodium chloride.

Scanning Electron Microscopy (SEM): The polydispersity of core particles was determined by scanning electron microscopy. Particle dispersions were deposited on a silicon wafer, dried in air at room temperature, and sputtered with a 12 nm layer of iridium using a Leica EM SCD 500 sputter coater. Images were recorded on an FEI Magellan 400 field-emission SEM, using a through-the-lens detector and an acceleration voltage of 2.0 kV.

Microscopy: Fluorescent images of composite microgels were recorded with a Zeiss LSM 5 EXCITER and Axiovert 200M confocal microscope, equipped with a 100× oil-immersion objective.

Viscometry: The volume fraction ϕ of particle stock solutions was determined by measuring the relative viscosity of dilute suspensions. For this, an Ubbelohde capillary viscometer was immersed in a water bath with a temperature precision of 0.1 °C. The relative viscosities of dilute suspensions at different particle concentrations were then measured. Using the Einstein-Batchelor relation $\eta/\eta_0 = 1 + 2.5(k \times wt) + 6.2(k \times wt)^2$ the data were fitted to determine the intrinsic volume fraction $k = \phi/wt$.^[15]

Rheology: Oscillatory rheology was performed on an Anton Paar rheometer (MCR 301 and MCR 501) using a double-walled couette geometry applying a strain of 1% at 1 Hz with a heating and cooling rate of 1.00 or 1.44 °C/min. A preshear of $\dot{\gamma} = 10^3 \text{ s}^{-1}$ and 5 minutes of equilibration were performed before every temperature cycle.

4.3 Results and Discussion

We prepare composite microgels (CMs) that have a latex core and a Microgel shell; the latex core allows embedding of high concentrations of a fluorescent dye, to aid visualization of the microstructures that form, without affecting the interparticle interactions.^[16] We first synthesize the latex core particles via an emulsion polymerization using sodium dodecyl sulfate (SDS) as an emulsifier. The particle size of the core can be tuned between 100 and 350 nm, by adjusting the concentration of SDS, while maintaining low polydispersity (Figure 4.1a,b). We use the monomers styrene, methyl methacrylate, and trifluoroethyl methacrylate to provide a range in refractive index and density. For example, the refractive index of cores prepared from trifluoroethyl methacrylate can be matched in aqueous mixtures of DMSO to yield transparent suspensions to be used in optical studies.^[17] Moreover, high loads of small molecular fluorescent dyes, dissolved in the monomer phase, can be directly embedded into the cores during synthesis, to aid visualization of the particles using confocal microscopy without influencing the interactions between the particles.

In the second step, a microgel shell is synthesized around the core particles by precipitation polymerization, composed of at least two components: *N*-isopropylacrylamide (NIPAM), and *N,N'*-methylenebis(acrylamide (MBAM). The thickness of the microgel shell is tuned by the mass ratio of microgel monomer to core particles, M_m/M_c (Figure 4.1c) and can be applied to a variety of microgel compositions. With this method a shell thickness of up to 300 nm in water, and up to 450 nm for carboxy-functional microgels suspended in 1×10^{-3} M NaOH is realized. For larger ratios of M_m/M_c , secondary nucleation occurs resulting in the presence of microgels without a fluorescent core. The core-shell particles retain the low polydispersity of the core particles within the range explored here. This is evidenced by the rapid crystallization of the particles at sufficiently high

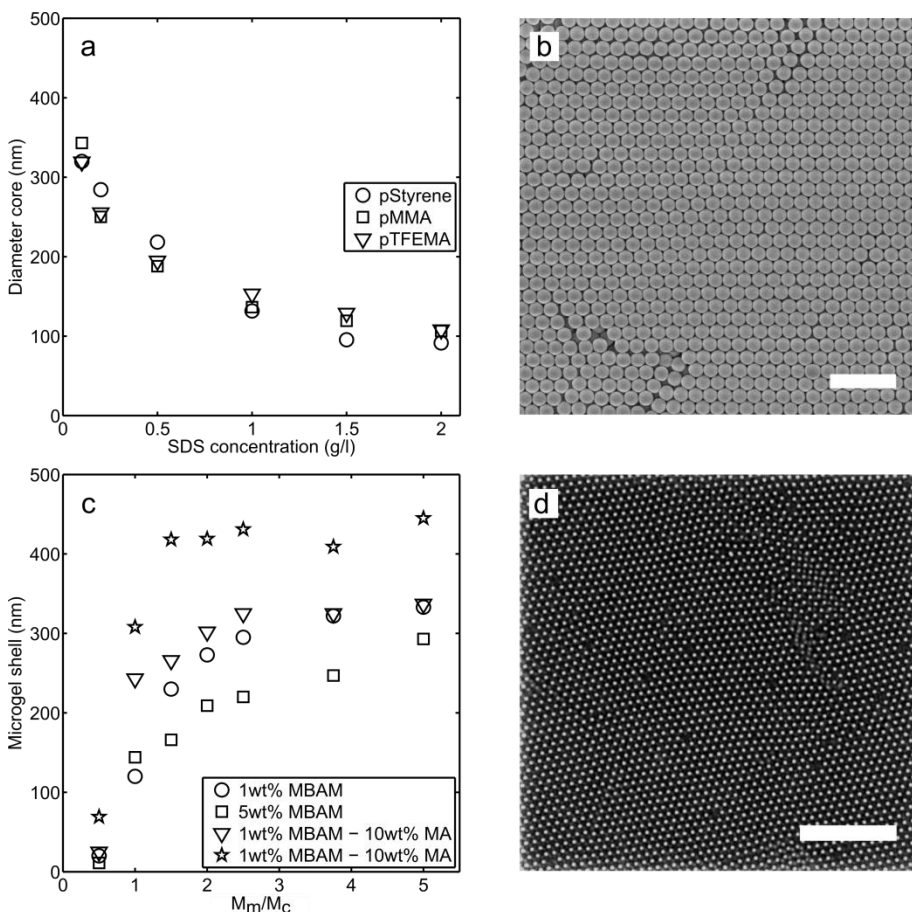


Figure 4.1: Particle size and polydispersity of the two-step synthesis method for composite microgels. a) Diameter of core particles at different SDS concentrations. b) SEM image of hexagonally packed polystyrene core particles at a SDS concentration of 0.5 g/L, scale bar is 1 μ m. c) Microgel shell thickness as a function of monomer to core mass ratio (M_m/M_c). d) Confocal microscopy image of a crystallized CM suspension, scale bar is 10 μ m.

volume fractions, as shown in Figure 4.1d. This two-step approach allows independent tuning of not only the core size and shell thickness, but also the refractive index of the core and shell. This allows the design of particles with specific scattering profiles, which could be of importance for photonic applications.^[18] The composition of the microgel shell determines the thermoresponsive character of the core-shell particles.^[19] To demonstrate this we synthesize CMs with different thermoresponsive characteristics by

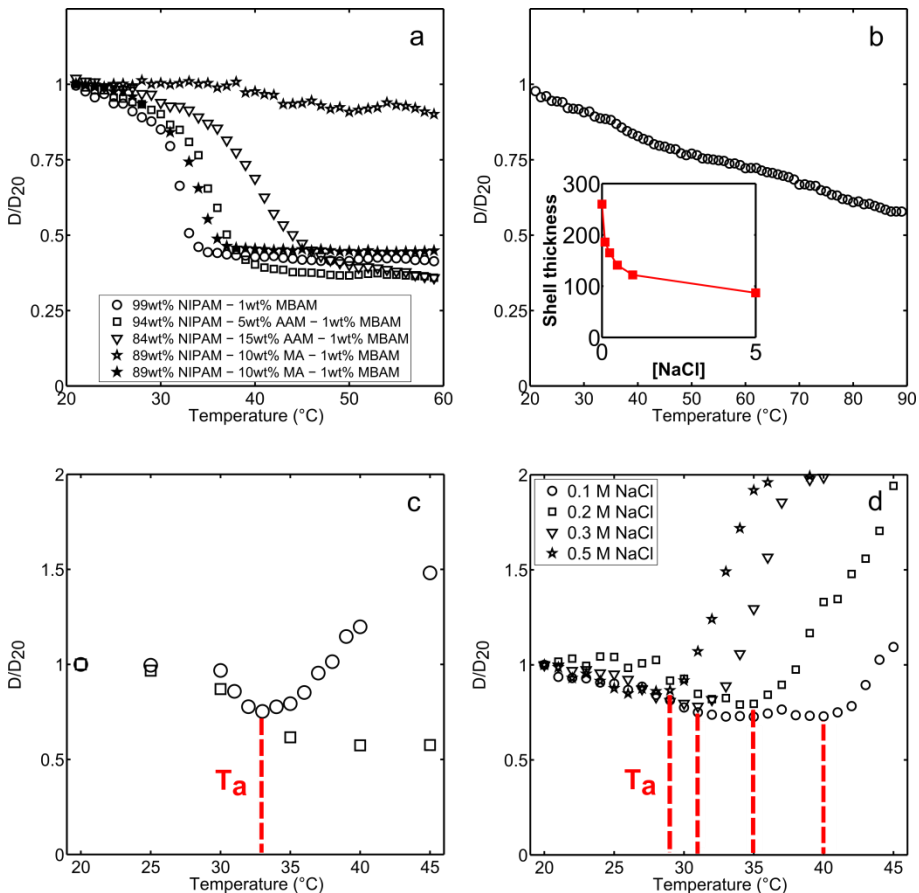


Figure 4.2: CM particle size at different temperatures and salt concentrations, measured with dynamic light scattering. a) Normalized particle size as a function of temperature for different CMs synthesized. Particles are suspended in water. The 89 wt% NIPAM-10 wt% MA-1 wt% MBAM CM is also measured in 1×10^{-3} M NaOH (open stars). b) Normalized particle size as a function of temperature and shell thickness as a function of salt concentration (inset) for a CM with 10 wt% SPMA. c) The aggregation temperature T_a is defined as the temperature at which the particles size starts increasing. d) T_a as a function of salt concentration for a CM with 1 wt% SPMA.

copolymerizing acrylamide (AAM), methacrylic acid (MA), or 3-sulfopropyl methacrylate (SPM) with NIPAM and MBAM. A poly(NIPAM-co-MBAM) microgel shell has a sharp collapse transition between 30 and 34 $^{\circ}\text{C}$ (Figure 4.2a). Copolymerizing AAM in the microgel shell increases the temperature

range over which the collapse takes place, 33-38 °C for 5 wt% AAM and 36-46 °C for 15 wt% AAM.

Copolymerization with MA and SPM, which are ionic monomers, introduce pH and ionic strength responsiveness for additional tuning of the colloidal interactions. For instance, 10 wt% MA shifts the collapse temperature in pure water by only a few degrees to 31-36 °C. However, in 1×10^{-3} M NaOH, electrostatic repulsions that arise inside the microgel shell, due to deprotonated carboxylic acid groups, increases the solvency to such an extent that no temperature-induced collapse is observed within the temperature range explored. Moreover, these highly charged core-shell microgels show rapid formation of extended crystals at high volume fractions, making them a useful model to study colloidal crystals.^[20] Remarkably, the introduction of a strongly charged ionic comonomer, SPM at 10 wt% changes the collapse behavior drastically; we observe a gradual and steady decrease in microgel shell thickness over a wide temperature range of 20-90 °C (Figure 4.2b). Even more remarkable is the strong response of this CM to ionic strength; at 20 °C, increasing the salt concentration from 0 to 5×10^{-3} M causes the microgel shell to collapse by ~70% (Figure 4.2b inset).

In general, these CMs decrease in size as the temperature increases, because the solvent quality decreases due to an increasing preference for the pNIPAM chains to form intramolecular hydrogen bonds. Above the lower critical solution temperature, this induces attractive interaction between the polymer chains of the microgel causing it to phase separate from the aqueous solution. However, at low ionic strength, this internal attraction does not translate into colloidal instability, as the particles are electrostatically stabilized by sulfonate groups at their periphery remnant from the radical initiator potassium persulfate. In addition, sulfonate or carboxylic acid groups from SPM and MA further increase the colloidal stability.

The electrostatic repulsion between CMs, which maintains colloidal stability across the collapse transition, has been used extensively to vary volume fraction with temperature, allowing rapid switching between liquid and amorphous or crystalline states.^[21-25] However, these electrostatic interactions can be screened by increasing the ionic strength. This leads to an interplay between electrostatic repulsion, tuned by salt concentration, and attractive interactions controlled by temperature. Therefore, the phase behavior of a CM suspension can be carefully tuned with these two

parameters. For a given, sufficiently high, ionic strength, we can identify a specific temperature T_a , at which the attractive interactions become sufficiently large to overcome the screened electrostatic repulsion, resulting in particle aggregation. From dynamic light scattering (DLS) measurements, we define T_a as the temperature above which we observe a sudden increase in particle diameter (Figure 4.2c), indicative of the onset of particle aggregation. By varying the ionic strength of the aqueous medium, we can tune the T_a , here demonstrated for CMs in which 1 wt% of SPM is copolymerized in the shell; as the salt concentration increases from 0.1 to 0.5 M, the T_a decreases from 40 to 29 °C (Figure 4.2d).

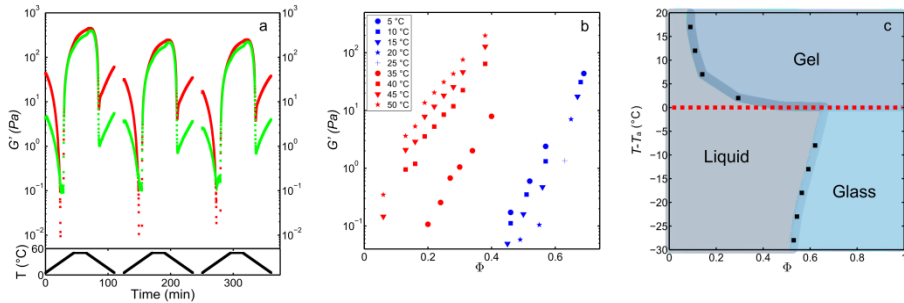


Figure 4.3: Viscoelastic moduli of CM suspensions at different temperatures and ϕ .
 a) Three consecutive temperature cycles between 5 and 50 °C of a $\phi = 0.5$ CM suspension. In each cycle, the glass, liquid, and gel states are identified by the temperature dependence of G' and G'' . The liquid state is highlighted by the gray areas. b) G' as function of ϕ at different temperatures. The blue markers are for the glass state, the red markers are for the gel state. c) Phase diagram for the glass, liquid, and gel states of composite microgel suspensions determined from G' measured at different temperatures and ϕ .

The phase behavior of colloidal suspensions is governed mainly by the volume fraction of particles and the interactions between the colloids. In our system, we can control particle size, thereby volume fraction, and particle interactions, switching from attractive to repulsive, by a combination of the initial number density of particles, the ionic strength, and temperature. This allows us to switch between repulsive glasses, repulsive liquids, and attractive colloidal gels with few experimental parameters. We explore these state transitions for a CM with a polystyrene core and a poly(NIPAM-MBAM) shell. Suspended in 5×10^{-3} M NaCl solution, these particles have a

T_a at 33 °C. To construct a diagram of states, we measure the temperature-dependent viscoelastic moduli G' and G'' using a rheometer over a temperature range from 5 to 50 °C, with a heating and cooling rate of 1 °C min⁻¹ and a fixed frequency and strain of 1 Hz and 1%, respectively (Figure 4.3a). Three temperature regimes are identified: between 5 and 25 °C, G' dominates over G'' indicating solid-like behavior. 25–35 °C, where G'' dominates over G' , indicating liquid-like behavior and a reentrant behavior starting at 35 °C, where the suspension adopts a solid-like behavior again. We identify these regimes as the glass, liquid, and gel states, respectively. A striking feature of these CM suspensions is that the state transitions are reversible. The heating and cooling curves display the same temperature regimes. We note some minor hysteresis, which is probably caused by the loosely crosslinked periphery of the microgel particles. In the attractive gel state, where the microgels are collapsed, it is possible that some entanglements between these outer surface brushes forms, which requires disentangling before the particles can dissociate upon decrease of temperature. In principle, this is a kinetic effect, and longer waiting times during cooling are expected to remove the hysteresis.

By measuring suspensions at different number concentrations of microgels, we determine the temperature-dependent state transitions. First, we determine the temperature-dependent volume fraction by measuring the diameter of the CMs as a function of temperature with dynamic light scattering and measuring the intrinsic viscosity of the suspension with an Ubbelohde viscometer. Fitting the Einstein-Batchelor equation for the viscosity of dilute suspensions, gives the intrinsic volume fraction, with which the effective volume fraction ϕ is determined.^[15] By plotting the elastic modulus G' as a function of ϕ at different temperatures, we identify the three states: (i) in the liquid state, G' is effectively zero; (ii) in the repulsive glass state, found at high volume fractions, G' is relatively small and caused by the elastic interactions between particles confined by their close-packed neighbors; (iii) in the gel state, at low volume fractions and temperatures above T_a , G' is significantly higher and caused by cohesive bonds between the aggregated colloids (Figure 4.3b). In the gel state, G' increases with increasing temperature, which we attribute to increasing bond strength between the particles as the temperature is increased above the collapse temperature.^[14] For the repulsive systems, the temperature dependence is much weaker, as expected.

We can now identify the critical volume fractions at which the state transitions occur, by assuming that the elastic modulus vanishes with a power-law upon approaching the critical volume fraction.^[26,27] Fitting these critical power laws to the measured G' data at different temperatures and ϕ then allows accurate determination of these transition points. The state transitions from liquid-to-glass and liquid-to-gel are determined in this manner, whereas the glass-to-gel transition, which is a solid-solid transition and does not exhibit a vanishing modulus, is fixed at the T_a . This allows us to construct a full diagram of state for this particular CM system as shown in Figure 4.3c. For hard spheres, the liquid-to-glass transition is independent of temperature and typically identified to occur at $\phi \approx 0.58$.^[28] Our data suggest that the liquid-to-glass transition in our experiments is weakly temperature dependent, with the glass transition at lower ϕ as the temperature decreases. This is probably due to the error between the measured hydrodynamic diameter of the CMs, which we use to compute the volume fraction, and the interaction diameter of the CMs in suspension, which may include short-range electrostatic repulsions or steric interactions from the dilute polymer brushes at the microgel surface. Moreover, the change in particle size as a function of temperature is measured by DLS at extremely dilute conditions, while the rheology is performed in concentrated suspensions, and it is well-established that microgels adapt their size at higher volume fractions to equilibrate against the osmotic pressure of the suspension.^[29] The liquid-to-gel transition exhibits a much stronger dependence on temperature, which is related to the increase of the attraction strength with increasing temperature.

A crucial question in exploring the nature of colloidal gels, and heterogeneous solids in general, is to establish clearly the relationship between macroscopic linear and non-linear rheology and microscopic structure. This is a difficult challenge as in many cases it is impossible to vary the microstructure of the colloidal gel while keeping all other parameters of the system constant. Using the temperature controlled tuning of particle size, volume fraction, and attractive interactions in the system presented above, we propose a strategy to accomplish this. We prepare mixtures of CMs with two distinctly different aggregation temperatures, by changing the co-monomer AAM concentration in the microgel shell. We mix particles with a T_a of 33 °C, with a green-emitting fluorescent core, and CMs with a T_a of 56 °C, with a red-emitting core, in different ratios and measure the storage modulus G' as a function of temperature.

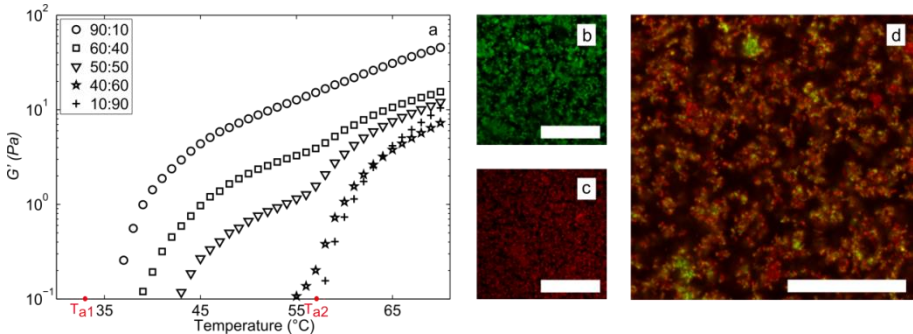


Figure 4.4: Temperature controlled gelation in a suspension of mixed CMs. a) G' as a function of temperature for different mixing ratios with initial $\phi = 0.3$. b,c) Confocal microscopy images of the gels formed by the individual particles at $70\text{ }^{\circ}\text{C}$. d) Confocal microscopy images of the gel formed by the sequential gelation of the particles at $70\text{ }^{\circ}\text{C}$, mixed in a 50:50 ratio. Scale bars are $20\text{ }\mu\text{m}$.

At low mixing ratios, G' develops as for a single component system, with a steep increase above the T_a of the major component (Figure 4.4a). Around equal mixing ratios however, G' has a stepwise increase, with the steps corresponding to the T_a values of the CMs. This is indicative of a temperature-dependent sequential gelation. The fluorescently labeled cores of the CMs allow us to image the gels formed by the CMs with confocal microscopy. Both CM types form gels in single-component suspensions at temperatures above T_a (Figure 4.4b,c). Interestingly, a 50:50 mixture, slowly brought to $70\text{ }^{\circ}\text{C}$ forms a gel with a distinct core-sheath architecture (Figure 4.4d). The CM with the lower T_a , shown in green, first aggregates to form a sparse and fractal colloidal gel of thin strands. When the second T_a is crossed, the remaining particles aggregate onto this rigid scaffold, thereby maintaining the overall gel structure but increasing the strand thickness.

The elasticity of a colloidal gel is governed by stretching and bending of the gel strands; both the resistance to stretching and bending increase with increased strand thickness, resulting in the increase in modulus observed during this sequential gelation process. This offers a unique approach to systematic variation of the microstructure of a heterogeneous colloidal solid while measuring its mechanical properties; moreover, due to the reversibility of the aggregation, this process can be repeated many times from reproducible initial conditions. This makes these sequentially gelling suspensions ideal systems to resolve the long-standing question on how

microscopic gel structure, and the attractive interactions between the colloidal building blocks, influence the linear and non-linear mechanics of colloidal gels.

4.4 Conclusion

In this chapter, we present a colloidal microgel system, which allows control of volume fraction, particle interactions, and the physical state of the suspension by means of environmental triggers alone. Changing the temperature and salt concentration enables transitioning between glass, liquid, and reentrant attractive solids states, known as colloidal gels. Moreover, as the synthetic protocol we develop can be applied to a variety of microgel chemistries, mixtures of particles can be prepared in which sequential phase transitions can be induced by means of gradual temperature ramp protocols. We demonstrate for a two-component mixture of composite microgels, the occurrence of sequential gelation, where the microgels with a lower gelation temperature form a scaffold gel structure on which the microgels with a higher gelation temperature aggregate. These results open the way for exploring dynamic arrest and kinetic pathways of complex phase transitions in an experimental colloidal model, in which the individual particles can be directly visualized and located accurately by means of confocal microscopy.

References

- [1] R. Mezzenga, P. Schurtenberger, A. Burbidge and M. Michel, *Understanding foods as soft materials*, Nature materials, **4** (2005), 729-740.
- [2] T. F. Tadros, Colloids in Cosmetics and Personnel Care, (2008) Wiley, Hoboken, NJ, USA.
- [3] K. Kroy, M. E. Cates and W. C. K. Poon, *Cluster Mode-Coupling Approach to Weak Gelation in Attractive Colloids*, Phys. Rev. Lett., **92** (2004), 148302.
- [4] M. Lattuada, H. Wu and M. Morbidelli, *Experimental Investigation of Colloidal Gel Structures*, Langmuir, **20** (2004), 4355-4362.
- [5] A. D. Dinsmore, V. Prasad, I. Y. Wong and D. A. Weitz, *Microscopic Structure and Elasticity of Weakly Aggregated Colloidal Gels*, Phys. Rev. Lett., **96** (2006), 185502.
- [6] P. J. Lu, E. Zaccarelli, F. Ciulla, A. B. Schofield, F. Sciortino and D. A. Weitz, *Gelation of particles with shortrange attraction*, Nature, **453** (2008), 499-503.
- [7] M. H. Lee and E. M. Furst, *Response of a colloidal gel to a microscopic oscillatory strain*, Phys. Rev. E, **77** (2008), 41408.
- [8] E. Zaccarelli and W. C. K. Poon, *Colloidal glasses and gels: The interplay of bonding and caging*, Proceedings of the National Academy of Sciences of the United States of America, **106** (2009), 15203-15208.
- [9] T. Gibaud, D. Frelat and S. Manneville, *Heterogeneous yielding dynamics in a colloidal gel*, Soft Matter, **6** (2010), 3482-3488.
- [10] J. Sprakel, S. B. Lindström, T. E. Kodger and D. A. Weitz, *Stress Enhancement in the Delayed Yielding of Colloidal Gels*, Phys. Rev. Lett., **106** (2011), 248303.
- [11] L. C. Hsiao, R. S. Newman, S. C. Glotzer and M. J. Solomon, *Role of isostaticity and load-bearing microstructure in the elasticity of yielded colloidal gels*, Proceedings of the National Academy of Sciences of the United States of America, **109** (2012), 16029-16034.
- [12] Z. Shao, A. S. Negi and C. O. Osuji, *Role of interparticle attraction in the yielding response of microgel suspensions*, Soft Matter, **9** (2013), 5492-5500.

- [13] S. B. Lindstrom, T. E. Kodger, J. Sprakel and D. A. Weitz, *Structures, stresses, and fluctuations in the delayed failure of colloidal gels*, Soft Matter, **8** (2012), 3657-3664.
- [14] T. E. Kodger and J. Sprakel, *Thermosensitive Molecular, Colloidal, and Bulk Interactions Using a Simple Surfactant*, Advanced Functional Materials, **23** (2013), 475-482.
- [15] G. Romeo, A. Fernandez-Nieves, H. M. Wyss, D. Acierno and D. A. Weitz, *Temperature-Controlled Transitions Between Glass, Liquid, and Gel States in Dense p-NIPA Suspensions*, Advanced Materials, **22** (2010), 3441-3445.
- [16] H. Monteillet, M. Workamp, J. Appel, J. M. Kleijn, F. A. M. Leermakers and J. Sprakel, *Ultrastrong Anchoring Yet Barrier-Free Adsorption of Composite Microgels at Liquid Interfaces*, Advanced Materials Interfaces, **1** (2014).
- [17] J. Appel, S. Akerboom, R. G. Fokkink and J. Sprakel, *Facile one-step synthesis of monodisperse micron-sized latex particles with highly carboxylated surfaces*, Macromolecular Rapid Communications, **34** (2013), 1284-1288.
- [18] A. Perro, G. Meng, J. Fung and V. N. Manoharan, *Design and Synthesis of Model Transparent Aqueous Colloids with Optimal Scattering Properties*, Langmuir, **25** (2009), 11295-11298.
- [19] R. Liu, M. Fraylich and B. R. Saunders, *Thermoresponsive copolymers: From fundamental studies to applications*, Colloid and Polymer Science, **287** (2009), 627-643.
- [20] R. Higler, J. Appel and J. Sprakel, *Substitutional impurityinduced vitrification in microgel crystals*, Soft Matter, **9** (2013), 5372-5379.
- [21] D. A. Sessoms, I. Bischofberger, L. Cipelletti and V. Trappe, *Multiple dynamic regimes in concentrated microgel systems*, Philosophical transactions, Series A, Mathematical, physical, and engineering sciences, **367** (2009), 5013-5032.
- [22] V. D. Nguyen, M. T. Dang, B. Weber, Z. Hu and P. Schall, *Visualizing the Structural SolidLiquid Transition at Colloidal Crystal-Fluid Interfaces*, Advanced Materials, **23** (2011), 2716-2720.
- [23] V. D. Nguyen, Z. Hu and P. Schall, *Single crystal growth and anisotropic crystal-fluid interfacial free energy in soft colloidal systems*, Phys. Rev. E, **84** (2011), 11607.
- [24] P. J. Yunker, K. Chen, M. D. Gratiale, M. A. Lohr, T. Still and A. G. Yodh, *Physics in ordered and disordered colloidal matter composed*

- of poly(N-isopropylacrylamide) microgel particles*, Reports on progress in physics, **77** (2014), 056601.
- [25] Y. Peng, F. Wang, Z. Wang, A. M. Alsayed, Z. Zhang, A. G. Yodh and Y. Han, *Two-step nucleation mechanism in solid-solid phase transitions*, Nature Materials, **14** (2015), 101-108.
 - [26] V. Trappe and D. A. Weitz, *Scaling of the Viscoelasticity of Weakly Attractive Particles*, Phys. Rev. Lett., **85** (2000), 449-452.
 - [27] V. Trappe, V. Prasad, L. Cipelletti, P. N. Segre and D. A. Weitz, *Jamming phase diagram for attractive particles*, Nature, **411** (2001), 772-775.
 - [28] G. L. Hunter and E. R. Weeks, *The physics of the colloidal glass transition*, Reports on Progress in Physics, **75** (2012), 66501.
 - [29] M. Muluneh, J. Sprakler, H. M. Wyss, J. Mattsson and D. A. Weitz, *Direct visualization of pH-dependent evolution of structure and dynamics in microgel suspensions*, Journal of Physics: Condensed Matter, **23** (2011) 505101.

II

Crystals, Glasses and Gels

Chapter 5

Substitutional Impurity-Induced Vitrification in Microgel Crystals

We study the effect of larger substitutional impurities on the structure of soft microgel crystals. At the size ratio we employ, $r_{small}/r_{large} = 0.67$, we observe the unexpected co-crystallisation of the large impurities with the base crystal, at low fractions of impurity particles. A single impurity takes the place of 4 tetrahedrally coordinated small particles within the lattice. However, as this is accompanied by local deformations of the particles, this distortion-minimizing structure transforms into a random surrounding of the impurity particle at higher fractions of large substitutional impurities. The distortions in the lattice become longer ranged through this transformation, and ultimately result in vitrification of the sample.

This chapter was published as:

Ruben Higler, Jeroen Appel, and Joris Sprakel: *Substitutional impurity-induced vitrification in microgel crystals*, Soft Matter **9** (2013), 5372-5379.

5.1 Introduction

The packing of spheres has been a subject of research for many centuries; in 1611 Kepler conjectured that the maximum packing fraction of monodisperse spheres cannot exceed 0.74.^[1] This can only be achieved when the spheres are arranged in a close packed ordered arrangement, accommodated by either hexagonally close packed or face-centered cubic symmetries. These crystal types can be stable in colloidal systems interacting solely through volume exclusion, i.e. hard spheres, or in systems with short ranged repulsion.^[2-4] Other commonly encountered crystal types, such as the body-centered cubic structure, require interactions that act over distances beyond a lattice constant, otherwise they are mechanically unstable; hence they are observed only in colloidal systems that interact through long ranged, e.g. electrostatic, repulsion.^[5]

Adding a single degree of complexity, by packing mixtures of (colloidal) particles composed of two populations of unequally sized spheres, increases the number of possibilities vastly. Depending on the mixing ratio of the two species and the size ratio α between large and small particles, a wide variety of ordered phases can be, theoretically, formed. For example, at size ratios $0 < \alpha > 0.22$ a XY₁₁ phase is predicted,^[6] in which the large spheres are close packed and small particles occupy their interstitial spaces, thus leading to too high packing fractions. At size ratios $0.528 < \alpha > 0.623$, another binary superlattice can occur in the AlB₂ (aluminium diboride) symmetry; this type of crystal lattice has been observed also in natural opals^[7] and manmade mixtures of colloidal hard spheres.^[8] However, above size ratios of 0.632, no stable binary ordered phases can exist, and the ground state of the system is that of two phase-separated crystals of either species. However, forming macroscopic domains of the two species in a mixture requires diffusive transport over large length scales, a process that is prohibitively slow in a solid.^[9] Computer simulations indicate that fractionated coexisting crystal phases can form spontaneously in polydisperse mixtures of colloidal particles; however, experimental evidence remains absent, possibly due to the long equilibration times required to achieve macroscopic demixing.^[10]

Due to the kinetic inaccessibility of these equilibrium states, sphere mixtures in this size ratio are considered excellent candidates to form

kinetically stable glasses; in the search for vitreous phases of binary metallic alloys, several size ratios of the metal atoms above this threshold value of 0.632 have been identified as most suitable to inhibit crystallization, with a large number of stable glasses found at a size ratio of approximately 0.7.^[11] This same size ratio of 0.7 has been employed to inhibit crystallization and ensure stable glasses in a wide variety of studies on athermal discs and spheres, and in studies on the structure and dynamics of glassy colloidal suspensions.^[6,12-18] In almost all of these studies, a fixed number ratio of large to small spheres, of around 1:1, is added to ensure a vitreous sample. The vitrification of a two-dimensional colloidal crystal, upon introduction of smaller impurity particles, at a size ratio of 0.7, was seen to occur already at very small fractions of impurities; a number fraction of 2% was sufficient to cause the crystal-to-glass transformation. At this transition point, the authors observed a peak in the susceptibility of the orientational bond order parameter; consequently they noted the resemblance to a melting transition, even though the mechanical rigidity of the colloidal solid was maintained.^[6] It can be envisioned that the addition of small impurity particles to a crystal of larger spheres introduces an extra vibrational volume into the crystal, which can ultimately lead to a similar vibrational instability, or Lindemann instability, that causes the crystal-to-fluid melting transition.

By contrast, when a crystal of smaller particles is disturbed by the introduction of impurities that are slightly too large to occupy a lattice space, another mechanism must be responsible for the vitrification. Yet, this scenario remains virtually unexplored, especially in colloidal systems. For highly asymmetric size ratios, the impurity-induced emergence of extended defects has been demonstrated in colloidal hard sphere crystals;^[19] yet how these phenomena translate to systems with only weak asymmetry in size $\alpha > 0.623$ is not known. This raises the question what local structural features, induced by the addition of mismatched substitutional impurities, cause global loss of order.

In this chapter, we study the crystal-to-glass transition in mixtures of soft microgel colloids, at a size ratio of 0.67, by the gradual substitution of small particles in the crystal by larger impurities. Using quantitative confocal microscopy we evaluate the structure of the sample; we uncover that the impurities induce a sudden and sharp decrease in the crystallinity of the sample. Surprisingly, at low fractions of large impurities, they co-crystallize with the smaller particles that form the base crystal; this can occur through

the substitution of 4 tetrahedrally coordinated particles in the crystal, with a single larger impurity. However, upon further increase of the fraction of impurities, this specific, distortion-minimizing configuration is lost, in favor of a disordered close-packed arrangement of the base particles around an impurity. At the same point, it appears that the global structure of the sample displays a phase inversion, from a continuous crystal with patches of glass, to a continuous glass with small crystalline islands.

5.2 Experimental Section

5.2.1 Materials

N-isopropylacrylamide (NIPAM), *N,N'*-methylenebis(acrylamide) (MBAM), methacrylic acid (MA), potassium peroxodisulfate (KPS), styrene and sodium dodecyl sulfate (SDS) were purchased from Sigma-Aldrich. The fluorescent dyes pyrromethene 546 and pyrromethene 605 were purchased from Exciton. All chemicals were used as received.

5.2.2 Preparation of Colloids

In this study we use microgel particles with a fluorescent polystyrene core; the high loading of fluorescent dye in the core and the separation of fluorescent centers by a non-fluorescent, and highly swollen, microgel shell allow accurate determination of the centroids of the particles using confocal microscopy. Core-shell microgel particles are synthesized in a two-step procedure. First, fluorescent cores, with a diameter $d \approx 300$ nm and polydispersity $< 5\%$, are prepared in an emulsion polymerization. 8 g styrene, 0.675 g NIPAM, 0.02 g SDS, and 0.01 g of fluorescent label are mixed with 26 mL of DI water. Following 15 minutes of purging of the reaction mixture with N_2 at 80 °C to remove dissolved oxygen, the reaction is initiated with 0.02 g KPS dissolved in 1 mL water. The reaction is left for 24 hours at 80 °C. The cores are purified by repeated centrifugation and resuspension in water. Then, a shell of poly(NIPAM-co-MA-co-MBAM) is grown around the core by suspending approximately 1 g cores in 100 mL water and adding 2.7 g NIPAM, 0.058 g MBAM, and 210 μL MA. After 15 minutes of purging with N_2 at 80 °C, the reaction is initiated with 0.1 g KPS

dissolved in 5 mL water. The reaction is allowed to proceed for 4 hours at 80 °C. Fifteen minutes into the reaction we added 5 mL of a 0.5 M MA solution in water to promote a high concentration of charge on the outside of the shells. The core-shell particles are purified by repeated centrifugation and resuspension in 1 mM NaOH and concentrated to ~ 7 wt%.

Green (Pyrromethene 546) and red (Pyrromethene 605) core-shell particles are used in this study, with total radii of 956 ± 24 nm and 645 ± 11 nm respectively, as determined by dynamic light scattering (Figure 5.1). The red particles will be referred to as the base particles and the green particles as the impurities. The size ratio base : impurity for this combination is 0.67.

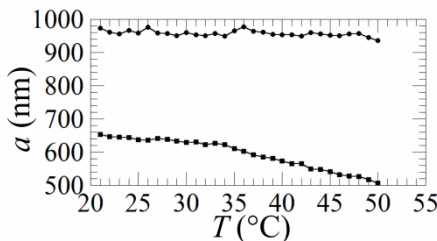


Figure 5.1: DLS data for base particles (bottom, squares) and impurities (top, circles) showing the small dependence of radius, a , on temperature, T , around our measurement temperature, 23 °C.

5.2.3 Sample Preparation

All experiments are conducted in a suspending medium of 1mM NaOH water; under these conditions all carboxylic acid groups in and on the microgel particles are charged, promoting crystallization of the particle suspension. Moreover, the particles are no longer thermoresponsive, as determined by DLS (Figure 5.1), such that we can perform our microscopy experiments at a room temperature of 23 °C without special precautions. At microgel concentrations < 4 wt%, crystallization is no longer observed, therefore all samples are prepared at a final concentration of 4.5 wt%, by diluting with 1 mM NaOH. Mixtures of small and large microgel particles, prepared from stock solutions at the same weight concentration, are thoroughly mixed before loading into glass sample chambers (18×20×0.25 mm), hermetically sealed with UV-curing epoxy. We leave the samples to equilibrate overnight at room temperature.

5.2.4 Confocal Microscopy

Images are recorded with a Zeiss LSM 5 EXCITER with Axiovert 200M confocal microscope, equipped with a 100 \times oil-immersion objective. We acquire two-dimensional images, in our three-dimensional sample, observing a field-of-view of 64.3 \times 64.3 mm. For each sample 20 images are acquired, taken at least several particle diameters away from sample walls, at independent random locations throughout the sample to obtain a statistically accurate representation of the sample structure. All data analysis is averaged over these 20 frames and all measurements were done at a room temperature of approximately 23 °C. Particle centroids are located using standard 2D particle tracking algorithms, with 15-20 nm spatial resolution.^[20]

5.3 Results and Discussion

Single component, monodisperse microgel suspensions, at the concentration 4.5 wt%, rapidly crystallize within several minutes, forming extended macroscopic crystallites. Upon the deliberate introduction of impurities that are larger than the particles that form the base crystal, with a size ratio $r_{base}:r_{impurity} = 0.67$, the crystallinity decreases until only a disordered packing remains, as can be seen in Figure 5.2c. It is clear that impurities of this size ratio are efficient at disrupting the crystal lattice. It is for this reason that binary suspensions, with a size ratio around 0.7, are often used to prevent crystal formation in colloidal and granular systems.^[6,12-18] To quantify this behavior as a function of the fraction of impurities, n_i/n , we compute the two-dimensional orientational bond order parameter Ψ_6 defined as^[21]:

$$\Psi_6 = \frac{1}{n_c} \sum_{j=1}^{n_c} e^{i6\theta(r_{ij})}$$

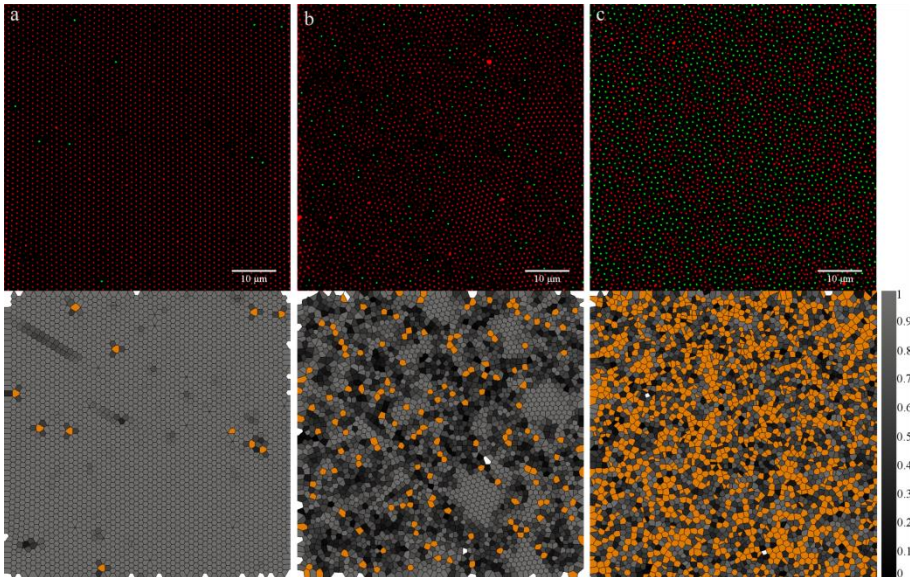


Figure 5.2: Top: confocal images of mixtures of small base particles (red) and impurities (green) at different impurity fractions $n_i/n =$ (a) 0.0084, (b) 0.056, and (c) 0.66. Bottom: corresponding Voronoi tessellations of the confocal images; the Voronoi cells are color coded in grey scale to represent the local bond order parameter $|\Psi_6|$. Substitutional impurities are coloured in orange. Scale bars are 10 μm .

This local order parameter quantifies the amount of average six-fold symmetry around a particle i with all of its n_c nearest neighbors j . $\theta(r_{ij})$ is the bond angle between particles i and j with a fixed yet arbitrary reference axis. For a perfect two-dimensional hexagonal lattice $\Psi_6 = 1$. We can use this bond order parameter to visualize the state of the sample by color-coding the Voronoi cells of each particle in an image according to their local $|\Psi_6|$ value. We can clearly see a few local distortions around the scarce impurities at low impurity mixing fractions, which transition into a fully disordered structure when they are mixed at one-to-one ratios or beyond (bottom row, Figure 5.2). We have investigated the spatial distribution of impurities in our samples, yet did not find statistically significant evidence that impurities cluster.

To investigate the crystal-to-glass transition in more detail, we compute the pair correlation function, $g(r)$; as we are investigating a mixed system, in which the two species are dyed distinctly, we can compute $g(r)$ for the base crystal particles and the impurities separately. At low

concentrations of impurities, $n_i/n > 0.033$, the $g(r)$ for base crystal particles shows distinct peaks at the locations expected for a planar hexagonal packing (Figure 5.3a). Upon increasing the fraction of impurities, the higher-order crystal peaks disappear. This is indicative of short-range order as expected for a glassy phase.^[16] The corresponding $g(r)$ for the impurity particles is initially very noisy due to low numbers of particles which can be averaged at low values of n_i/n . Nevertheless, we still observe peaks corresponding to distances on the crystal lattice for impurities; it appears that at low n_i/n , the larger substitutional impurities co-crystallize with the base crystal matrix. At higher n_i/n , also the pair correlation functions for the impurities show a fluid-like amorphous structure as they do for the base particles (Figure 5.3b).

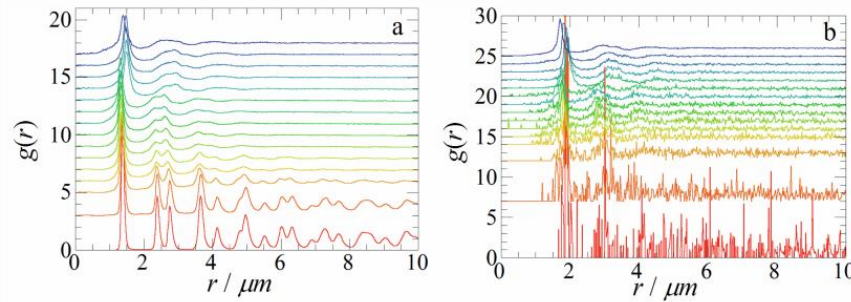


Figure 5.3: Pair correlation function $g(r)$ for $n_i/n = 0.008$ (red, bottom) up to $n_i/n > 0.660$ (blue, top). (a) $g(r)$ for base particles and (b) $g(r)$ for substitutional impurities.

In the $g(r)$ for the small particles at moderate impurity concentrations, $0.008 < n_i/n > 0.081$, we see a split double-peak at $r = 2.5 \mu\text{m}$ (Figure 5.3a); this phenomenon is often observed in glasses of monodisperse particles.^[22-26] For these samples, both the confocal microscopy images and corresponding Voronoi tessellations in Figure 5.2b display the coexistence of a continuous glass phase with small islands of crystal. These regions of medium-ranged crystalline order (MRCO) are responsible for the ordered remnant in the $g(r)$.^[27-32] This MRCO persists up to $n_i/n = 0.081$, after which the $g(r)$ is purely liquid-like.

The apparent gradual loss of crystallinity we observed in the pair correlation functions can be further substantiated by investigating the range

of the order in our samples through the spatial correlation of the bond order parameter^[33]:

$$g_6(r = |r_i - r_j|) = \langle \Psi_6(r_i) \Psi_6(r_j) \rangle$$

For the crystals, as expected, we observe a long ranged order, shown by the plateau in $g_6(r)$ ($n_i/n = 0.008$ in Figure 5.4a), while for the completely vitreous samples, $n_i/n > 0.050$, $g_6(r)$ decays very rapidly, suggesting no long ranged order, and a fluid like structure. Interestingly, in a small regime of impurity fractions ($n_i/n = 0.033$) we appear to see signs of decay with a finite characteristic length scale spanning over several particle diameters; this suggests that indeed MRCO plays an intermediary role in the crystal-to-glass transition.^[31] This is surprising, as for a classical first-order crystal-to-fluid, or melting, transition the change from long-ranged to short-ranged order is expected to be abrupt.

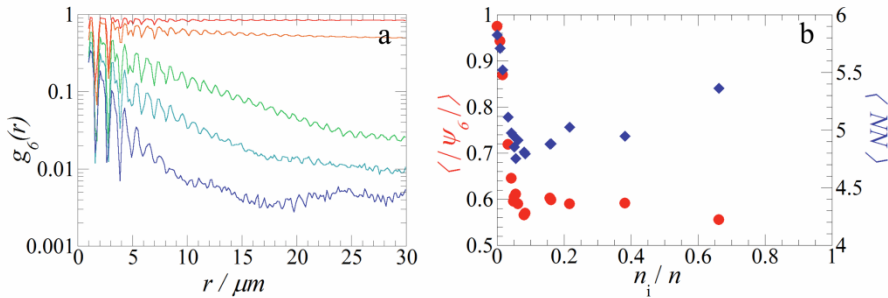


Figure 5.4: Spatial correlation function $g_6(r)$ of the bond orientational order parameter for $n_i/n = 0.008; 0.017; 0.033; 0.043; 0.050$ (from top to bottom). b) Ensemble-averaged values of $\langle |\Psi_6| \rangle$ (circles, red) and mean number of nearest neighbors $\langle NN \rangle$ (diamonds, blue) as a function of the fraction of impurity particles n_i/n .

Clearly, the transition from crystal to glass occurs already at small amounts of substitutional impurities. To further quantify this transition we first compute the mean value of the orientational bond order parameter $\langle |\Psi_6| \rangle$ and the mean number of nearest neighbors $\langle NN \rangle$ (Figure 5.4b). We can clearly see a steep decay of the mean value of the bond order parameter, indicative of the overall loss of crystallinity of the sample. Correspondingly, the number of nearest neighbors starts at just below six, as expected for a

hexagonal arrangement in the plane, and decreases only mildly when the sample vitrifies; even in the glass state, due to the high particle concentration, particles are apparently surrounded by on average 5-5.5 neighbors. We can use these metrics, to get a more detailed view on the transition, by calculating the fraction of crystalline particles in our sample.

First, we consider a particle crystalline when it has exactly six nearest neighbors, characteristic of a hexagonal arrangement; note that the bond angles between the central particle and its neighbors are not taken into account here. The fraction of crystalline particles as determined by the number of nearest neighbors, α_{NN} , shows a steep linear decrease with increasing impurity fraction up to $n_i/n = 0.050$ beyond which the fraction of crystalline particles remains constant at $\alpha_{NN} \approx 0.23$ (diamonds in Figure 5.5). This apparent persistence of crystallinity originates from the fact that even in a fully amorphous material some particles will still have six nearest neighbors, which are not necessarily arranged at the correct 60° bond angles.

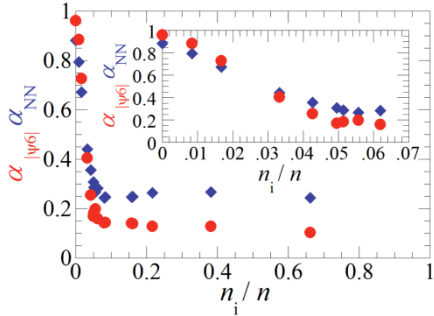


Figure 5.5: Fraction of crystalline particles, measured through the bond order parameter $|\Psi_6|$, a) $\alpha_{|\Psi_6|}$ (circles, red) and through counting the number of nearest neighbors, α_{NN} (diamonds, blue) as a function of the fraction of impurity particles n_i/n . Inset shows a close-up view of the initial decay.

We can also consider particles crystalline when the bond angles of their nearest neighbors meet the criterion for a hexagonal packing; we quantify this through the local bond order parameter $|\Psi_6|$. Here we choose a cut-off value of $|\Psi_6| > 0.9$ for a particle to be considered crystalline. The fraction of crystalline particles, $\alpha_{|\Psi_6|}$, determined in this method exhibits the same trend as α_{NN} and reaches a plateau value at the same fraction of impurities (circles in Figure 5.5). The non-zero plateau value of

$\alpha_{|\Psi_6|} \approx 0.1$ in the glass state results from the fact that we use local measurements only and that even in an amorphous system local order is expected to be present.

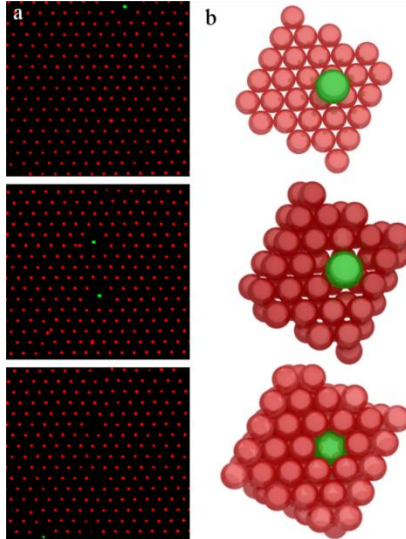


Figure 5.6: (a) Confocal image series of a substitutional impurity in three consecutive lattice planes. (b) 3D illustration of the substitutional impurity and the surrounding base crystal.

At low impurity concentrations, $n_i/n < 0.033$, it appears that the structure of the base crystal is unaffected around the impurity (Figure 5.2a); beyond this concentration the overall structure of the sample becomes more amorphous and the fraction of crystalline particles reaches a low, yet finite, plateau. We thus identify this concentration of $n_i/n = 0.033$ as the transition point. It is surprising that at $n_i/n < 0.033$ the impurities co-crystallize with the crystal matrix as the size difference between the particles in the crystal and the substitutional impurities does not allow one base particle to be substituted by one impurity particle. For the size ratio we employ $r_{small}/r_{large} = 0.67$, geometry dictates that a large impurity can be closely surrounded by seven impurity particles in the 2D plane. Remarkably, this is not the situation we observe at low impurity fractions. Rather, it appears that within the plane, an impurity particle substitutes three base particles. As a result, a single impurity is surrounded, in plane, by a triangular structure composed of nine base crystal particles; this gives rise to

the “propeller”-like features in the Voronoi tessellations in Figure 5.2a, bottom row. In addition to the three particles substituted in the plane that holds the center of mass of the impurity, a fourth base crystal particle is substituted in a layer above, or below. The confocal images clearly show the substitution of 4 tetrahedrally coordinated base crystal particles by a single impurity (Figure 5.6); the impurity thus occupies the space of a tetrahedral substitution cluster (TSC).

To evaluate at what size ratio this specific type of substitution can occur, we generate a perfect virtual face-centered cubic crystal, and select four tetrahedrally coordinated particles, three in-plane and one above, to represent the substitution void. We then numerically fit the largest possible sphere into this cavity; we find that this type of substitution can theoretically only occur for size ratios of $r_{small}/r_{large} = 0.74$ and above. Our size ratio, of 0.67, thus theoretically does not allow such a substitution to occur; in fact, our impurity particles are ~ 170 nm too large to fit in the formed void. However, since we are working with soft compressible particles, we can imagine that the impurity particle shrinks to adapt to the crystal lattice to minimize the lattice strain; such lattice-induced shrinking of an impurity was observed previously.^[34]

This also raises the question if the stress thus accumulated at the impurity leads to local strain in the crystal lattice. We therefore measured the local separation distance between hexagonal nearest-neighbors in the lattice as a function of their distance to a tetrahedrally coordinated impurity substitution, but did not find any signs of lattice distortions beyond the resolution of our particle tracking of approximately 15 nm. This suggests that the impurity particle shrinks due to the pressure imposed by the lattice, in order to minimize any unfavorable lattice distortions and defects.

In the dilute impurity regime $n_i/n < 0.033$, lattice distortions are minimized by the unique tetrahedral substitution clusters (TSCs); this allows for the co-crystallization of impurities and base particles, as evident in their pair correlation functions (Figure 5.3). In plane, the TSCs are characterized by a triangular surrounding with nine nearest neighbors, corresponding to $360^\circ/9 = 40^\circ$ angles between the particle-impurity bonds. Through analysis of the histogram of bond angles of those particles directly surrounding an impurity, we can indeed see that the distribution is strongly peaked at 40° (Figure 5.7a).

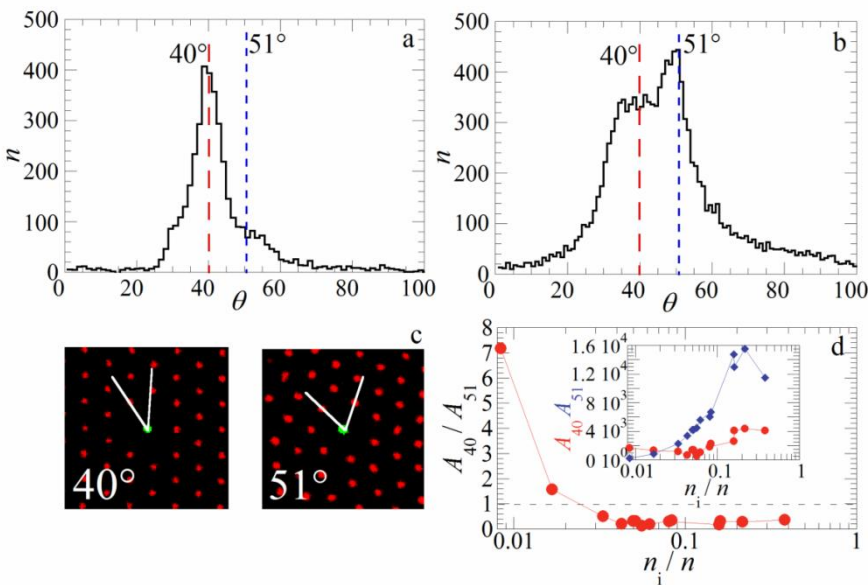


Figure 5.7: Bond angle histograms of particles directly surrounding an impurity, for $n_i/n = 0.008$ (a) and 0.033 (b). The confocal images in (c) illustrate the two different local structures and their characteristic bond angles, (d) relative abundance of the 40° and 51° angles from deconvolution of the bond angle histograms.

When we increase the impurity fraction to 0.033 we observe the sudden appearance of a new peak at 51° . This new peak, which first appears when $0.017 < n_i/n > 0.033$ and persists in samples with higher n_i/n values, is indicative of an in-plane surrounding of seven base particles (Figure 5.7b), which is what we expect for a close-packed organization of base particles around a single impurity, at our size ratio of 0.67 . In order to quantify this transition in the local structure around an impurity, we deconvolve the bond-angle histograms, and calculate the area of the two individual peaks for every sample, thus representing the relative abundance of either a tetrahedral surrounding A_{40} or a random surrounding A_{51} . We see a clear increase in the peak at 51° with increasing fraction of impurities and a decline of the peak at 40° . The curves cross between $n_i/n = 0.017$ and $n_i/n = 0.033$; this cross-over becomes more apparent when plotting the ratio A_{40}/A_{51} (Figure 5.7d). This implies that at concentrations $n_i/n < 0.033$ the distortion-minimizing TSC structure is most abundant, while at $n_i/n > 0.033$ a random, distortion-inducing surrounding becomes dominant.

This becomes even more evident when we plot the average crystallinity, quantified through the average local bond order parameter, as a function of the distance to an impurity particle; at low impurity fractions, where the tetrahedral-substitution structure dominates, only a very short-range distortion of the sample structure is observed, spanning no more than one or a few particle diameters (circles in Figure 5.8). When the fraction of impurities is increased, and the structure around an impurity becomes more random, the lattice distortions become longer ranged (diamonds and triangles in Figure 5.8); this ultimately leads to the complete vitrification of the sample.

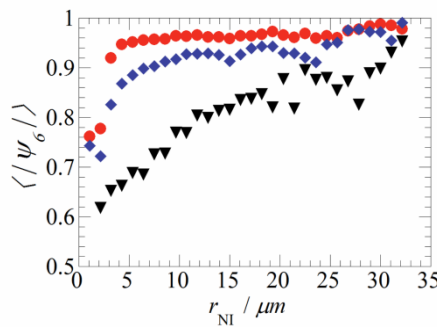


Figure 5.8: Mean value of the bond order parameter as a function of the distance to an impurity, for $n_i/n = 0.008$ (circles), 0.017 (diamonds) and 0.033 (triangles).

It is interesting to note that the transition from a continuous crystal, with patches of disordered material, to a continuous glass with small crystallites dispersed throughout occurs at approximately the same impurity fraction where the transition from a tetrahedral-substitution of base particles to the random surrounding of an impurity with long-ranged distortions of the lattice occurs. We hypothesize that the local stress generated by the, slightly too large, impurity particle, prevents the co-crystallization to persist for increasing impurity fractions. It is imaginable that the transition from co-crystallization of the impurities to the vitrification of the sample occurs when the zones in which the stress around the TSC is distributed begin to overlap. However, with the current optimal tracking resolution of 15-20 nm this hypothesis cannot be rigorously verified.

5.4 Conclusion

At low number ratios, large impurities in a crystal of smaller microgel particles, with a size ratio of 0.67, unexpectedly co-crystallize. This is accommodated by the substitution of 4 tetrahedrally coordinated small particles from the crystal by a single impurity; in this configuration distortions of the lattice are minimized to very short length scales. However, this is only possible due to the softness of the particles, as theoretically, only impurity particles with a size ratio of 0.74 and up, which are thus smaller than our impurity particles, should fit in such a tetrahedral void. As a result, we hypothesize that stress is built up in the crystal lattice surrounding an impurity. At high enough impurity concentrations, where $n_i/n > 0.033$, this results in a change in the local surrounding of an impurity particle to a random packing. Consequently, this loss of order surrounding an impurity distorts the lattice over much larger length scales and ultimately leads to vitrification of the sample. Our results show that the crystal-to-glass transition can be accurately investigated in these systems. In this paper we focused on the static structure of the increasingly vitreous samples, but future study will focus on the accompanying changes in the dynamics and dynamical heterogeneity; this might answer open questions relating to the fragility of the glass transition in soft systems.^[35]

References

- [1] J. Kepler and J.F. Nims, *The six-cornered snowflake: a new year's gift*, Paul Dry Books, Philadelphia, PA, (2010).
- [2] M. Marechal, M. Hermes and M. Dijkstra, *Stacking in sediments of colloidal hard spheres*, The Journal of Chemical Physics, **135** (2011), 034510.
- [3] D. Frenkel and A. J. C. Ladd, *New Monte Carlo method to compute the free energy of arbitrary solids. Application to the fcc and hcp phases of hard spheres*, The Journal of Chemical Physics, **81** (1984), 3188-3193.
- [4] P. N. Pusey, W. van Megen, P. Bartlett, B. J. Ackerson, J. G. Rarity and S. M. Underwood, *Structure of crystals of hard colloidal spheres*, Phys. Rev. Lett., **63** (1989), 2753-2756.
- [5] E. B. Sirota, H. D. Ou-Yang, S. K. Sinha, P. M. Chaikin, J. D. Axe and Y. Fujii, *Complete phase diagram of a charged colloidal system: A synchrotron x-ray scattering study*, Phys. Rev. Lett., **62** (1989), 1524-1527.
- [6] P. Yunker, Z. Zhang and A. G. Yodh, *Observation of the Disorder-Induced Crystal-to-Glass Transition*, Phys. Rev. Lett., **104** (2010), 15701.
- [7] J. V. Sanders, *Close-packed structures of spheres of two different sizes I. Observations on natural opal*, Philosophical Magazine A, **42** (1980), 705-720.
- [8] A. B. Schofield, P. N. Pusey and P. Radcliffe, *Stability of the binary colloidal crystals $A\{B\}_2$ and $A\{fB\}_{13}$* , Phys. Rev. E, **72** (2005), 31407.
- [9] P. Sollich and N. B. Wilding, *Crystalline Phases of Polydisperse Spheres*, Phys. Rev. Lett., **104** (2010), 118302.
- [10] P. Sollich and N. B. Wilding, *Polydispersity induced solid-solid transitions in model colloids*, Soft Matter, **7** (2011), 4472-4484.
- [11] D. B. Miracle, D. V. Louzguine-Luzgin, L. V. Louzguina-Luzgina and A. Inoue, *An assessment of binary metallic glasses: correlations between structure, glass forming ability and stability*, International Materials Reviews, **55** (2010), 218-256.

- [12] W. Götze and Th. Voigtmann, *Effect of composition changes on the structural relaxation of a binary mixture*, Phys. Rev. E, **67** (2003), 21502.
- [13] R. Kurita and E. R. Weeks, *Glass transition of two-dimensional binary soft-disk mixtures with large size ratios*, Phys. Rev. E, **82** (2010), 41402.
- [14] T. Narumi, S. V. Franklin, K. W. Desmond, M. Tokuyama and E. R. Weeks, *Spatial and temporal dynamical heterogeneities approaching the binary colloidal glass transition*, Soft Matter, **7** (2011), 1472-1482.
- [15] C. R. Nugent, K. V. Edmond, H. N. Patel and E. R. Weeks, *Colloidal Glass Transition Observed in Confinement*, Phys. Rev. Lett., **99** (2007), 25702.
- [16] D. Paloli, P. S. Mohanty, J. J. Crassous, E. Zaccarelli and P. Schurtenberger, *Fluid-solid transitions in soft-repulsive colloids*, Soft Matter, **9** (2013), 3000-3004.
- [17] S. R. Williams and W. van Megen, *Motions in binary mixtures of hard colloidal spheres: Melting of the glass*, Phys. Rev. E, **64** (2001), 41502.
- [18] Z. Zhang, N. Xu, D. T. N. Chen, P. Yunker, A. M. Alsayed, K. B. Aptowicz, P. Habdas, A. J. Liu, S. R. Nagel and A. G. Yodh, *Thermal vestige of the zero-temperature jamming transition*, Nature, **459** (2009), 230-233.
- [19] V. W. A. de Villeneuve, R. P. A. Dullens, D. G. A. L. Aarts, E. Groeneveld, J. H. Scher, W. K. Kegel and H. N. W. Lekkerkerker, *Colloidal hard-sphere crystal growth frustrated by large spherical Impurities*, Science, **309** (2005), 1231-1233.
- [20] Y. Gao and M. L. Kilfoil, *Accurate detection and complete tracking of large populations of features in three dimensions*, Opt. Express, **17** (2009), 4685-4704.
- [21] P. J. Steinhardt, D. R. Nelson and M. Ronchetti, *Bond-orientational order in liquids and glasses*, Phys. Rev. B, **28** (1983), 784-805.
- [22] F. Ebert, P. Keim and G. Maret, *Local crystalline order in a 2D colloidal glass former*, The European Physical Journal E, **26** (2008), 161-168.

- [23] J. L. Finney, Random Packings and the Structure of Simple Liquids. I. The Geometry of Random Close Packing, *Proceedings of the Royal Society of London A: Mathematical, Physical and Engineering Sciences*, **319**(1970), 479-493.
- [24] W. K. Kegel and A. van Blaaderen, *Direct Observation of Dynamical Heterogeneities in Colloidal Hard-Sphere Suspensions*, *Science*, **287** (2000), 290-293.
- [25] T. M. Truskett, S. Torquato, S. Sastry, P. G. Debenedetti and F. H. Stillinger, *Structural precursor to freezing in the hard-disk and hard-sphere systems*, *Phys. Rev. E*, **58** (1998), 3083-3088.
- [26] A. van Blaaderen and P. Wiltzius, *Real-Space Structure of Colloidal Hard-Sphere Glasses*, *Science*, **270** (1995), 1177-1179.
- [27] C. A. Angell, *Spectroscopy simulation and scattering, and the medium range order problem in glass*, *Journal of Non-Crystalline Solids*, **73** (1985), 1-17.
- [28] T. Kawasaki, T. Araki and H. Tanaka, *Correlation between Dynamic Heterogeneity and Medium-Range Order in Two-Dimensional Glass-Forming Liquids*, *Phys. Rev. Lett.*, **99** (2007), 215701.
- [29] H. W. Sheng, W. K. Luo, F. M. Alamgir, J. M. Bai and E. Ma. *Atomic packing and short-to-medium-range order in metallic glasses*, *Nature*, **439** (2006), 419-425.
- [30] H. Shintani and H. Tanaka, *Frustration on the way to crystallization in glass*, *Nature Physics*, **2** (2006), 200-206.
- [31] H. Tanaka, T. Kawasaki, H. Shintani and K. Watanabe, *Critical-like behaviour of glass-forming liquids*, *Nature materials*, **9** (2010), 324-331.
- [32] K. Watanabe and H. Tanaka, *Direct Observation of Medium-Range Crystalline Order in Granular Liquids Near the Glass Transition*, *Phys. Rev. Lett.*, **100** (2008), 158002.
- [33] P. Dillmann, G. Maret and P. Keim, *Comparison of 2D melting criteria in a colloidal system*, *Journal of Physics: Condensed Matter*, **24** (2012), 464118.
- [34] A. St. John Iyer and L. A. Lyon, *Self-Healing Colloidal Crystals*, *Angewandte Chemie International Edition*, **48** (2009), 4562-4566.
- [35] J. Mattsson, H. M. Wyss, A. Fernandez-Nieves, K. Miyazaki, Z. Hu, D. R. Reichman and D. A. Weitz, *Soft colloids make strong glasses*, *Nature*, **462** (2009), 83-86.

Chapter 6

Mechanics at the Glass-to-Gel Transition of Thermoresponsive Microgel Suspensions

We study the rheology of systems of thermoresponsive microgels at the transition between a repulsive glass and an attractive gel state. We find marked differences between these two colloidal solids, within the same experimental system, due to the different origins for their dynamic arrest. While the rigidity of the repulsive systems depends solely on particle volume fraction, we find that the change in linear elasticity upon introducing attractive bonds in the system scales linearly with the adhesive bond strength which can be tuned with the temperature in our experiments. And while the glasses yield reversibly and with a rate-dependent energy dissipation, bond-reorganization in the gels is suppressed so that their rupture is irreversible and accompanied by a high, but rate-independent, dissipation. These results highlight how colloids with responsive interactions can be employed to shed new light onto solid-solid transitions.

This chapter was published as:

Jeroen Appel, Bart Fölker and Joris Sprakel: *Mechanics at the Glass-to-Gel Transition of Thermoresponsive Microgel Suspensions*, Soft Matter **12** (2016), 2515-2522.

6.1 Introduction

The physical state of a colloidal suspension depends sensitively on the volume fraction of particles and the interactions that act between them. The simplest case is that of colloidal hard spheres, which are governed by entropy, where fluid, crystalline and glassy states can be reached by changing the particle volume fraction and polydispersity. Introducing enthalpic contributions, either repulsive or attractive, creates a much wider array of phases that can be prepared, such as fluids,^[1-5] gels,^[6-10] glasses,^[11-15] crystals^[16-20] and quasicrystals.^[21-25] The study of these phases has provided new insight not only into the colloidal domain, but in some aspects of the properties of matter at large.^[26-28] Colloidal systems can also be prepared to exhibit a responsivity to environmental triggers, which can be easily controlled in an experiment, such as pH,^[29] temperature^[30] or light.^[31] Colloids whose interactions can be tuned by an external trigger can thus in principle be switched between different physical states which allows the study of phase transitions, in much detail. To date, this has been used extensively to study for example the transition between liquids and gels or glasses.^[32-34] Yet, solid-solid transitions have received significantly less attention.

Colloidal microgels have proven a particularly appealing experimental system to study temperature-induced phase transitions. Solvent-swollen microgel particles composed of the thermoresponsive polymer poly(N-isopropyl acrylamide) (pNIPAM) undergo a volume phase transition when the temperature of the surrounding aqueous phase is increased above the lower critical solution temperature (LCST) or cloud point.^[35,36] These particles are typically charge stabilized, such that the particle size can be adjusted with temperature, while they remain colloidally stable. This is for example used to quench systems from a liquid to glass^[37-39] or to create superheated colloidal crystals to study melting.^[40] However, when the ionic strength of the surrounding medium is increased above a critical value, the particles remain colloidally stable below the LCST, due to steric interactions between the swollen pNIPAM hairs, but become attractive once the LCST is crossed.^[30,41,42] This allows a dilute suspension of microgels to reversibly undergo a fluid-gel transition. Moreover, in mixtures of particles with different transition temperatures, sequential gelation of the

multiple components can be achieved by quenching the system along different kinetic.^[42] It remains unknown however, how such a system changes when the initial particle volume fraction below the LCST is sufficiently high to create a glass. This would allow switching between a repulsive glass, arrested by the formation of configurational cages, and an attractive gel, which owes its rigidity to enthalpic bonds between the particles. It remains unknown how the properties of the colloidal suspension change when it undergoes such a transition between two amorphous solids governed by very different microscopic mechanisms.

Here we explore the glass-to-gel transition by studying the rheology of dense suspensions of thermoresponsive pNIPAM microgels, in a temperature range where the system transforms from a glass to a colloidal gel. We first explore the linear rheology at this solid-solid transition and find that the strength of the gel depends only on the adhesive strength of interparticle bonds. While the glass shows only weak frequency-dependence, the gel exhibits a clear poroelastic relaxation mode. Also in the non-linear rheology, marked differences between the glass and gel states appear, exhibiting a distinct discontinuity in non-linear mechanics at the glass-to-gel transition.

6.2 Experimental Section

6.2.1 Materials

N-isopropylacrylamide, *N,N'*-methylenebis(acrylamide), potassium peroxodisulfate, styrene, divinylbenzene and sodium dodecyl sulfate were purchased from Sigma-Aldrich. The fluorescent dye pyrromethene 546 was purchased from Exciton. All chemicals were used as received.

6.2.2 Composite microgel synthesis

Composite microgels with a core-shell structure were synthesized according to a previously described two-step procedure.^[42] First, polystyrene core particles were synthesized in an emulsion polymerization. 670 g water, 186.9 g styrene, 21.0 g *N*-isopropylacrylamide, 2.1 g divinylbenzene, 0.35 g sodium dodecyl sulfate and 0.05 g fluorescent dye were mixed and flushed

with nitrogen for 30 minutes at 75 °C. The polymerization was initiated by addition of 0.35 g potassium peroxodisulfate dissolved in 30 g water. The reaction was left at 75 °C for 24 hours, after which the reaction mixture is filtrated. A microgel shell was then synthesized around the core particles in a precipitation polymerization. 900 g water, 100 g core particle reaction mixture (~20 g core particles), 19.6 g *N*-Isopropylacrylamide and 0.40 g *N,N'*-methylenebisacrylamide were mixed and flushed with nitrogen for 30 minutes at 75 °C. The polymerization was initiated by addition of 0.20 g potassium peroxodisulfate dissolved in 10 g water. The reaction was left to proceed at 75 °C for 4 hours, after which the reaction mixture was filtrated. The composite microgel particles were then washed twice against 0.1 M potassium chloride using centrifugation.

6.2.3 Suspension characterization

Dynamic light scattering: Hydrodynamic particle sizes were measured as a function of temperature by dynamic light scattering (Malvern Zetasizer 2000) at a scattering angle of 173° and a wavelength of 632.8 nm.

Viscometry: The volume fraction of particle stock solutions was determined by measuring the relative viscosity of dilute suspensions. For this, an Ubbelohde capillary viscometer was immersed in a thermostat controlled water bath with a temperature precision of 0.1 °C. The relative viscosities of dilute suspensions were then measured as a function of particle concentration. These data are then fitted to the Einstein- Batchelor relation to determine the volume fraction.

Microscopy: Colloidal suspensions were imaged by fluorescence microscopy (Zeiss LSM 5 EXCITER) using a 100× oil-immersion objective. The temperature was controlled with an Instec TSA02i temperature control stage mounted on the microscope, with 0.01 °C accuracy.

Rheology: Rheological measurements were performed on a TA Discovery HR-3 hybrid rheometer equipped with a 40 mm steel plate-plate geometry and 500 μm plate separation. To prevent solvent evaporation, a solvent trap was placed over the sample. To exclude memory effects, a fresh sample was loaded into the rheometer for each measurement. After loading and equilibration at 20 °C for 5 minutes, the temperature is ramped to a designated temperature at a rate of 1 °C/s, during heating and at the final temperature we probe the linear viscoelasticity of the suspension under mild

oscillation with a strain of $\gamma = 0.1\%$ and frequency $\omega = 0.628 \text{ rad/s}$. The sample is then subjected to a frequency sweep with $\omega = 10^{-1} - 10^2 \text{ rad/s}$, with $\gamma = 0.1\%$. We investigate how the material yields in a strain amplitude sweep with increasing strain of $\gamma = 10^{-1} - 10^4\%$, at a fixed frequency $\omega = 0.628 \text{ rad/s}$. Finally we probe how the sample yields in rotational shear start-up experiments, in the glass state at 20°C and the gel state at 45°C , to investigate how shear rate affects the yielding process. We vary the shear rate $\dot{\gamma}$ between 10^{-2} and 10^1 1/s .

6.3 Results and Discussion

6.3.1 Suspension characteristics

Thermoresponsive microgels can be synthesized following widely differing recipes, which give rise to microgels with subtly different characteristics.^[43-49] Here we synthesize composite microgels, with a fluorescent polystyrene core ($d_{\text{core}} = 210 \text{ nm}$) and a thick cross-linked pNIPAM shell of 150 nm at 20°C , giving the composite microgel a diameter (d) of 500 nm at 20°C . We have previously shown that these composite particles allow both tuning of the pair interactions and accurate visualization in confocal microscopy, e.g. in capillary ordering^[50] and crystal-to-glass transitions.^[51] Despite the presence of a solid core, the thermal responsivity of the pNIPAM shell is maintained, characterized by the lower critical solution temperature (LCST) at 31°C ; this gives rise to a temperature dependent shell size as shown in Figure 6.1a. From capillary viscosimetry, the volume fraction (ϕ) of the suspension at 20°C is known. With the temperature-dependent size of the microgels determined from DLS we can now compute the volume fraction at other temperatures. As can be seen in Figure 6.1a, the volume fraction of our suspensions decreases between 20 and 34°C by almost an order of magnitude, and remains constant above 35°C as the particles are fully collapsed for $T \gg T_{\text{LCST}}$.

Above the LCST, pNIPAM becomes insoluble and phase separates from its aqueous solvent. As a result, collapsed layers of pure pNIPAM induce an attractive interaction between surfaces.^[30] For our microgels, this attraction is mitigated by the presence of charged moieties at the particle surface; in absence of salt, increasing T above the LCST leads to particle

shrinkage but no aggregation. However, upon adding salt to screen these repulsive interactions that keep the suspension stable above the collapse temperature, a temperature-dependent attraction develops in the system. Due to the interplay between electrostatic repulsion, tuned by salt concentration, and attraction strength, tuned by temperature, the physical state of the microgel suspension can be carefully controlled with two environmental parameters.^[41,42] Confocal microscopy imaging reveals that a diluted microgel suspension, with $\phi = 0.39$ at 20 °C and $[K^+][Cl^-] = 0.1\text{ M}$, transitions from a dispersed fluid state at 30 °C (Figure 6.1b) to a percolated gel state at 35 °C (Figure 6.1c). Interestingly, this temperature-induced gelation is almost completely reversible.

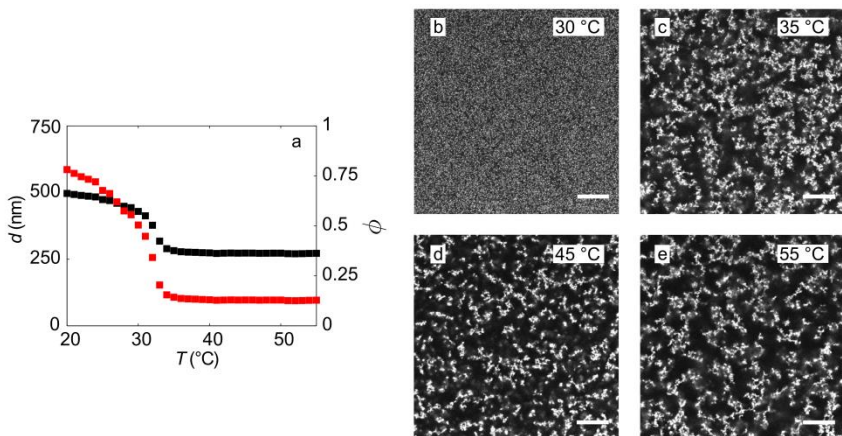


Figure 6.1: a) Hydrodynamic diameter of core-shell microgels as a function of temperature (red squares) and corresponding change in volume fraction (black squares) of the suspension used in the rheology experiments. Confocal microscopy images of microgel suspensions below (b, 30 °C) and above the LCST (c, 35 °C, d, 45 °C, e, 55 °C). Scale bars indicate 10 μm .

The phase behavior of colloidal suspensions depends on particle volume fraction, polydispersity and interparticle interactions, exhibiting solid phases such as crystals, glasses or gels. The structure, dynamics and mechanics of these colloidal solids have been extensively studied with rheology and microscopy.^[18,52-58] By contrast, much less is known about the nature of the transition between two of these distinct solid states. In this paper, we focus

on the glass-to-gel transition which is readily accessible in these thermoresponsive colloidal systems.^[39,41,42,59,60]

We concentrate the microgels in 0.1 M [K⁺][Cl⁻] to $\phi = 0.78$ using centrifugation. At low temperatures the suspension is in a repulsive soft glassy state at this volume fraction. Upon increasing the temperature, the volume fraction decreases gradually, weakening the glass, until at 31 °C, which we denote as T_{gel} , attractive interactions come into play. At $T > T_{gel}$, the microgels aggregate into a sample-spanning, heterogeneous colloidal gel. This temperature-induced glass-to-gel transition, which is fully reversible, thus allows us to study in detail the rheology of suspensions at this transition between two disordered colloidal solids governed by distinctly different microscopic mechanisms. Whereas elasticity in the glass is provided by repulsive contact interactions of colloids caged by neighboring particles, the gel is mechanically rigid due to the formation of attractive particle bonds and a heterogeneous percolated structure.

6.3.2 Linear rheology

We use oscillatory rheology to probe the temperature-dependent viscoelastic properties of the suspension in a wide range of temperatures (20-55 °C) across the gelation point. At temperatures below T_{gel} , where the sample is in its repulsive state, the shear elasticity of the suspension is finite and constant over time (Figure 6.2a). This is consistent with a densely-packed glassy state, in which microgels are caged by their neighbors and cannot diffuse freely.^[53,61-65] Colloidal glasses, including microgel systems, are known to exhibit distinct ageing behavior when they are quenched from a liquid state to the solid regime.^[66-68] In our experiments, we always quench the temperature from low to high, thus only lowering the volume fraction at temperatures below the gelation point. In our experiments, we do not observe any noticeable signs of de-aging in this quench from high to lower packing density. Above T_{gel} , the suspension transforms into an attraction-driven percolated gel (Figure 6.1c-e), characterized by a shear storage modulus G' that increases with time as the network begins to form and ages (Figure 6.2a). Colloidal gels are not equilibrium states. In an attempt to maximize the number of attractive interactions, gels will continuously reorganize and coarsen as individual bonds between particles break and

reform due to thermal fluctuations.^[16] As this process proceeds until the gel rigidity is lost and the material fails catastrophically from within in order to phase separate,^[69] a true steady-state does not exist for colloidal gels. As a proxy for the gel elasticity we take the viscoelastic moduli after 30 minutes of aging. We confirmed that using a different choice for this interval does not change the trends we discuss below. The elastic moduli as a function of temperature show the distinct transition between glass and gel (Figure 6.2b).

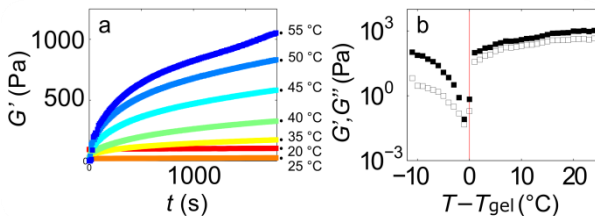


Figure 6.2: a) Evolution of the storage modulus over time during heating with a ramp rate of 1 °C/s to a final temperature as indicated b) Shear moduli (G' , filled squares = G' , open squares = G'') taken at $t = 1800$ s after the quench, exhibiting a glass-gel transition at T_{gel} (solid line).

In the gel state, $T > T_{gel}$, we find that G' and G'' increase proportionally with temperature. Both at temperatures below the LCST and those above, we find that the storage modulus is in excess of the loss modulus, indicative of solid-like behavior at this frequency. Only exactly at the transition temperature, we find $G' \approx G''$, which indicates a liquid-like behavior separating the glass and gel states. A similar intermediate state is observed in the repulsive-to-attractive glass transition for hard sphere colloids.^[53] As the volume fraction remains constant at 0.13 above 35 °C, this effect cannot be explained by further changes in volume fraction. In fact, the change in shear moduli of the gel phase with respect to the transition point, plotted as $\Delta G'$ and $\Delta G''$ in Figure 6.3a, increases linearly with distance from the gel point $T - T_{gel}$. This could either result from changes in the gel microstructure or from an increase in particle bonding strength as T is increased. From the confocal microscopy images (Figure 6.1c-e) we see no obvious changes in gel microstructure as the temperature is increased further above T_{gel} .

It is known that the adhesive interactions between grafted pNIPAM chains increase in strength above the LCST.^[70] This is due to the reduction of water content in the collapsed pNIPAM coacervate as the temperature is

raised above the LCST; this results in an increase of the interfacial tension between the insoluble pNIPAM phase and the surrounding aqueous solution. Previously, we measured the temperature-dependent adhesion energy (U_a) between pNIPAM layers at colloidal surfaces using colloidal probe Atomic Force Microscopy.^[30] We indeed find an excellent linear correlation between the experimentally-determined adhesion energy between particle surfaces and the increase in gel elasticity due to bonding interactions (Figure 6.3b). In theory, for bond-stretching mechanics, we expect the shear elasticity to be set by the spring constant of the interparticle bonds, determined by the curvature of the minimum in the interaction potential. However, with a fixed range of interaction, set by the thickness of the collapsed pNIPAM layer (~25 nm), a change in attraction strength will give rise to a concomitant change in the effective spring constant of the particle bonds. This linear dependence of modulus with interparticle attraction appears to be more generic in nature, as it was observed previously for hard colloids decorated with short thermoresponsive hairs.^[30] This allows us to explore with relative ease how the properties of a colloidal gel change when the bond strength is adjusted, while the gel microstructure remains unaltered, whereas these properties are intricately linked in most other attractive colloidal systems.^[71]

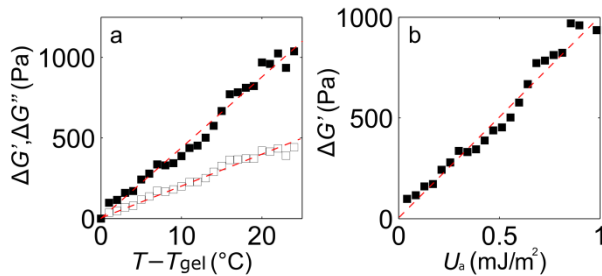


Figure 6.3: a) Differential shear moduli $\Delta G' = G'(T) - G'(T_{gel})$ (filled symbols) and $\Delta G'' = G''(T) - G''(T_{gel})$ (open symbols) as a function of distance to the transition point, b) $\Delta G'$ plotted as a function of adhesion energy (U_a) between the particles. Dotted lines to guide the eye.

Not only the magnitude of the shear elasticity exhibits a distinct change at the glass-to-gel transition, but also the frequency-dependence of the shear moduli is very different between the glass and gel states. Typical frequency sweeps in the glass ($T = 20$ °C), around the transition ($T = 35$ °C) and deep

in the gel regime ($T = 50$ °C) are shown in Figure 6.4a. For the repulsive glasses, we find the characteristic frequency-dependence for soft glassy materials. The shear elasticity G' shows a frequency-independent plateau over the measured frequency range. By contrast G'' exhibits a distinct minimum, which is attributed to the timescale for particle de-caging in the glass. In the gel state a strong frequency-dependence of both G' and G'' are observed. Even though the gels exhibit a finite yield stress, and thus remain solid like at all frequencies, we find that G' and G'' cross at a finite frequency. At low frequencies, the solid-like behavior of the kinetically-arrested network dominates and $G' > G''$. At higher frequencies, contributions from both fluid flow through the porous network^[72] and thermal fluctuations of the colloidal gel strands^[73] begin to contribute to the mechanics, causing a crossover between storage and loss moduli. The characteristic time scale for this crossover is virtually-independent of the distance to the gel point (Figure 6.4b). This suggests that the high-frequency behavior is governed by poroelasticity rather than gel strand fluctuations, as we would expect the stiffness of aggregated strands of attractive colloids to increase with increasing attraction strength, which would decrease the flexibility of the strands.

6.3.3 Non-linear rheology

Colloidal glasses and gels are two disordered colloidal solids which are governed by different mechanisms for dynamic arrest. While relaxation is halted in glasses due to the formation of configurational cages, the solid-like behavior of gels originates from the formation of enthalpic interparticle bonds. Not only does this change in microscopic physics alter the linear rheology as discussed above, it has a marked effect on the non-linear mechanics as well.

Non-linear rheology experiments on soft solids often suffer from pronounced wall slip. Microgels made of pNIPAM tend to adhere strongly to surfaces.^[74] To verify that this is sufficient to prevent severe wall slip, we perform strain sweeps in the gel state (40 °C) at three different gap sizes (Figure 6.5a). Indeed, the linear and non-linear regimes in the strain amplitude sweep are independent of gap width, verifying that wall slip is not severe for these samples and this measurement geometry.

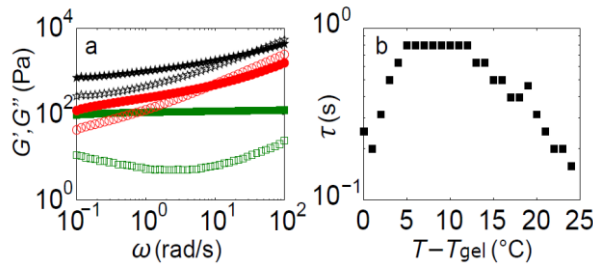


Figure 6.4: a) Shear moduli G' (closed symbols) and G'' (open symbols) as a function of frequency at 20 (green squares), 35 (red circles) and 50 °C (black stars). b) The characteristic time for the cross-over in moduli observed in the gel state.

Characteristic strain sweeps for the glass and gel are shown in Figure 6.5b. In both cases, the shear moduli are strain-independent for low strains, until nonlinearities emerge and the material yields at a characteristic yield strain (γ_y). For the soft glasses, a peak in the loss modulus is observed when yielding occurs. This is attributed to distinct non-affine, cooperative, rearrangements in the glass, which dissipate strain energy. Their frequency increases as the yielding transition is approached, thus increasing the rate of viscous dissipation.^[75-77] In the gel, yielding is more abrupt without precursors in G'' ; due to the high bonding energy (Figure 6.3b), which we calculate to range from several tens to hundreds of $k_B T$ /bond, stress-driven structural rearrangements prior to bond rupture and yielding are suppressed. It thus appears that the yielding of the glass exhibits some degree of plasticity or ductility, while that of the gel is more “brittle” in nature.

Sufficiently far away from the transition, the yield strains appear independent of temperature, both in the glass and gel states. However, close to the glass-to-gel transition, a discontinuity in the non-linear rheology becomes apparent. While the yield strain appears to diverge as the glass weakens upon approaching the transition, the yield strain of the gel vanishes at T_{gel} (Figure 6.5c). As the glass approaches the transition, $T < T_{gel}$, the volume fraction decreases which lowers the glass elasticity. In a purely repulsive glass, the yield strain decreases as the volume fraction decreases,^[78] however, in our system an attractive potential arises as the volume fraction decreases, causing the yield strain to increase. If gelation would be suppressed, the glass would melt into a liquid without a significant shear modulus. As the glass-to-liquid transition is continuous^[58] and the

liquid does not exhibit yielding, the yield strain must grow to infinity close to the glass-to-liquid transition. In our experiment however, the sample gels before the glass melts completely. Very close to the gel point, the percolated colloidal gels are very weak as the bond strength is barely sufficient to stabilize the solid phase. Even small deformations, stretching the marginally-stable bonds, are sufficient to cause the structure to yield. In fact, upon approaching the gel point, the stability of the gel vanishes critically[79] and may thus be expected to reach a fragile state where the linear regime vanishes.

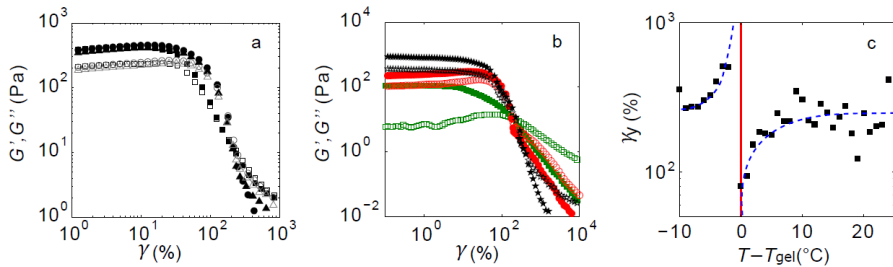


Figure 6.5: a) Shear moduli G' (closed symbols) and G'' (open symbols) as a function of strain amplitude at 40 °C for three different gap sizes: 0.25 mm (squares), 0.50 mm (circles) and 1.00 mm (triangles), b) Strain sweeps at different temperatures at 20 (squares), 35 (circles) and 50 °C (stars). c) Yield strain as a function of distance to the transition point indicated by the solid line. Dotted lines are a guide to the eye.

The discontinuity in non-linear rheology at the glass-to-gel transition demarcates two solid phases of which both structure, linear and non-linear dynamics are governed by completely different microscopic mechanisms. Yielding in the glass state involves the transformation of local configurational cages which reform as soon as the applied deformation is removed. Indeed, sequential ramping of the strain amplitude from low to high and back, shows no hysteresis for the repulsive soft glasses at 20 °C (Figure 6.6a). This suggests that no noticeable anisotropy is generated in the microstructure of the system which is governed by repulsive interactions alone. By contrast, yielding in a colloidal gel involves breaking of enthalpic bonds between particles. The colloidal gel is a kinetically-trapped non-equilibrium structure en-route to complete phase separation.^[80] The re-

association of broken bonds will thus occur with a tendency towards configurations that increase the local contact number, thereby coarsening the structure and reducing its connectivity.^[81,82] Even under very weak gravitational stresses this can lead colloidal gels to a spontaneous yielding transition in absence of mechanical deformation.^[69,83,84] For the gels, at 45 °C, we find strong hysteresis when the gel is continuously yielded, reformed, and yielded again (Figure 6.6b); not only does the yield strain gradually shift to lower values, but also the gel elasticity reduces as connectivity of the structure is gradually lost. Clearly, while the structural rearrangements that cause yielding in repulsive glasses are reversible, those in colloidal gels are irreversible in nature.

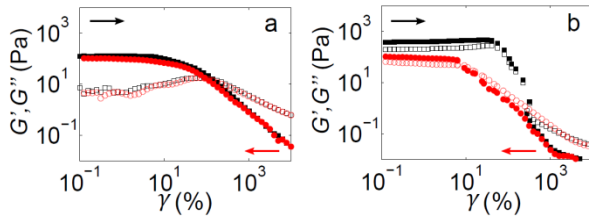


Figure 6.6: Yielding hysteresis probed by forward- and backward-strain sweeps as indicated by the arrows for the glass (a, 20 °C) and gel (b, 45 °C).

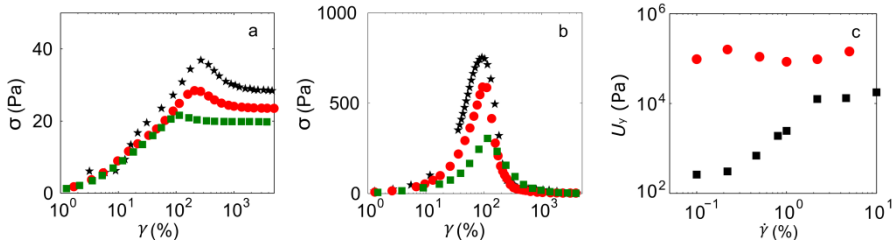


Figure 6.7: Shear start-up experiments for different strain rates for the glass (a, 20 °C) and the gel (b, 45 °C). c) Corresponding energy dissipation during yielding, from the integral of the stress-overshoot, as a function of strain rate for the glass (squares) and gel (circles).

We finally explore the rate-dependence of the yielding transition. To do so, we perform rotational shear start-up experiments as a function of the applied strain rate. A distinct stress overshoot is observed during yielding both for the glass and gel states (Figure 6.7a). To evaluate the energy dissipation U_y

during yielding, we integrate the area under the stress overshoot. Interestingly, we find a strong rate-dependence for the yielding process of the glass, which we attribute to the competition between the shear deformation rate and the inherent rate of thermal re-arrangements in the glass. By contrast, energy dissipation in the gel is significantly larger, as it involves the breaking of enthalpic bonds, but shows virtually no rate dependence. Clearly, thermally activated bond rupture in the gel does not occur at these frequencies, probably due to the high bonding energy sufficiently far away from T_{gel} .

6.4 Conclusion

In this paper we have studied the rheology of suspensions of thermoresponsive microgels across the transition from repulsive glass to attractive gel. We find that gels from these particles whose adhesive forces can be tuned by temperature, exhibit a shear elasticity governed by bond strength alone. This allows us to investigate how the mechanics of the colloidal gel are affected by weakening the bond strength while keeping its microstructure intact. We find that the non-linear rheology of the gel exhibits a fragile state at the transition point, which exhibits a discontinuity in the yield strain. Due to the high bond strength between these thermoresponsive colloids, at temperatures well above the gel point, thermally-activated bond-rupture is suppressed. This results in yielding which exhibits no rate dependency and is irreversible. By contrast, thermal relaxation modes exist in the glass, which renders its yielding rate-dependent but reversible. These results show how these systems which exhibit temperature-triggered interactions allow exploration of the mechanics at and around solid-solid transitions. In the system explored here, attractive interactions coincided with a collapse of the particles; as a result, the repulsive glass melts partially before it transforms into a gel. Using a different particle architecture in which only a very thin thermoresponsive shell is present, could allow introducing temperature-dependent attractions while keeping suspension volume fraction constant. In the future, this could make it possible to also study the repulsive-to-attractive glass transition, of which many details remain elusive to date.

References

- [1] N. A. M. Verhaegh, J. S. van Duijneveldt, J. K. G. Dhont and H. N. W. Lekkerkerker, *Fluid-fluid phase separation in colloid-polymer mixtures studied with small angle light scattering and light microscopy*, Physica A: Statistical Mechanics and its Applications, **230** (1996), 409-436.
- [2] G. H. Koenderink, S. Sacanna, D. G. A. L. Aarts and A. P. Philipse, *Rotational and translational diffusion of fluorocarbon tracer spheres in semidilute xanthan solutions*, Phys. Rev. E, **69** (2004), 21804.
- [3] D. G. A. L. Aarts, M. Schmidt and H. N. W. Lekkerkerker, *Direct Visual Observation of Thermal Capillary Waves*, Science, **304** (2004), 847-850.
- [4] D. Derks, D. G. A. L. Aarts, D. Bonn, H. N. W. Lekkerkerker and A. Imhof, *Suppression of Thermally Excited Capillary Waves by Shear Flow*, Phys. Rev. Lett., **97** (2006), 38301.
- [5] G. S. Redner, M. F. Hagan and A. Baskaran, *Structure and Dynamics of a Phase-Separating Active Colloidal Fluid*, Phys. Rev. Lett., **110** (2013), 55701.
- [6] P. N. Pusey and W. van Megen, *Phase behaviour of concentrated suspensions of nearly hard colloidal spheres*, Nature, **320** (1986), 340-342.
- [7] U. Gasser, E. R. Weeks, A. Schofield, P. N. Pusey and D. A. Weitz, *Real-Space Imaging of Nucleation and Growth in Colloidal Crystallization*, Science, **292** (2001), 258-262.
- [8] S. Wong, V. Kitaev and G. A. Ozin, *Colloidal Crystal Films: Advances in Universality and Perfection*, Journal of the American Chemical Society, **125** (2003), 15589-15598.
- [9] P. Schall, I. Cohen, D. A. Weitz and F. Spaepen, *Visualization of Dislocation Dynamics in Colloidal Crystals*, Science, **305** (2004), 1944-1948.
- [10] V. N. Manoharan, *Colloidal matter: Packing, geometry, and entropy*, Science, **349** (2015), 1253751.
- [11] T. G. Mason and D. A. Weitz, *Linear Viscoelasticity of Colloidal Hard Sphere Suspensions near the Glass Transition*, Phys. Rev. Lett., **75** (1995), 2770-2773.

- [12] E. R. Weeks, J. C. Crocker, A. C. Levitt, A. Schofield and D. A. Weitz, *Three-Dimensional Direct Imaging of Structural Relaxation Near the Colloidal Glass Transition*, *Science*, **287** (2000), 627-631.
- [13] D. Bonn, S. Tanase, B. Abou, H. Tanaka and J. Meunier, *Laponite: Aging and Shear Rejuvenation of a Colloidal Glass*, *Phys. Rev. Lett.*, **89** (2002), 15701.
- [14] E. R. Weeks and D. A. Weitz, *Properties of Cage Rearrangements Observed near the Colloidal Glass Transition*, *Phys. Rev. Lett.*, **89** (2002), 95704.
- [15] K. H. Nagamanasa, S. Gokhale, A. K. Sood and R. Ganapathy, *Direct measurements of growing amorphous order and non-monotonic dynamic correlations in a colloidal glass-former*, *Nature Physics*, **11** (2015), 403-408.
- [16] L. Cipelletti, S. Manley, R. C. Ball and D. A. Weitz, *Universal Aging Features in the Restructuring of Fractal Colloidal Gels*, *Phys. Rev. Lett.*, **84** (2000), 2275-2278.
- [17] P. Varadan and M. J. Solomon, *Shear-Induced Microstructural Evolution of a Thermoreversible Colloidal Gel*, *Langmuir*, **17** (2001), 2918-2929.
- [18] V. J. Anderson and H. N. W. Lekkerkerker, *Insights into phase transition kinetics from colloid science*, *Nature*, **416** (2002), 811-815.
- [19] C. J. Rueb and C. F. Zukoski, *Viscoelastic properties of colloidal gels*. *Journal of Rheology*, **41** (1997), 197-218.
- [20] N. Koumakis and G. Petekidis, *Two step yielding in attractive colloids: Transition from gels to attractive glasses*, *Soft Matter*, **7** (2011), 2456-2470.
- [21] M. Schmiedeberg and H. Stark, *Colloidal Ordering on a 2D Quasicrystalline Substrate*, *Phys. Rev. Lett.*, **101** (2008), 218302.
- [22] D. V. Talapin, E. V. Shevchenko, M. I. Bodnarchuk, X. Ye, J. Chen and C. B. Murray, *Quasicrystalline order in self-assembled binary nanoparticle superlattices*, *Nature*, **461** (2009), 964-967.
- [23] S. Fischer, A. Exner, K. Zielske, J. Perlich, S. Deloudi, W. Steurer, P. Lindner and S. Förster, *Colloidal quasicrystals with 12-fold and 18-fold diffraction symmetry*, *Proceedings of the National Academy of Sciences*, **108** (2011), 1810-1814.

- [24] M Schmiedeberg and H Stark, *Comparing light-induced colloidal quasicrystals with different rotational symmetries*, Journal of Physics Condensed Matter, **24** (2012), 284101.
- [25] L. Zaidouny, T. Bohlein, J. Roth and C. Bechinger, *Periodic average structures of colloidal quasicrystals*, Soft Matter, **10** (2014), 8705-8710.
- [26] W. C. K. Poon, *Colloids as Big Atoms*, Science, **304** (2004), 830-831.
- [27] T. H. Zhang and X. Y. Liu, *Nucleation: What happens at the initial stage?*, Angewandte Chemie-International Edition, **48** (2009), 1308-1312.
- [28] S. M. Liddle, T. Narayanan and W. C. K. Poon, *Polydispersity effects in colloid-polymer mixtures*, Journal of Physics: Condensed Matter, **23** (2011), 194116.
- [29] H. Monteillet, M. Workamp, J. Appel, J. M. Kleijn, F. A. M. Leermakers and J. Sprakel, *Ultrastrong Anchoring Yet Barrier-Free Adsorption of Composite Microgels at Liquid Interfaces*, Advanced Materials Interfaces, **1** (2014), 1300121.
- [30] T. E. Kodger and J. Sprakel, *Thermosensitive Molecular, Colloidal, and Bulk Interactions Using a Simple Surfactant*, Advanced Functional Materials, **23** (2013), 475-482.
- [31] I. de Feijter, L. Albertazzi, A. R. A. Palmans and I. K. Voets, *Stimuli-Responsive Colloidal Assembly Driven by Surface-Grafted Supramolecular Moieties*, Langmuir, **31** (2015), 57-64.
- [32] C. P. Royall, S. R. Williams, T. Ohtsuka and H. Tanaka, *Direct observation of a local structural mechanism for dynamic arrest*, Nature Materials, **7** (2008), 556-561.
- [33] H. Tanaka, J. Meunier and D. Bonn, *Nonergodic states of charged colloidal suspensions: Repulsive and attractive glasses and gels*, Phys. Rev. E, **69** (2004), 31404.
- [34] H. Tanaka, T. Kawasaki, H. Shintani and K. Watanabe, *Critical-like behaviour of glass-forming liquids*, Nature materials, **9** (2010), 324-331.
- [35] C. Boutris, E. G. Chatzi and C. Kiparissides, *Characterization of the LCST behaviour of aqueous poly(*N*-isopropylacrylamide) solutions by thermal and cloud point techniques*, Polymer, **38** (1997), 2567-2570.

- [36] I. Berndt, J. S. Pedersen and W. Richtering, *Temperature-sensitive core-shell microgel particles with dense shell*, Angewandte Chemie-International Edition, **45** (2006), 1737-1741.
- [37] Z. Zhang, N. Xu, D. T. N. Chen, P. Yunker, A. M. Alsayed, K. B. Aptowicz, P. Habdas, A. J. Liu, S. R. Nagel and A. G. Yodh, *Thermal vestige of the zero-temperature jamming transition*, Nature, **459** (2009), 230-233.
- [38] M. Siebenbürger, M. Fuchs, H. Winter and M. Ballauff, *Viscoelasticity and shear flow of concentrated, noncrystallizing colloidal suspensions: Comparison with mode-coupling theory*, Journal of Rheology, **53** (2009), 707-726.
- [39] V. Carrier and G. Petekidis, *Nonlinear rheology of colloidal glasses of soft thermosensitive microgel particles*, Journal of Rheology, **53** (2009), 245-273.
- [40] Z. Wang, F. Wang, Y. Peng, Z. Zheng and Y. Han, *Imaging the homogeneous nucleation during the melting of superheated colloidal crystals*, Science, **338** (2012), 87-90.
- [41] G. Romeo, A. Fernandez-Nieves, H. M. Wyss, D. Acierno and D. A. Weitz, *Temperature-Controlled Transitions Between Glass, Liquid, and Gel States in Dense p-NIPA Suspensions*, Advanced Materials, **22** (2010), 3441-3445.
- [42] J. Appel, N. de Lange, H. M. van der Kooij, T. van de Laar, J. B. ten Hove, T. E. Kodger and J. Sprake, *Temperature Controlled Sequential Gelation in Composite Microgel Suspensions*, Particle & Particle Systems Characterization, **32** (2015), 764-770.
- [43] C. D. Jones and L. A. Lyon, *Synthesis and Characterization of Multiresponsive CoreShell Microgels*, Macromolecules, **33** (2000), 8301-8306.
- [44] I. Berndt and W. Richtering, *Doubly Temperature Sensitive CoreShell Microgels*, Macromolecules, **36** (2003), 8780-8785.
- [45] S. Chai, J. Zhang, T. Yang, J. Yuan and S. Cheng, *Thermoresponsive microgel decorated with silica nanoparticles in shell: Biomimetic synthesis and drug release application*, Colloids and Surfaces A: Physicochemical and Engineering Aspects, **356** (2010), 32-39.

- [46] R. Acciaro, T. Gilányi and I. Varga, *Preparation of Monodisperse Poly(N-isopropylacrylamide) Microgel Particles with Homogenous Cross-Link Density Distribution*, Langmuir, **27** (2011), 7917-7925.
- [47] T. Still, K. Chen, A. M. Alsayed, K. B. Aptowicz and A. G. Yodh, *Synthesis of micrometer-size poly(N-isopropylacrylamide) microgel particles with homogeneous crosslinker density and diameter control*, Journal of Colloid and Interface Science, **405** (2013), 96-102.
- [48] D. Suzuki and C. Kobayashi, *Raspberry-Shaped Composite Microgel Synthesis by Seeded Emulsion Polymerization with Hydrogel Particles*, Langmuir, **30** (2014), 7085-7092.
- [49] B. P. Tripathi, N. C. Dubey and M. Stamm, *Hollow Microgel Based Ultrathin Thermoresponsive Membranes for Separation, Synthesis, and Catalytic Applications*, ACS Applied Materials & Interfaces, **6** (2014), 17702-17712.
- [50] D. Ershov, J. Sprakel, J. Appel, M. A. Cohen Stuart and J. van der Gucht, *Capillarity-induced ordering of spherical colloids on an interface with anisotropic curvature*, Proceedings of the National Academy of Sciences of the United States of America, **110** (2013), 9220-9224.
- [51] R. Higler, J. Appel and J. Sprakel, *Substitutional impurity induced vitrification in microgel crystals*, Soft Matter, **9** (2013), 5372-5379.
- [52] Y. Xia, B. Gates, Y. Yin and Y. Lu, *Monodispersed Colloidal Spheres: Old Materials with New Applications*, Advanced Materials, **12** (2000), 693-713.
- [53] K. N. Pham, A. M. Puertas, J. Bergenholz, S. U. Egelhaaf, A. Moussaid, P. N. Pusey, A. B. Schofield, M. E. Cates, M. Fuchs and W. C. K. Poon, *Multiple Glassy States in a Simple Model System*, Science, **296** (2002), 104-106.
- [54] F. Sciortino, *Disorderd materials: One liquid, two glasses*, Nature Materials, **1** (2002), 145-146.
- [55] V. Prasad, D. Semwogerere and E. R. Weeks, *Confocal microscopy of colloids*, Journal of Physics: Condensed Matter, **19** (2007), 113102.
- [56] A. Yethiraj, *Tunable colloids: control of colloidal phase transitions with tunable interactions*, Soft Matter, **3** (2007), 1099-1115.

- [57] E. Zaccarelli, *Colloidal gels: equilibrium and non-equilibrium routes*, Journal of Physics: Condensed Matter, **19** (2007), 323101.
- [58] G. L. Hunter and E. R. Weeks, *The physics of the colloidal glass transition*, Reports on Progress in Physics, **75** (2012), 66501.
- [59] H. Senff, W. Richtering, C. Norhausen, A. Weiss and M. Ballauff, *Rheology of a Temperature Sensitive CoreShell Latex*, Langmuir, **15** (1999), 102-106.
- [60] M. Siebenburger, M. Fuchs and M. Ballauff, *Core-shell microgels as model colloids for rheological studies*, Soft Matter, **8** (2012), 4014-4024.
- [61] K. A. Dawson, *The glass paradigm for colloidal glasses, gels, and other arrested states driven by attractive interactions*, Current Opinion in Colloid & Interface Science, **7** (2002), 218-227.
- [62] E. R. Weeks and D. A. Weitz, *Subdiffusion and the cage effect studied near the colloidal glass transition*, Chemical Physics, **284** (2002), 361-367.
- [63] C. Mayer, E. Zaccarelli, E. Stiakakis, C. N. Likos, F. Sciortino, A. Munam, M. Gauthier, N. Hadjichristidis, H. Iatrou, P. Tartaglia, H. Löwen and D. Vlassopoulos, *Asymmetric caging in soft colloidal mixtures*, Nature Materials, **7** (2008), 780-784.
- [64] E. Zaccarelli and W. C. K. Poon, *Colloidal glasses and gels: The interplay of bonding and caging*, Proceedings of the National Academy of Sciences of the United States of America, **106** (2009), 15203-15208.
- [65] C. Christopoulou, G. Petekidis, B. Erwin, M. Cloitre and D. Vlassopoulos, *Ageing and yield behaviour in model soft colloidal glasses*, Philosophical Transactions of the Royal Society of London A: Mathematical, Physical and Engineering Sciences, **367** (2009), 5051-5071.
- [66] X. Di, K. Z. Win, G. B. McKenna, T. Narita, F. Lequeux, S. R. Pullela, and Z. Cheng, *Signatures of structural recovery in colloidal glasses*, Phys. Rev. Lett., **106** (2011), 095701.
- [67] X. Di, X. Peng and G. B. McKenna, *Dynamics of a thermoresponsive microgel colloid near to the glass transition*, The Journal of Chemical Physics, **140** (2014), 054903.

- [68] X. Peng and G. B. McKenna, *Comparison of the physical aging behavior of a colloidal glass after shear melting and concentration Jumps*, Phys. Rev. E, **90** (2014), 050301.
- [69] J. Sprakel, S. B. Lindström, T. E. Kodger and D. A. Weitz, *Stress Enhancement in the Delayed Yielding of Colloidal Gels*, Phys. Rev. Lett., **106** (2011), 248303.
- [70] I. B. Malham and L. Bureau, *Density Effects on Collapse, Compression, and Adhesion of Thermoresponsive Polymer Brushes*, Langmuir, **26** (2010), 4762-4768.
- [71] A. D. Dinsmore and D. A. Weitz, *Direct imaging of three-dimensional structure and topology of colloidal gels*, Journal of Physics: Condensed Matter, **14** (2002), 7581-7597.
- [72] V. Trappe and D. A. Weitz, *Scaling of the Viscoelasticity of Weakly Attractive Particles*, Phys. Rev. Lett., **85** (2000), 449-452.
- [73] M. L. Gardel, J. H. Shin, F. C. MacKintosh, L. Mahadevan, P. A. Matsudaira and D. A. Weitz, *Scaling of F-Actin Network Rheology to Probe Single Filament Elasticity and Dynamics*, Phys. Rev. Lett., **93** (2004), 188102.
- [74] S. Schmidt, T. Hellweg and R. von Klitzing, *Packing Density Control in p(NIPAM-co-AAc) Microgel Monolayers: Effect of Surface Charge, pH, and Preparation Technique*, Langmuir, **24** (2008), 12595-12602.
- [75] P. Sollich, *Rheological constitutive equation for a model of soft glassy materials*, Phys. Rev. E, **58** (1998), 738-759.
- [76] C. Derec, A. Ajdari and F. Lequeux, *Rheology and aging: A simple approach*, The European Physical Journal E, **4** (2001), 355-361.
- [77] K. Miyazaki, H. M. Wyss, D. A. Weitz and D. R. Reichman, *Nonlinear viscoelasticity of metastable complex fluids*, Europhysics Letters, **75** (2006), 915-921.
- [78] P. Menut, S. Seiffert, J. Sprakel and D. A. Weitz, *Does size matter? Elasticity of compressed suspensions of colloidal- and granular-scale Microgels*, Soft Matter, **8** (2012), 156-164.
- [79] V. Trappe, V. Prasad, L. Cipelletti, P. N. Segre and D. A. Weitz, *Jamming phase diagram for attractive particles*, Nature, **411** (2001), 772-775.

- [80] P. J. Lu, E. Zaccarelli, F. Ciulla, A. B. Schofield, F. Sciortino and D. A. Weitz, *Gelation of particles with short-range attraction*, Nature, **453** (2008), 499-503.
- [81] T. Kawasaki, T. Araki and H. Tanaka, *Correlation between Dynamic Heterogeneity and Medium-Range Order in Two-Dimensional Glass-Forming Liquids*, Phys. Rev. Lett., **99** (2007), 215701.
- [82] Z. Shao, A. S. Negi and C. O. Osuji, *Role of interparticle attraction in the yielding response of microgel suspensions*, Soft Matter, **9** (2013), 5492-5500.
- [83] S. Manley, J. M. Skotheim, L. Mahadevan and D. A. Weitz, *Gravitational Collapse of Colloidal Gels*, Phys. Rev. Lett., **94** (2005), 218302.
- [84] W. C. K. Poon, L. Starrs, S. P. Meeker, A. Moussaid, R. M. L. Evans, P. N. Pusey and M. M. Robins, *Delayed sedimentation of transient gels in colloid-polymer mixtures: dark-field observation, rheology and dynamic light scattering studies*, Faraday Discuss., **112** (1999), 143-154.

Chapter 7

General Discussion

Colloidal suspensions are a powerful experimental model system for studying the individual and collective phenomena of matter at the microscopic length scales. In analogy to atoms and molecules, which act at much smaller length scales, colloids in suspension also form a variety of solid phases, both crystalline and amorphous. The inherently larger length and time scales that govern colloidal systems, allow these phases to be studied with easily accessible techniques such as microscopy, light scattering and rheology, which give insight into both structural and mechanical properties.

With the development of high resolution microscopes and increased sensitivity of rheometers, colloidal suspensions can now be studied with increased precision at microscopic length scales. Together with the improvement and automation of analysis techniques, and the development of colloids with new characteristics, such as active propulsion or adjustable size, this signals the advent of many new opportunities to study structure and mechanics in colloidal systems and develop colloid-based materials. In this thesis we contribute to this endeavor, by presenting five experimental chapters on both the development of new colloidal particles and the study of solid-solid phase transformations.

Synthesis of “model” colloids

The term “model” colloid, while often used, is ambiguous and depends on the criteria required for the system or phenomena under investigation. However, there are some criteria which are often encountered, in particular within the colloids as big atoms paradigm. Starting with the synthesis of colloidal particles, there are three criteria which should be considered: i) is the synthesis method simple or laborious, ii) are potentially hazardous or environmentally-unfriendly chemicals or methods involved in the synthesis and iii) is the method reproducible. Especially criterion ‘iii’ appears to be highly challenging; many of the published synthetic protocols are

notoriously difficult to reproduce. In Chapter 2, we present a method to synthesize colloids in aqueous solution in a single step. The method we develop is so straightforward, that it can be executed by first year chemistry students without an elaborate experimental set-up. Water is the medium in which the reaction occurs and the temperature stays well below its boiling point. The strength of this method however, is the fact that it works with different latex monomers, giving control over the density and refractive index of the colloids. This is interesting because generally, colloid synthesis protocols focus on a single monomer to produce the colloid and changing the monomer involves a change in the recipe.^[1-4] Finally, the method is highly reproducible, which is proven by two synthesis runs performed with identical recipe except with different fluorescent dye. Figure 7.1a shows a confocal microscopy image of these mixed particles, which co-crystallize, meaning that there is less than 5% difference in their size and shape.

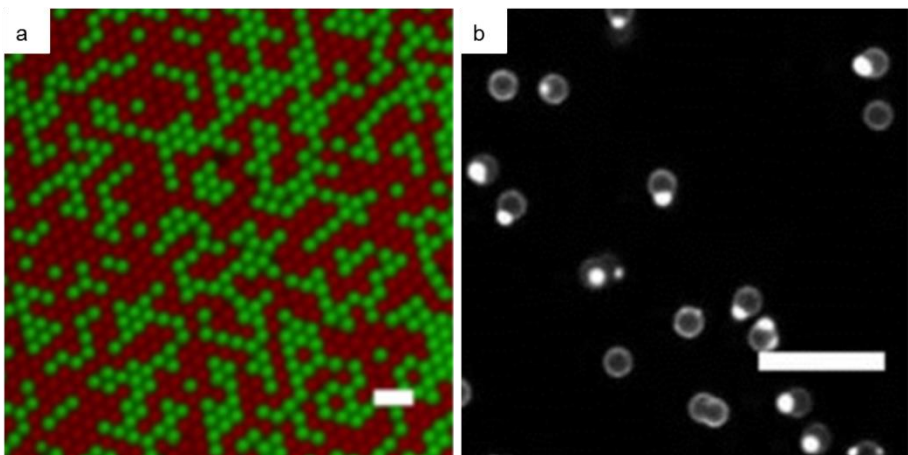


Figure 7.1: a) A crystallized mixture of two fluorescently distinct colloids, synthesized following the same reaction protocol. The co-crystallization of both types of colloids demonstrates the reproducibility of the synthesis method. b) A confocal microscopy image of core-shell particles with protrusions of conjugated polymer due to an excess of monomer in the reaction. Scale bars 5 μm .

Chapters 3 and 4 present the synthesis of core-shell particles, which are performed in a more difficult two-step method. Even though this synthesis is somewhat more laborious than the one-pot recipes in Chapter 2, we have verified that also here the procedures are highly reproducible. In a first step

the core particle is synthesized, either from polymeric or inorganic precursors, which is then used as a seed particle in the second reaction step, where a shell is grown around it. Chapter 3 demonstrates that this approach has the advantage of creating anisotropic particles, simply by choice of seed particles. Once more, a versatile range of colloids can be used as core particles, however, as the particle shape becomes more elaborate, so does the synthesis protocol.^[5-7] Interestingly, the optical properties of the shell can be tuned with monomer composition and a broad range of conjugated shells can be synthesized. There is however a limit to the thickness of the shells synthesized in Chapter 3. As the shell thickness increases, the anisotropic shape of the seed colloids no longer determines the final particle shape as surface tension will round-off the anisotropic features until a spherical particle results for thick shells. More interesting however, is the case of excess amounts of monomer during synthesis. This creates secondary particles, which adsorb and anchor to the core-shell particles, creating distinct and relatively monodisperse protrusions as shown in figure 7.2b.

In Chapter 4 we demonstrate the facile synthesis of core-shell microgel particles in aqueous media. The core particle is a solid latex particle which, similar to the colloids described in Chapter 2, can be synthesized from different latex monomers and can incorporate fluorescent dye molecules. The hydrogel shell that is synthesized to surround the solid core, has the interesting property of responsiveness to temperature, ionic strength and pH. The obtained core-shell particles have two distinct features; i) the responsive hydrogel shell can be used to change both the size and interaction potentials between the particles, which can be used for an application such as drug delivery^[8] or to study phase transformations^[9,10] in colloidal suspensions (Chapters 5 and 6), ii) the fluorescent core acts as a beacon that allows accurate particle tracking using high-resolution quantitative confocal microscopy without overlap of fluorescent emission between the soft and deformable shells.

In addition to the need for well-explained, facile and reproducible synthesis protocols, there is often the need for particles with low size polydispersity and with tailored properties. For example to form colloidal crystals the polydispersity of the particles must be <5%.^[11] By contrast, to induce glass formation, polydispersity >10% is often desired to reduce the crystal nucleation rate thus ensuring sufficient stability of the glass phase.

Chapters 2, 3 and 4 demonstrate methods to synthesize particles with low polydispersity, which is evidenced by the fact that the concentrated suspensions crystalize. The desired properties of colloidal particles often dictate the appropriate synthetic route. In Chapter 2, the density and refractive index of the colloids can be controlled by choice of monomer; this allows tuning the scattering contrast to enable a variety of characterization techniques to be used and to minimize gravitational effects which are known to alter the phase behavior and dynamics of suspensions. In addition, we demonstrate that this method allows for a homogenous incorporation of a fluorescent dye, to enable their observation with fluorescence microscopy methods. The surface properties of the colloids are largely determined by the high loading of carboxylic acid groups, which provide not only stability by electrostatic repulsion but allow us to use standard coupling reactions to modify the colloidal surface.

In Chapter 3 we demonstrate the use of different types of seed particles, which by themselves have different properties such as different shapes, densities, refractive indices and responsivity to for example magnetic field. The two-step approach allows for a core-shell architecture of two very distinct materials, each of which can be tailored at will. We show for instance, that an inert silica core particle is covered with a conjugated polymer shell, which has interesting properties for photonic materials as the emission and scattering profile of the particles can be controlled.^[12]

The core-shell particles described in Chapter 4 are fluorescent and responsive to temperature, ionic strength and pH. In experiments, the fluorescent core allows for excellent particle discrimination and tracking. Homogeneously dyed particles, such as those in Chapter 2, are difficult to locate in three-dimensional confocal microscopy images, especially in dense systems, due to the overlap of the fluorescence emission from neighboring particles. The use of a non-fluorescent shell, separated the emission centers physically, increasing the reliability and resolution of computer-based particle location algorithms, which is crucial to study the structure of for example glasses and crystals in detail (Chapter 5). It is likely that a number of other small molecules and particles can also be incorporated in the core following this synthesis protocol. This will further increase the functionalities of the core particles. The hydrogel shell is responsive in water and allows control over the particle size and interaction potential, with which phase transformation can be induced with a simple environmental trigger

(Chapter 6). These core-shell particles can be further functionalized to impart them for example with catalytic properties by incorporation of nanoparticles in the shell.^[13]

Crystals, glasses and gels

When a colloidal suspension is prepared which meets the criteria discussed above, it can be used to effectively study the structure and microscopic dynamics of solid phases, for example using confocal microscopy. Typically, the mechanical properties of the same suspensions can be measured with a rheometer. Since the mechanics of these materials relies on the specific details of microstructure and particle dynamics, this approach enables the study of the relations between the microscopic structure and the macroscopic mechanics.

For the final chapters of this thesis, we have used the core-shell microgel particles presented in Chapter 4. With these colloids we can switch the state of the suspension from a glass, to a liquid or gel phase by adjusting the temperature by a few degrees. Upon mixing two or more different species of these core-shell colloids, we can design systems that have a dual response at two different temperatures. For example, when using two species of particles that gel upon increasing the temperature at two different critical temperatures, we find a step-wise increase in the elastic modulus as the temperature is raised across the two transition points. Using confocal microscopy, we learned that gelation in these mixtures happens in a sequential manner. This is an interesting complex phase transition, because there is a first aggregation process where one species of particles forms a gel-like scaffold structure. At a higher temperature the scaffold is coated by gelation of the other particles onto the scaffold, thus generating a complex and hierarchical gel structure. It is interesting for future study to explore the effect of different mixing ratios and volume fractions. These factors will influence the microstructure and thus the mechanical properties of these core-sheath gels. It is even more interesting to investigate if the chemistry of the colloids can be modified so that the two species do not aggregate on to each other, instead they form a double network. This can lead to the development of colloidal materials with tunable mechanical properties.

In Chapter 5 we study the crystal-to-glass transition in a concentrated suspension of colloids, which is an order-to-disorder transition without liquefaction of the sample. Hence the transition, unlike the melting transition of crystals to liquids, is purely structural in origin. Repulsive forces due to charged carboxylic acid groups in the microgel shells assure that these suspensions easily crystallize in a face centered cubic lattice. However, when we introduce particles that are sufficiently larger, and thus do not fit into the crystal lattice, the crystal formation is hampered by these impurity defects. We found that as the number of impurities is increased, the system can at first accommodate impurities by placing the impurities in the lattice position of four tetrahedrally coordinated particles, thus creating a new type of crystalline defect. At increasing impurity numbers, the co-crystal transforms into a polycrystal with amorphous regions around the crystallites. Finally, from impurity number fractions of 0.05 and higher the whole system becomes amorphous. It is interesting that at low impurity numbers, the impurity particles occupy a space in the lattice which does not disturb the lattice. A geometric argument tells us that this is the effect of the size ratio between the particles. These defects require further investigation, because carefully mixed colloidal crystals with these type of defects could have interesting photonic properties where light propagation through the periodic lattice is perturbed.

In Chapter 6 we present measurements of the mechanics at another solid-solid transition; that between two amorphous solids, i.e. the glass-to-gel transition. These two states are interesting because they are both amorphous solids, however at very different volume fractions with different interparticle interactions and different microstructures. We found that the attractive interactions between the particles in the gel state can be controlled as a function of temperature and this allowed us to study the mechanics of the gel system with different attractive interactions between the particles. We further explore the differences between the glass and gel states of the suspension and found a discontinuity in the yield strain at the transition point. This system has potential for studying another largely unexplored transition between two amorphous solids, namely the repulsive-to-attractive glass transition. In this transition, interparticle interactions change from repulsive to attractive. While the microstructure remains unaffected, the mechanical properties of the suspension change distinctly,^[14,15] which is important in for example material processing.

Peptide-functionalized colloids

In chapter 4 we first discuss responsive colloids, which have a temperature dependent interaction potential. In this chapter, the particles have a microgel shell of which the polymer has a lower-critical solution. However, this results in highly aspecific attractions between all particles in the system. To create controllable and complex ordered colloidal structures, it is essential that the particles are functionalized with molecules that interact specifically and direct the particles to assemble. Together with Geert Daudey and Alexander Kros of Leiden University, we set out to functionalize colloids with complementary coiled-coil peptides. These peptides, inspired by SNARE fusion proteins, have specific interactions, that can direct membrane fusion.^[16,17] They are made up from two specific amino acid heptad repeats (EIAALEK₃ and KIAALK₃) that form heterodimeric coiled-coils. The peptides bind to each other with a hydrophobic patch and are directed to specific heterodimeric interactions by complementary charged groups flanking the hydrophobic patch. Figure 7.2 shows a helical wheel representation of this coiled-coil interaction.

Particular sets of peptides have a specific melting temperature and should bind only to their heterodimeric partner with high specificity. The hypothesis leading this research line was that with multiple complementary sets with different melting temperatures, a complex mixture could be created, in which temperature controlled orthogonal clustering could be studied.

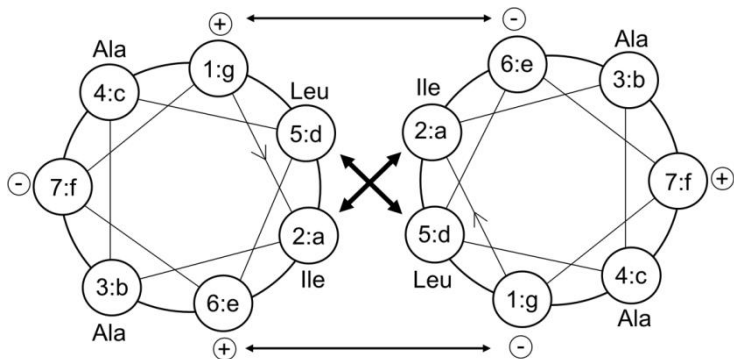


Figure 7.2: A helical wheel representation of coiled-coil dimer, residues a and d form a hydrophobic side, which directs binding between the coiled-coils, residues e and g direct heterogeneous binding via electrostatic interactions.^[18]

We started with the conjugation of one set of well-studied coiled-coil peptides, peptides E and K, to the surface of micron sized latex particles. We discovered in our initial experiments that there was strong homo-coiling between the K-peptide functionalized particles which resulted in aggregates of K-peptide functionalized particles even in absence of their complementary partner. The E-peptide functionalized particles on the other hand did not self-interact and were properly suspended in solution. Mixing the peptide functionalized particles resulted in mixed aggregates in which one could identify E-K interactions, however, the majority of interactions seemed to be aspecific in origin, due to aggregation of the K-peptide functionalized particles. By increasing the temperature we hoped to melt the aggregates and then reinitiate their assembly by slowly lowering the temperature. The aggregates however, would never melt despite mechanical agitation and being heated to tens of degrees above the melting point of the heterodimeric coils in solution. This aspecific effect which can increase the melting point of peptide-functionalized colloids was also described previously for DNA-functionalized colloids.^[19]

Subsequently, we explored an alternative strategy. The colloids were decorated with lipid bilayers by means of vesicle adsorption. The E- or K-peptides were anchored into these bilayers via a cholesterol anchor. While this approach has shown specific docking and fusion of small vesicles in solution,^[16,17] also here we observed strong homo-coiling of the K-peptides and subsequent aggregation of the individual species. This prevented us from determining the correct number of peptides on the surface required to ensure hetero-aggregation. What we overlooked however, was the fact that upon mixing these lipid coated particles, large undefined homo-aggregated clusters formed, together with a small population of heterobound structures. Figure 7.3. shows some of the characteristic specific and non-specific assemblies we found. At the same time, a new study demonstrated that membrane-coated particles interact via membrane fusion when E- and K-peptides are anchored in the membranes leading to mixing and exchange of peptides between initially pure E- or K-decorated colloids thus loosing specificity as soon as binding begins.^[20] With this knowledge we concluded that membrane fusion and fast exchange dynamics of the peptides over the membrane was the reason we saw these small properly self-assembled structures. At the same time, a similar system using DNA instead of peptides

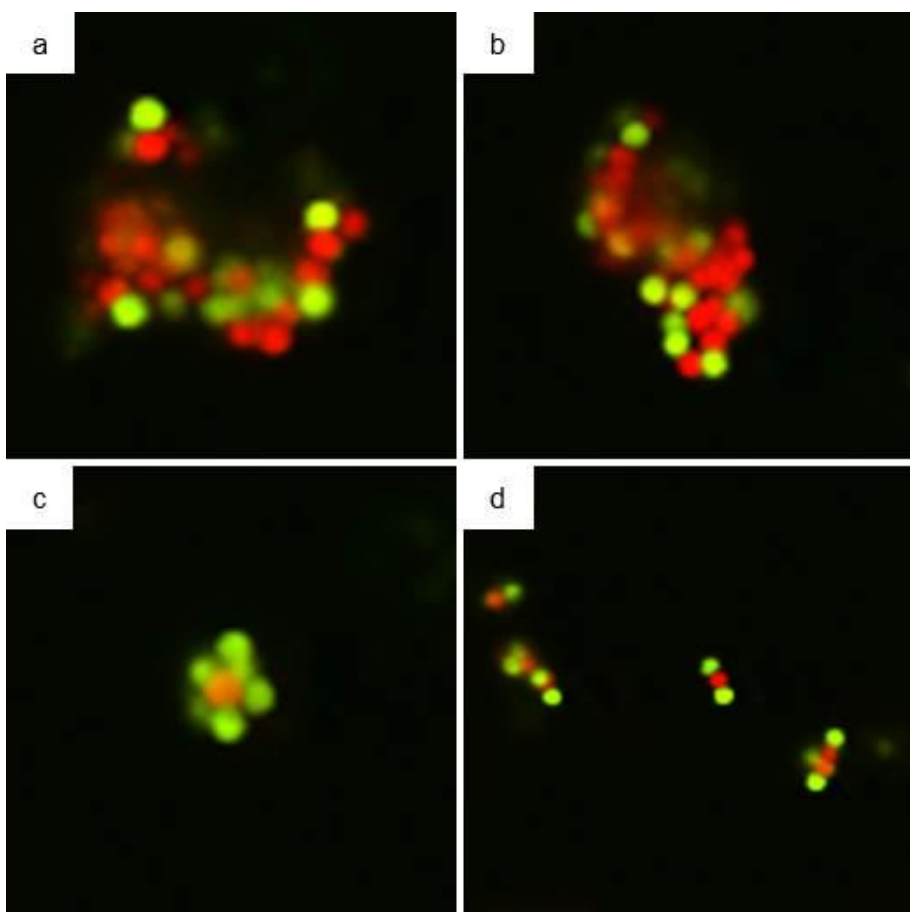


Figure 7.3: Confocal microscopy images of typical large clusters (a,b) formed by mixing E- and K-peptide functionalized colloids, and small proper assemblies (c,d). The particles in these images have a diameter of 1300 nm.

anchored in membrane decorated colloids demonstrated that temperature controlled self-assembly is possible in these systems.^[21]

Finally, we put our efforts in four sets of coiled-coil peptides with different melting temperatures designed initially by Woolfson.^[22] We assumed that a lower melting temperature would give us more control over the self-assembly process, because the interactions would be weaker and more readily tuned by temperature. However, we encountered the same problems as with the E- and K-peptides and we were unable to resolve these issues at the time. A similar strategy to exploit peptides for colloidal assembly, is to re-design peptides following the principles governing DNA

hybridization. Here hydrogen-bonding is the driving force for interaction and this might be more suitable for directing the self-assembly of micron-sized colloids. Peptide sequence inspiration can for example be taken from natural occurring protein β -sheets.

Concluding remarks

Microscopic particles suspended in a liquid are a fascinating form of matter with an extensive variety of composition and mesoscopic properties. This thesis describes our efforts of developing novel colloids and understanding fundamental concepts of phase transformations within colloidal suspensions. We hope the research presented here will inspire others to further develop the field of colloid science to create and understand advanced soft materials.

References

- [1] W. Stöber and A. Fink, *Controlled growth of monodisperse silica spheres in the micron size range*, Journal of Colloid and Interface Science, **26** (1968), 62-69.
- [2] K. P. Lok and C. K. Ober, *Particle size control in dispersion polymerization of polystyrene*, Canadian Journal of Chemistry, **63** (1985), 209-216.
- [3] L. Antl, J. W. Goodwin, R. D. Hill, R. H. Ottewill, S. M. Owens, S. Papworth and J. A. Waters, *The preparation of poly(methyl methacrylate) latices in non-aqueous media*, Colloids and Surfaces, **17** (1986), 67-68.
- [4] T. Still, K. Chen, A. M. Alsayed, K. B. Aptowicz and A. G. Yodh, *Synthesis of micrometer-size poly(N-isopropylacrylamide) microgel particles with homogeneous crosslinker density and diameter control*, Journal of Colloid and Interface Science, **405** (2013), 96-102.
- [5] C. C. Ho, A. Keller, J. A. Odell and R. H. Ottewill, *Preparation of monodisperse ellipsoidal polystyrene particles*, Colloid and Polymer Science, **271** (1993), 469–479.
- [6] B. Liu and D. Y. Wang, *High-Throughput Transformation of Colloidal Polymer Spheres to Discs Simply via Magnetic Stirring of Their Dispersions*, Langmuir, **28** (2012) 6436-6440.
- [7] T. Sugimoto, M. M. Khan, A. Muramatsu and H. Itoh, *Formation mechanism of monodisperse peanut-type- Fe_2O_3 particles from condensed ferric hydroxide gel*, Colloids and Surfaces A: Physicochemical and Engineering Aspects, **79** (1993), 233-247.
- [8] J. K. Oh, R. Drumright, D. J. Siegwart and K. Matyjaszewski, *The development of microgels/nanogels for drug delivery applications*, Progress in Polymer Science, **33** (2008), 448-477.
- [9] G. Romeo, A. Fernandez-Nieves, H. M. Wyss, D. Acierno and D. A. Weitz, *Temperature-Controlled Transitions Between Glass, Liquid, and Gel States in Dense p-NIPA Suspensions*, Advanced Materials, **22** (2010), 3441-3445.
- [10] Y. Peng, F. Wang, Z. Wang, A. M. Alsayed, Z. Zhang, A. G. Yodh and Y. Han, *Two-step nucleation mechanism in solid-solid phase transitions*, Nature Materials, **14** (2015), 101-108.
- [11] S. Auer and D. Frenkel, *Suppression of crystal nucleation in polydisperse colloids due to increase of the surface free energy*, Nature, **413** (2001), 711-713.

- [12] A. J. C. Kuehne, M. C. Gather and J. Sprakel, *Monodisperse conjugated polymer particles by Suzuki–Miyaura dispersion polymerization*, Nature Communications, **3** (2012).
- [13] Y. Lu, Y. Mei, M. Dreschler and M. Ballauff, *Thermosensitive Core–Shell Particles as Carriers for Ag Nanoparticles: Modulating the Catalytic Activity by a Phase Transition in Networks*, Angewandte Chemie-International Edition, **45** (2006), 813-816.
- [14] Z. Zhang, P. J. Yunker, P. Habdas and A. G. Yodh, *Cooperative Rearrangement Regions and Dynamical Heterogeneities in Colloidal Glasses with Attractive Versus Repulsive Interactions*, Phys. Rev. Lett., **107** (2011), 208303.
- [15] N. Koumakis and G. Petekidis, *Two step yielding in attractive colloids: Transition from gels to attractive glasses*, Soft Matter, **7** (2011), 2456-2470.
- [16] H. R. Marsden and A. Kros, *Self-Assembly of Coiled Coils in Synthetic Biology: Inspiration and Progress*, Angewandte Chemie-International Edition, **49** (2010), 2988-3005.
- [17] F. Versluis, H. R. Marsden and A. Kros, *Self-Assembly of Coiled Coils in Synthetic Biology: Inspiration and Progress*, Chemical Society Reviews, **39** (2010), 3434-3444.
- [18] F. Versluis, *Peptide Amphiphiles and their use in supramolecular Chemistry*, Doctoral Thesis, Universiteit Leiden (2013), <http://hdl.handle.net/1887/22801>.
- [19] R. Dreyfus, M. E. Leunissen, R. Sha, A. V. Tkachenko, N. C. Seeman, D. J. Pine and P. M. Chaikin, *Simple Quantitative Model for the Reversible Association of DNA Coated Colloids*, Phys. Rev. Lett., **102** (2009), 048301.
- [20] C. Bao, G. Pähler, B. Geil and A. Janshoff, *Optical Fusion Assay Based on Membrane-Coated Spheres in a 2D Assembly*, Journal of the American Chemical Society, **135** (2013), 12176-12179.
- [21] S. A. J. van der Meulen and M. E. Leunissen, *Solid Colloids with Surface-Mobile DNA Linkers*, Journal of the American Chemical Society, **135** (2013), 15129-15134.
- [22] D. N. Woolfson and M. G. Ryadnov, *Peptide-based fibrous biomaterials: some things old, new and borrowed*, Current Opinion in Chemical Biology, **10** (2006), 559-567.

Chapter 8

Summary

Mayonnaise, shaving foam and paint are everyday examples of soft solid materials that have both liquid-like and solid-like characteristics. We refer to these materials as soft matter and they comprise different systems such as emulsions, suspensions and polymer solutions. Due to the mesoscopic length scales inherent to structure in these systems they can be readily studied with techniques such as optical microscopy, light scattering and rheology, giving insight in both structural and mechanical properties of the system.

A particular class of soft materials are colloidal suspensions; small particles suspended in a fluid. Depending on the volume fraction of particles and the interaction potential between the particles colloidal dispersions can exist in different thermodynamic or non-equilibrium phases, such as fluids, liquids, glasses, crystals or gels. Each of these phases has its specific structural and mechanical features; the fact that the link between structure and mechanics can be studied in one system at the single-particle level, makes colloidal suspensions a powerful experimental model system to study soft materials.

In this thesis, which is divided into two parts, we try to both advance the possibilities of colloids as experimental models by developing novel colloids with controllable interactions and study the different solid-like phases found in colloidal suspensions such as crystals, glasses and gels. In particular, we use the fact that clever design of the particles allows us to manipulate the particle interactions using temperature, thus enabling the study of the crystal-to-glass and glass-to-gel transition using microscopy and rheology.

In **Part I** of this thesis, methods to synthesize novel well-defined monodisperse colloids are presented. A facile method to synthesize surface-functional latex colloids is presented in **Chapter 2**, where we show that the combination of 4,4'-azobis(4-cyanovaleic acid) (ACVA) as the radical initiator, together with itaconic acid as a comonomer, yields single-pot highly carboxylated, monodisperse particles of a variety of polymers. The method provides excellent control over the size, refractive index and density of the particles, together with the ability to modify the surface. More complex colloids require several synthesis steps, therefore, in **Chapter 3**, a

two-step method is introduced to synthesize conjugated polymer shells on colloids of variable composition and shape. Colloidal seed particles of organic as well as inorganic materials are surface functionalized with an aryl halide, which are then used as a template for a conjugated polymer shell grown using a Suzuki-Miyaura dispersion polymerization. Monodisperse core-shell particles with various shapes and various conjugated polymers were synthesized, creating novel composite conjugated polymer particles. In **Chapter 4** we present a two-step method to synthesize core-shell composite microgels. These microgels have a hard polystyrene core, which can be functionalized with a fluorescent dye. Different responsive microgel shells were synthesized around these core particles, creating monodisperse core-shell particles with excellent control over the particle size. The microgel shells are responsive to temperature, pH and salt concentration and can be tuned with monomer composition. We characterize a dense suspension of these microgels, which transitions from a glass, to a liquid, to a gel phase, as temperature is increased. We also demonstrate that a suspension with two different types of composite microgels, forms a gel with a core-sheath structure in a sequential manner.

The core-shell microgels are the basis for **Part II**, in which we use these colloids to study solid-solid transitions in dense suspensions. In **Chapter 5**, we study the vitrification of microgel suspensions from the crystal phase, by doping the crystal with increasing amounts of impurity particles. The fluorescent core of the microgels allows for single particle tracking and different fluorescent dyes discriminate the impurity particles from the base particles. The impurities, with a size ratio of 0.67, unexpectedly co-crystallize at low number fractions by replacing a cluster of four tetrahedrally coordinated small particles in a face centered cubic lattice. However, as the number of impurities is increased, long range distortions occur on the crystal lattice, eventually vitrifying the system. Surprisingly, the transition from crystal to glass shows striking similarities to the melting transition of crystals into a liquid phase. Finally, in **Chapter 6**, a suspension of thermoresponsive microgels is studied, in which we can induce a transition from a repulsive glass to an attractive gel using a temperature-induced decrease of particle volume fraction and a switch from a repulsive interaction to an attractive interaction between the particles. Using rheology, we probe the mechanical properties in both the linear and non-linear regimes

and find marked differences in the way these two amorphous solids respond, due to particle volume fraction and interparticle interactions. There is a clear discontinuity in the yield strain at the gelation temperature. Furthermore, the glass phase yields with a rate dependency in a reversible manner, contrary to the gel phase which yields without a rate dependency and irreversible. These chapters demonstrate how in a thermoresponsive suspension, solid-solid phase transitions which have remained relatively unexplored to date, can be effectively studied.

List of Publications

J. J. Davis, B. Peters, W. Xi, J. Appel, A. Kros, T. J. Aartsma, R. Stan and G. W. Canters, *Large amplitude conductance gating in a wired redox molecule*, The Journal of Physical Chemistry Letters **1** (2010), 1541-1546.

D. Ershov, J. Sprakel, J. Appel, M. A. Cohen Stuart and J van der Gucht, *Capillarity-induced ordering of spherical colloids on an interface with anisotropic curvature*, PNAS **110** (2013), 9220-9224.

R. Higler, J. Appel and J. Sprakel, *Substitutional impurity-induced vitrification in microgel crystals*, Soft Matter **9** (2013), 5372-5379.

J. Appel, S Akerboom, R. G. Fokkink and J. Sprakel, *Facile one-step synthesis of monodisperse micron-sized latex particles with highly carboxylated surfaces*, Macromolecular Rapid Communications **34** (2013), 1284-1288.

J. B. ten Hove, J. Appel, J. M. van den Broek, A. J. C. Kuehne and J. Sprakel, *Conjugated polymer shells on colloidal templates by seeded SuzukiMiyaura dispersion polymerization*, Small **10** (2014), 957-963.

H. Monteillet, M. Workamp, J. Appel, J. M. Kleijn, F. A. M. Leermakers and J. Sprakel, *Ultrastrong anchoring yet barrier-free adsorption of composite microgels at liquid interfaces*, Advanced Materials Interfaces **1** (2014), 1300121.

S. Akerboom, J. Appel, D. Labonte, W. Federle, J. Sprakel and M. Kamperman, *Enhanced adhesion of bioinspired nanopatterned elastomers via colloidal surface assembly*, Journal of the Royal Society Interface **12** (2015), 20141061.

R. Stan, A. Kros, N. Akkilic, J. Appel, and N. J. M. Sanghamitra, *Conductance switching and organization of two cognate molecular wires on gold*, Langmuir **31** (2015), 953-958.

J. Appel, N. de Lange, H. M. van der Kooij, T van de Laar, J.B. ten Hove, T. E. Kodger and J. Sprakel, *Temperature controlled sequential gelation in composite microgel suspensions*, Particle and Particle Systems Characterization **32** (2015), 764-770.

J. Appel, B. Fölker and J. Sprakel, *Mechanics at the glass-to-gel transition of thermoresponsive microgel suspensions*, Soft Matter **12** (2016), 2515-2522.

R. C. Stan, A. Kros, J. Appel and N. J. M. Sanghamitra, *Probing the Active Site of an Azurin Mutant Hot-Wired to Gold Electrodes*, The Journal of Physical Chemistry C **120** (2016), 7639-7645.

R. C. Stan, A. Kros, N. Akkilic, N. J. M. Sanghamitra and J. Appel, *Direct wiring of the azurin redox center to gold electrodes investigated by protein film voltammetry*, Journal of Electroanalytical Chemistry **787** (2017), 14-18.

Acknowledgements

This thesis is an account on scientific research conducted over a period of four years, which I present to Wageningen University and the Academic Board to be able to receive the degree of Philosophiae Doctor. Of course my contribution to the research is significant, but fortunately I did not do it all by myself and I would like to take a moment to gratefully thank the following people for their involvement.

As significant as my contribution is that of Joris Sprakel, who supervised and supported me over the course of this thesis project. Joris, you have a remarkably good eye for recognizing meaningful results and outstanding skills in presenting these results to an academic audience. You guided this research to a success with your enormous dedication and a mindset to succeed. Thank you for working together with me.

Alexander Kros and Geert Daudey, timewise, most of my time was spent on our common project on colloidal LEGO during which we experimented with the E and K peptides as surface ligands on micron sized colloids to control colloid-colloid interactions. Unfortunately we were not able to produce an additional chapter on this subject in this thesis, however your effort is gratefully appreciated.

Frans Leermakers as my promotor you had the first and final decision on the judgement of this thesis and during the project we had discussions about this and other research. Your enthusiasm and knowledge were certainly appreciated.

Four chapters of this thesis could not have been possible without the help of the following brilliant and dedicated students. Ruben Higler, your thorough analysis of the vitrification of microgel suspensions guided our understanding of this phenomenon. Jan Bart ten Hove, your ability to redesign and perform experiments on a daily basis lead us to the development of a novel hybrid colloid. Niek de Lange, your dedication and meticulousness presented us the experimental data on the synthesis of core-shell microgel particles and the mechanical properties of their suspensions.

Bart Fölker, also your dedicated and meticulous way of working lead us to a further understanding of phase transformations in microgel suspensions.

Sabine Akerboom, when I started the thesis project, you and I were in search for the same result, micron-sized carboxylated polystyrene particles. Together we found a recipe for these particles relatively quick and I am proud to present that recipe as part of chapter 2 in this thesis.

Maria Oikonomou, your research was similar to mine, except your focus was on nanoparticles and mine was on micron-sized particles. This allowed us to discuss our research with great enthusiasm and on an exclusive level of detail.

Thomas Kodger, your enthusiasm for colloids and experience with pNIPAM microgels which you shared with me, has been the basis for most of the work presented in this thesis.

Rui Rijo Pedro da Costa Carvalho, you helped me also outside the lab for which I am truly grateful. You never tried to teach me a word of Português, however this sentence I will never forget “Trabalho é trabalho, conhaque é conhaque”.

Hanne van der Kooij, sharing an office with you has been a great privilege. You have an exceptional academic level and you were a listening ear for personal and professional matters.

Johannes Lyklema you have a monumental status in the field of colloid and interface science and it was a pleasure to be able to discuss with you something as simple as the titration of carboxylic acids on a colloidal surface.

Tom Wenckes and Bas van den Berg, whenever I had a problem related to organic chemistry, your doors were always open and you gave me great advice. Bas, your effort went beyond advice and I thank you for the many efforts on thiolated silica

Frank Versluis, we know each other now for almost a decade and every time we talk, we end up with a smile on our face. During your year in Wageningen, we shared many smiles.

Huanhuan Feng, thank you for the inspirational talks which carried a lot of Chinese wisdom. All the best to you, Tingting and Leo.

Ties van de Laar, you also became a microgel enthusiast and together we further developed and characterized these particles.

Maarten van Heek, you were always of great assistance in finding solutions to Matlab related problems.

I greatly appreciate the assistance and company of all the people that are and were part of Physical Chemistry and Soft Matter. Aljosha, Aldrik, Anita, Anton K., Anton B., Armando, Bert, Camilla, Céline, Chistian, Diane, Dirk, Dmitry, Duc, Esio, Evan, Frank, Gerben, Gosia B., Gosia W., Hande, Hannie, Harke, Hélène, Herman, Ilse, Inge, Jacob, Jan, Jan Maarten, Jasper, Joanne, Johan, Joshua, Josie, Juan, Junyou, Junus, Kamuran, Katarzyna, Kris, Lennart, Lione, Liyakat, Mara, Marcel, Marleen, Martien, Merve, Mieke, Monika, Nadia, Natalia, Peter, Pieter, Prachi, Rahim, Ran, Remco, Renko, Rene, Rojman, Ronald, Soumi, Surender, Simeon, Stan, Sten, Thao, Tingting, Vittorio, Willem and Wolf.

I would also like to acknowledge Thad Castle (BMS) for the occasional inspiration and the Matlab/Latex/Inkscape/Google support team for their effort.

Finally I would like to thank the people closest to me for their inspiration, support and love. Maria, Rafael, Arthur, Bert, Annelies, Thijs, Oma, Lefteris and Chrysoula.

About the Author

Jeroen Appel was born the 25th of November 1981 in Beverwijk, the Netherlands. He obtained his bachelor degree in chemistry from the Hogeschool Inholland Alkmaar, for which he did a thesis project in the Academic Medical Center Amsterdam, at the department of Medical Biochemistry. Under the supervision of dr. Rolf G. Boot, he studied the effect of iminosugars on the proteome of obese mice for further understanding diabetes type II. He then obtained his master degree in chemistry from Leiden University, where he did a thesis project at the department of Metallo Proteins. Supervised by prof. dr. Gerard W. Canters, he studied the use of biarsenical fluorophores as bioconjugated sensor molecules to determine the redox state of copper proteins. At the department of Soft Matter Chemistry he performed an internship, supervised by prof. dr. Alexander Kros, where he synthesized oligo(phenylenevinylene) molecules for the use as electron transfer molecules. In 2011 he joined the laboratory of Physical Chemistry and Soft Matter at Wageningen University, where he started his PhD research on a ChemThem grant from the Netherlands Organization for Scientific Research under the supervision of dr. Joris Sprakel and prof. dr. Frans A.M. Leermakers. The result of his PhD research is this thesis.

Overview of Completed training Activities

Discipline specific courses and conferences

- Colloid Science, Wageningen, 2012.
- Microscopy and Spectroscopy in Food and Plant Sciences, Wageningen, 2012.
- 13th Dutch Soft Matter Meeting, Wageningen, 2012. †
- Physics@FOM, Veldhoven, 2013. †
- Chemistry in relation to Physics and Material Sciences, Veldhoven, 2013. †
- InterM, Antalya (Turkey), 2013. †
- Han-sur-Lesse Winterschool, Han-sur-Lesse (Belgium), 2014.
- Gordon Research Seminar, Colloidal, Macromolecular Polyelectrolyte Solutions, Ventura, CA (USA), 2014. †
- Gordon Research Conference, Colloidal, Macromolecular Polyelectrolyte Solutions, Ventura, CA (USA), 2014. †
- 17th Dutch Soft Matter Meeting, Leiden, 2014.
- Advanced Chemistry, Wageningen, 2014-2015.
- Gordon Research Seminar, Macromolecular Materials, Ventura, CA (USA), 2015. †‡
- Gordon Research Conference, Macromolecular Materials, Ventura, CA (USA), 2015. †
- 18th Dutch Soft Matter Meeting, Eindhoven, 2015.
- 19th Dutch Soft Matter Meeting, Utrecht, 2015.
- Julich Soft Matter Days, Bad Honnef, (Germany), 2015. †
- CHAINS, Veldhoven, 2015.

General courses

- Information Literacy including EndNote Introduction, Wageningen, 2014.
- Data Management Planning, Wageningen, 2014.
- Mobilising Your Scientific Network, Wageningen, 2014.
- Scientific Writing, Wageningen, 2014.
- Career Assessment, Wageningen, 2015.
- Writing Grant Proposals, Wageningen, 2015.

Other activities

- Group meetings and colloquia, 2012-2016. †
- Journal club, 2014-2016.
- PhD trip, California (USA), 2013. ‡
- PhD trip, England (UK), 2015. ‡

Notes: † poster, ‡ oral presentation

This research was financially supported by the Netherlands Organisation for Scientific Research (NWO).

Printed by Proefschriftmaken.nl || Digiforce Vianen
Published by Uitgeverij BOXPress, Vianen